Author:
Qiao, Mengmeng

Title:
Genetic and molecular analysis of lawd-1, an essential gene in epithelial development and morphogenesis

Genetic and molecular analysis of *lawd-1*, an essential gene in epithelial development and morphogenesis

Mengmeng Qiao

Supervisor: Professor Patricia Kuwabara

A dissertation submitted to the University of Bristol in accordance with the requirements for award of the degree of Doctor of Philosophy in the Faculty of Medical and Veterinary Sciences

School of Biochemistry

February 2018

Word count: 37681

Table of contents

Abstract

Epithelial cells are capable of undergoing dynamic rearrangements to form sheets and tubes during morphogenesis. These dynamic changes are controlled by a network of proteins responsible for inducing and maintaining polarity, cell junctions and cytoskeletal associations. In this study, I analysed the function of a novel *C. elegans* gene named *lawd-1* (lumen associated with WD40 domain). Genetic analyses revealed that *lawd-1* mutants exhibit variable morphogenetic defects throughout development. The first allele was identified because of the appearance of a Notched-head. Later characterisation of a *lawd-1* null allele confirmed that *lawd-1* has essential roles in development. Co-expression studies using fluorescent proteins as intracellular markers and a mCherry tagged LAWD-1 revealed the dynamic pattern of LAWD-1 expression. LAWD-1 was shown to be enriched along the apical membrane of epithelial tissues beginning in the late embryo. LAWD-1 continues to be expressed at post-embryonic stages of development. Evidence is presented showing that LAWD-1 is associated with the actomyosin contractility network. LAWD-1 encodes multiple protein isoforms; the largest isoforms carry the protein-protein interaction WD40 domain. A screen to identify potential LAWD-1 interacting proteins was carried out by performing co-immunoprecipitation followed by mass spectroscopy. Characterisation of one of the proteins identified by this screen, VAB-10B, a spectraplakin cytoskeleton linker is presented. A model is presented speculating that LAWD-1 functions in controlling cytoskeletal dynamics through its interaction with VAB-10B.

Acknowledgement

I owe my deepest gratitude to my supervisor Prof. Patricia Kuwabara, who gave me the opportunity to do this project and has supported me unconditionally throughout my PhD, who has provided guidance not only in my research, but for my life too.

I would like to thank the University of Bristol for giving me this opportunity to pursue this PhD and I am very grateful to have been funded by the University of Bristol Overseas Studentship.

I am grateful for having Jade and Marion not only as good friends, but also as valuable colleagues in the lab. You both have taught me so much and I am so glad our friendship goes beyond our time together at the university.

I am thankful for all the previous and current colleagues with whom I have spent great time. I will never forget all the big and little advice given to me when I was stuck, and the fun we had when we went out for food together.

I also need to mention Ruby and her chicken soup, both helped me get through the most frustrating time I had. You rock.

I truly appreciate my parents, my mother and father in-law, whose gave me care, encouragement and love more than I could ask for.

Finally, I have to thank my best friend, my dearest husband Sulide, I owe you the most and I know you are beyond happy to see me complete this part of the journey of my life.

Declaration

I declare that the work in this dissertation was carried out in accordance with the requirements of the *University's Regulations* and *Code of Practice for Research Degree Programmes* and that it has not been submitted for any other academic award. Except where indicated by specific reference in the text, the work is the candidate's own work. Work done in collaboration with, or with the assistance of, others, is indicated as such. Any views expressed in the dissertation are those of the author.

Signature: 

Date: 2023.9.19

Table of figures

Table of tables

List of Abbreviations

AP	Anterior-posterior
APS	Ammonium Persulfate
BCMP1	Brain cell membrane protein
BLAST	Basic local alignment search tool
BPAG	Bullous pemphigoid antigen
CCC	Catenin-cadherin complex
cDNA	complementary Deoxyribonucleic acid
CeAJ	*C. elegans* Apical Junction
CeHD	*C. elegans* Hemidesmosome Junction
CFB	Circumferential F-actin bundle
CIP	Calf intestinal phosphatase
co-IP	co-immunoprecipitation
CRISPR	Clustered regularly interspaced short palindromic repeats
DAC	DLC-1-AJM-1 complex
DIC	Differential interference contrast
dNTP	deoxyribonucleotide triphosphate
Dpy	Dumpy
DTC	Distal tip cell
DTT	Dithiothreitol
EB	Epidermolysis bullosa
ECM	Extracellular matrix
EDTA	Ethylenediaminetetraacetic acid
EGTA	Ethylene glycol-bis(β-aminoethyl ether)-N,N,N',N'-tetraacetic acid
Eph	Ephrin
FRAT	Fluorescent recovery after photobleaching
FO	Fibrous organelle
GAP	GTPase activating protein
GEF	Guanine nucleotide exchange factor
GFP	Green fluorescent protein
GSL	Glycosphingolipids
HEPES	4-(2-hydroxyethyl)-1-piperazineethanesulfonic acid
HRP	Horse radish peroxidase
HSS	High speed supernatant
IF	Intermediate filament
IPTG	Isopropyl β-D-1-thiogalactopyranoside
JAM	Junctional adhesion molecules
KASH	Klarscicht, ANC-1 and Syne-homology
kbp	kilo base pair
kDa	kilo Dalton
Lgl	Lethal giant larva
LGV	Linkage group V
MACF	Microtubule actin cross-linking factor
MAGuK	Membrane-associated guanylate kinase
mCh	mCherry
MET	Mesenchymal-epithelial transition
mRFP	monomeric red fluorescent protein
MT	Microtubule

MTOC	Microtubule organising centre
NGM	Nematode growth media
nt	nucleotide
PAM	Protospacer adjacent motif
PBS	Phosphate-buffered saline
PCM	Pericentriolar materials
PCR	Polymerase chain reaction
PKC	Protein kinase C
PMSF	Phenylmethane sulfonyl fluoride
RNAi	RNA interference
Rol	Roller
RPM	Rounds per minute
SDS PAGE	Sodium dodecyl sulfate polyacrylamide gel electrophoresis
sgRNA	single guide Ribonucleic acid
SMAC	SAX-7/MAGI-1/AFD-1 complex
SNARE	Soluble N-ethylmaleimide-sensitive factor activating protein receptor
ssODN	single-stranded oligodeoxynucleotides
SUN	Sad-1 and UNC-84
TAE	Tris-acetic ethylenediaminetetraacetic acid
TBE	Tris-borate ethylenediaminetetraacetic acid
Unc	Uncoordinated
UV	Ultraviolet
Vab	Variable abnormal
γ-TuRC	Gamma-tubulin ring complex

Chapter 1 **Introduction**

1.1 *C. elegans* as a model organism to study epithelia morphogenesis.

C. elegans is a 1 mm small and transparent nematode which was first introduced as a model organism by Sydney Brenner (1) to understand developmental biology and neurology. There are many advantages to use *C. elegans* as a model organism. It is genetically tractable, being able to self-propagate as hermaphrodite and mate with males. This allows various genetic manipulations to be carried out such as genetic screening, gene deficiency studies and genetic interaction studies, which had uncovered functions of essential genes and provided insight into its higher organism homologues. It had its invariable whole cell lineage mapped, which allows study on development from a single cell prospective (2). It was the first model organism to have its genome completed sequenced (3), forming a large data base where functions of unknown genes based on verified cDNA clones or predictions can be explored. This work has also aided the completion of human whole genome sequencing (4). Approximately 35% of *C. elegans* genes are closely related to human (5). Its transparent body allows easy visualisation of tissues and organs in which proteins can be tagged by fluorescent markers such as green fluorescent protein (GFP) as firstly developed by Marty Chalfie and co.(6) and their subcellular localisations studied by electron and fluorescent microscopy. RNAi reverse genetic approach was also developed in *C. elegans* which allows gene function analyses without altering the endogenous gene (7). Complete RNAi library is also available for such analyses (8). In addition, it has a relative short lifecycle of about 3 days from embryo to grown adult at 20 °C, which enables short experimental

cycles (1). In recent years, CRISPR-Cas9 genome editing technique was adapted from mammalian cell line research and further developed in the *C. elegans* system, which allows precise manipulations of any gene (9) (10) (11) (12) (13).

1.2 General features of epithelium and using *C. elegans* as tool to study epithelial development.

Epithelial tissues form barriers which prevent harmful materials from entering organisms, and as such they have a number of distinctive features. They are polarised along the apical-basal axis and the presence of junction complexes allow them to adhere to each other and form polarised sheets and tubes (14). Polarity is defined and maintained by differentially localised protein complexes such as the PAR polarity determining proteins and the junction complexes (15). Due to their polarised nature, they can also form chemical gradient and transfer materials between tissues. They can also secrete materials to the internal and external surfaces of the organisms (14).

The *C. elegans* epithelium consists of cells from the epidermis/hypodermis and other tubular tissues such as the intestine and spermatheca (16). Similar to epithelial cells in other multicellular organisms such as in *Drosophila* and human, they are capable of forming strong cell-cell adhesions through apical junctions (CeAJ) and hemi-desmosome-like junctions (CeHD) (16); Adhesion complexes undergo rearrangements controlled by endocytosis (17), endosomal recycling (18), and cytoskeleton remodelling (16) to allow epithelia to form cells of different size and shapes.

Essential components in *C. elegans* epithelia development had firstly been identified by a range of monoclonal antibodies developed by Francis and Waterson (19) (20). Genetic screens were subsequently used to uncover the function of genes in which mutations cause defects in embryonic and larval patterning and elongation, and other variable abnormal body morphological changes (16). Studies using fluorescent imaging have identified the subcellular localisation of polarity proteins

and apical and basolateral junction proteins. Progress in recent years has provided a better understanding of the mechanisms by which cell trafficking contributes to cell polarity maintenance, the dynamics of junctional and cytoskeletal remodelling (21) (22), and has led to the identification and characterization of new genes in CeHD formation (23). The results from these pioneering experiments will be discussed in detail in later sections of this chapter. The precise mechanisms underlying the direct and indirect interactions between the adhesion complexes and the cytoskeleton network, especially microtubules, remains poorly understood. Also unclear are the biochemical and mechanical signalling pathways that control how epithelial junctions change during morphogenesis (16)

1.3 Polarity proteins and their functions in epithelia development.

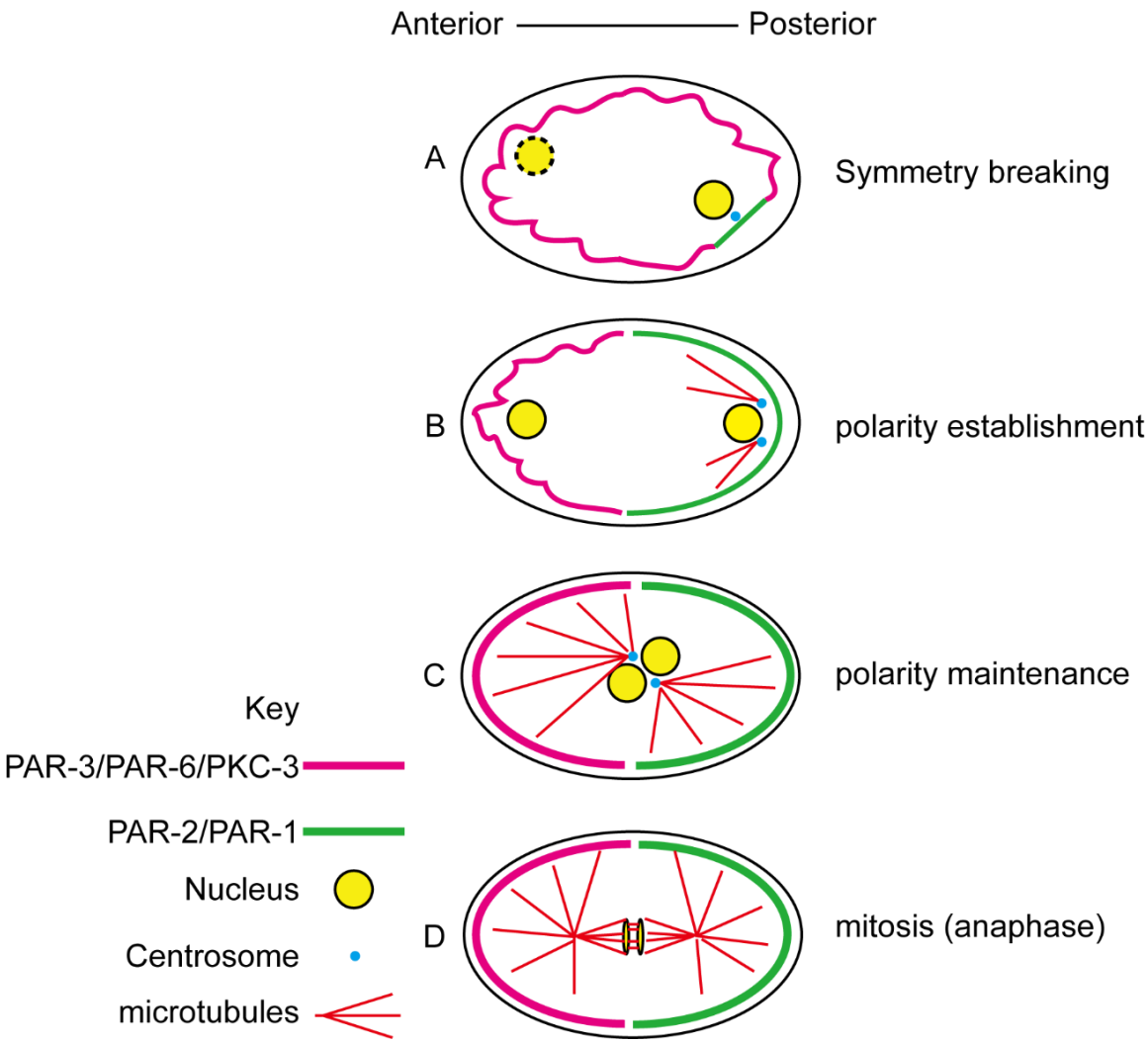

Figure 1-1 Establishment and maintenance of polarity in *C. elegans* early embryo.

A. Symmetry breaking occurs when centrosomes cause local inactivation of contractility of the actomyosin network which results in a small domain of smooth cortical area. **B.** During polarity establishment, the small cortical area expands in an anterior direction until it reaches ~50% egg length. **C. D.** Polarity is maintained by mutual exclusion of PAR proteins. Modified based on (24)

1.3.1 Discovery of PAR proteins in *C. elegans* early embryo.

During the development of multicellular organisms, cells adopt distinctive fates through differentiation and morphogenesis. The mechanism underlying these events involves the uneven distribution and partitioning of cellular content, which results in asymmetric cell division. A key determinant in asymmetric cell division is the establishment of cell polarity. Cell polarity is essential for cell growth, development, signal transduction and the transport of molecules across epithelial cell membranes (25). Research based on *C. elegans* early embryonic development helped to pioneer our understanding on cell polarity establishment and maintenance. In searching for the key molecular players for cell polarity determination and control, Kemphues *et al* found the first 6 genes during asymmetric division in *C. elegans* zygote through forward genetic screens and named them *par* (for partition defective) genes (26). Unspecified Mutations in these genes cause defects in zygotic cleavage, embryo patterning and developmental timing and also contribute to the abnormal distribution of P granules, which are large non-membrane bound ribonucleoprotein organelles in *C. elegans* germ cells (27). These events can then cause cell size and fate changes in daughter cells, altered spindle positions and cell cycle progression defects (28). Following on from the identification of the *par* genes, many studies have since established other aspects of the mechanisms controlling polarity establishment, asymmetric cell division and cell fate determination in *C. elegans*; similar processes have also been observed in higher organisms.

In *C. elegans*, establishment of embryonic polarity starts in the one cell zygote and the first embryonic cell division. At anaphase of meiosis II, an actomyosin network beneath the plasma membrane at cell cortex begins to contract (Figure 1-1A) in a process controlled by the Rho family GTPase RHO-1 and Rho-

binding kinase LET-502 (29) (30). Such contractions depend on the non-muscle myosin II heavy chain (NMY-2) as *nmy-2* knockdown by RNA interference (RNAi) leads to a *par*-like phenotype in *C. elegans* embryos (31). Knockdown of the regulatory myosin light chain MLC-4 also results in diminished cortical flow due to the reduction of actomyosin contractility, as demonstrated by GFP::PAR-6 (32). Asymmetry in the zygote starts to form in a process called symmetry breaking when inactivation of the local actomyosin network contractility occurs (Figure 1-1A) (33). Studies have shown that symmetry breaking is brought about by the centrosomes, which are assembled from the centrioles carried over from the sperm and the maternal pericentriolar material (24). When centrosomes are juxta positioned in proximity of the cell cortex by random movement along cortical microtubules, a reduction of local contractility occurs (34, 35). Laser ablation experiments also showed that centrosomes, and the short microtubules that they nucleate, are essential for the next stage of polarity establishment (34). Inactivation of local actomyosin contractility is caused by decreasing the activity of ECT-2, a RHO-1 positive regulator GTPase exchange factor (GEF), (29), or by increasing the activity of CYK-4, a negative regulator of the RHO-1 GTPase-activating protein (GAP), in the vicinity of centrosomes (36). CYK-4 is provided by sperm and its depletion results in uniform contractions (36). The local cortical region near centrosomes forms a small non-contractile actomyosin domain, which expands in the anterior direction until it reaches ~50% of the egg length before stopping (Figure 1-1B). A cortex flow is established through altered contractility at the cell cortex as anterior cortical tension, measured along the longitudinal axis, is twice as much as posterior cortical tension (37). PAR proteins come into play at this stage when PAR-3 and PAR-6, both of which contain PDZ domains capable of anchoring membrane

proteins to cytoskeletons in the cytosol, are localised to the anterior cortex of the cell. GFP::PAR-6 is initially detected throughout the cell cortex before symmetry breaking, but it retracts from posterior cortex during polarity establishment (32). PAR-3 and PAR-6 together with PKC-3, which encodes an atypical protein kinase C (38), form the 'anterior PAR complex' (24). PAR-1, a serine/threonine kinase (39), and PAR-2, a zinc finger domain protein of E3 ligase class (40), are localised at posterior cell cortex during polarity establishment. In contrast to GFP::PAR-6, the GFP::PAR-2 signal expands from the posterior cortex towards the anterior cortex during polarity establishment (41). PAR-4, a serine/threonine kinase (42), and PAR-5, a 14.3.3 protein, are found diffused uniformly throughout the cytoplasm (43). Taken together, contraction of the actomyosin network is responsible for establishing embryonic polarity by distributing different PAR proteins into mutually exclusive domains in a process controlled by RHO-1. It has also been observed that the anterior expansion of the PAR-2::GFP signal is faster than NMY-2::GFP posterior retraction (44). This observation indicates that PAR-2 can function independently of the actomyosin contractile network, as described above. Genetic analysis has further revealed that *par-2* is essential in a partial loss-of-function *etc-2(ax751)* mutant to establish polarity, which indicates that PAR-2 works in parallel pathway with the actomyosin network (45). PAR-2 has been shown to associate with centrosomes and biochemical analysis indicates it can bind with microtubules (46). Inactivation of PAR-2 by PKC-3 phosphorylation normally prevents PAR-2 from expanding along the anterior cortex; however, microtubule binding can protect PAR-2 from PKC-3 activity (46). PAR-2 is also capable of interacting with phospholipids *in vitro*, which also helps to protect it from negative control by PKC-3 (46). Furthermore, binding with phospholipids allows PAR-2 to recruit more PAR-2, which

in turn, promotes PAR-2 posterior expansion (46). Thus, PAR-2 provides an alternative pathway for polarity establishment through microtubule-dependent manner, although the actomyosin contractile network still remains the main player.

After polarity is established, ablation of the actomyosin contractile network is no longer capable of altering anterior-posterior (AP) polarity, suggesting that there is a need for additional polarity mechanisms (34). Maintaining polarity requires the mutual exclusion of PAR proteins and polarity components between the anterior and posterior cortical domains as illustrated in Figure 1-1 C, D and this is mainly achieved by the *par-2* gene function. A mutation in *par-2* causes posterior distribution of PAR-6::GFP (41) and NMY-2::GFP (32). NMY-2 was speculated to be another regulator, however recent research has shown that it only plays a minor role (47). The maintenance of PAR-2 polarity is achieved in part by PKC-3 phosphorylation (48). As mentioned earlier, PKC-3 phosphorylation is responsible for inactivating PAR-2 during polarity establishment. Structural and functional analysis of PAR-2 has shown that it can be phosphorylated by PKC-3 at seven different serine/threonine residues (48). Mutating these residues so that they can no longer be phosphorylated leads to uniform distribution of GFP::PAR-2. By contrast, modifying these amino acids to mimic constitutive phosphorylation prevents the localisation of GFP::PAR-2 (48). PAR-2 can then recruit PAR-1 through direct interaction (46). PAR-1 is capable of phosphorylating PAR-3 *in vitro* and can exclude the ‘anterior polarity complex’ in a PAR-2 dependent manner (46). Therefore, AP polarity and the mutually exclusive domains are maintained by the exertion of mutually inhibitory PAR protein activities.

Several other proteins have been extensively studied which all have important roles in establishing and maintaining polarity in *C. elegans* early embryos.

They are the *Drosophila* tumor-suppressor protein Giant Lethal Larvae homologue LGL-1, an Hsp90 co-chaperone CDC-37 and the small G protein CDC-42. Mutations in *lgl-1* enhances the lethality caused by partial inhibition of *par-2* and causes abnormal distribution of cortical NMY-2. Conversely, increasing LGL-1 activity improves the *par-2* (RNAi) phenotype (49) (47). This indicates that LGL-1 works in a redundant parallel pathway with PAR-2. Like PAR-2, LGL-1 is also subject to phosphorylation control by PKC-3, as similar results compared with manipulations of PAR-2 phosphorylation residues were observed when changing the properties of its own predicted phosphorylation sites (49) (47). CDC-37 is thought to stabilise PKC-3, because RNAi reduction of *cdc-37* revealed defects in exclusions of anterior and posterior proteins (50). CDC-42 can physically interact with PAR-6 (51), and the two proteins are co-dependent on each other for their proper cortical localisation (52). Image analysis revealed that CDC-42 initially appears at the anterior cortex before moving to the posterior cortex and disappearing (53). A targeted RNAi screen has identified the GEF protein CGEF-1 and the GAP protein CHIN-1 as regulators of CDC-42 (53). These regulators have been shown to be linked to the CDC-42 effector PAR-6, because depletion of CHIN-1 causes a reduction in the cortical distribution of PAR-6, and an increase in CHIN-1 causes an increase in PAR-6 cortical distribution (47). CDC-42 appears to have more important roles than discussed above, as it has been implicated in earlier polarity establishment phase in a PAR-2 dependent manner as well (30). CDC-42 regulators CGEF-1 and CHIN-1 may also act in a third parallel pathway to PAR-2 and LGL-1 mediated polarity maintenance, as in PAR-2 and LGL-1 depleted embryos, CDC-42 distributes in a polarised manner in a CGEF-1- and CHIN-1- dependent manner (47).

Proteins involved in basic cellular processes can also contribute to polarity establishment and maintenance, as evidenced by DYN-1, the dynamin GTPase, which has a wide variety of functions in endocytosis, actin dynamics and cell trafficking (54). DYN-1 becomes restricted to the anterior cortex during epithelial development in a manner similar to PAR-6, dependent on PAR-6 and PAR-3 (54). FRAP experiments suggest that DYN-1 can promote PAR-6 cortical association (54). Depletion of DYN-1 causes reduction of cortical GFP::PAR-6 and anterior expansion of GFP::PAR-2 (54). Because the polarity proteins PAR-6, PAR-3, PKC-3 and CDC-42 also contribute to endocytosis (55), this has been taken to indicate that there is an interplay between cell trafficking and polarity control. The early endosome protein RAB-5 might also play a role in controlling polarity, as depletion of RAB-5 causes minor changes in GFP::PAR-6 cortical distribution, and no change in GFP::PAR-2 cortical localisation (56). It is likely that these changes are only secondary effects resulting from the perturbation of basic cellular processes. A more refined relationship between basic cellular regulators and polarity proteins remains to be explored (24).

1.3.2 AP polarity establishment and maintenance in *C. elegans* epithelia.

In *C. elegans*, epithelial polarisation begins when apical junction proteins Catenin-Cadherin Complex (CCC), and DLG-1-AJM-1 Complex (DAC) redistribute from a uniform cytoplasmic pool to the apical domain (Figure 1-2) (57). These complexes will be discussed in detail in later sections. The correct localisation of the apical junction proteins is therefore key in forming a polarised epithelium. Epithelia are capable of forming sheets and tubes through morphogenesis and they require slightly different mechanisms of polarisation (16).

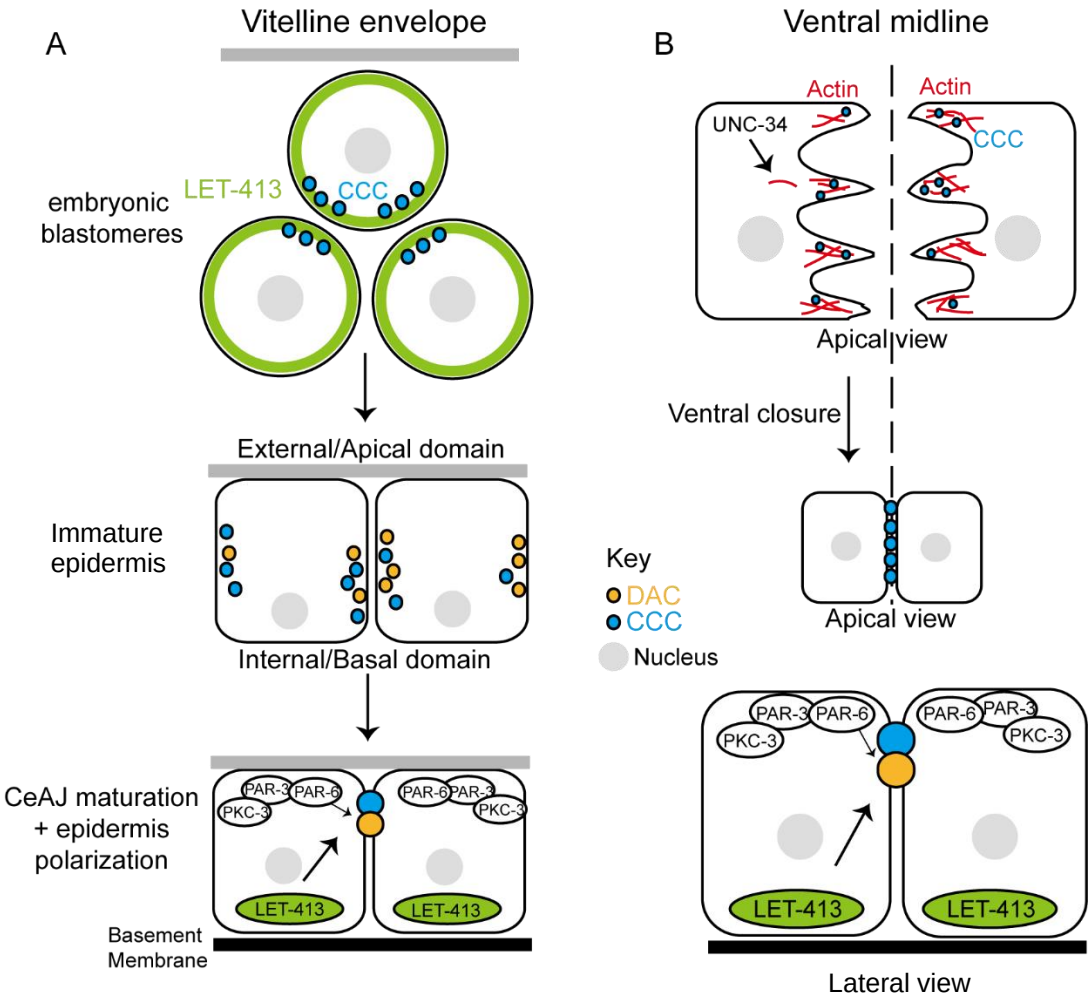

Figure 1-2 Polarity establishment in *C. elegans* epidermis.

A. LET-413 is initially uniformly distributed in embryonic blastomeres. Outer membrane is in contact with the vitelline envelope. CCC components are expressed at this stage. During early epidermis development, CCC and DAC are localised along the lateral membrane as puncta structures. LET413 begins to localise to the basolateral membrane during polarisation of epidermis and it is required for the coalescence of CeAJ to the apical domain. PAR-6 is also required for CeAJ maturation. **B.** Polarity is re-established, and AJ reformed during the ventral closure process in epidermis morphogenesis. CCC are mobilised along actin-rich protrusions to prime for new AJ formation. Actin regulator UNC-34/Enabled is required for stabilisation of AJ. In mature epidermis, PAR-3, PAR-6 and PKC-3 are all localised to the apical membrane. The schematic representation of PAR proteins in this figure does not reflect their interacting relationship. Modified based on (58) (57) (59) (60)

1.3.2.1 AP polarity establishment in *C. elegans* epidermis.

The *C. elegans* epidermis is equivalent to a thin layer of skin which acts as a structural and permeability barrier and has important functions in innate immunity, mechanosensation, endocrine and exocrine secretion and wound healing (57). The epidermis has an internal basal surface, which is covered with basement membrane, and an external apical surface covered by cuticle (57). Epidermal cells become polarised in two instances: First is the initial polarisation during the early developmental stage when non-polarised epidermal cells differentiate into polarised epithelium. Second is the formation of new junctions during epidermal morphogenesis in later developmental stage (Figure 1-2). Epidermal morphogenesis starts at a mid-embryonic stage in which the dorsal epidermal cells first intercalate with each other in a process called dorsal intercalation. These cells then migrate towards the ventral side of the animal wrapping around the ventral neurons in a process called epiboly. When these cells meet at the ventral midline, new junctions are formed between the epidermal cells in a process called ventral closure (Collectively reviewed in (61)). During epidermal morphogenesis, polarity is re-established while new junctions are formed. Therefore, the interplay between adhesion complexes and polarity determinants should be viewed as a highly dynamic process.

In *C. elegans*, unlike in *Drosophila*, neither polarity nor adhesion is affected when CCC components are lost (62), which indicates that there are redundant mechanisms involved in polarity establishment. As discussed in 1.2, PAR proteins are important polarity determinants in *C. elegans* early embryo development. PAR-3, PAR-6 are PKC-3 are all present in *C. elegans* epithelia and are localised to the apical membrane (Figure 1-2) (63) (64) (65) (66). Since these proteins are essential

for early development, experimental strategies were developed in which they were tagged with PIE-1 Zn-finger that mediates PIE-1 degradation in somatic cells in later developmental stage in order to understand their contributions for polarity determination in epithelia (67) (68) (69) (70). In the epidermis, surprisingly, neither PAR-3 nor PAR-6 is required for the correct assembly of CeAJ proteins, hence PAR-3 and PAR-6 are dispensable for polarity establishment (68) (69). However, in the absence of PAR-6, the assembled CeAJ fails to coalesce into mature junctions, indicating that it is required for maturation of the CeAJ (68). Loss of PAR-3 causes embryo elongation defects, although the ability of the CeAJ to undergo coalescence remains normal (69). The molecular mechanism underlying the role of PAR-6 in junction maturation remains to be investigated and the precise role of PAR-3 remains unclear.

Recent studies in *Drosophila* indicate that the small GTPase Cdc-42 works together with Par6 to control the trafficking of junctional proteins within cells (55) (71). Whether the role of PAR-6 in *C. elegans* junction maturation depends on CDC-42 remains to be investigated. The reason why PAR-3 and PAR-6 do not appear to be as critical in establishing polarity in epithelia of the epidermis compared with their roles in establishing early embryo polarity may be explained by the fact that unlike the single cell zygote, epithelial precursor cells are already in an intrinsically polarised environment by the time they start to become polarised (57). In *C. elegans*, the homologues of Crb CRB-1 and EAT-20 appear to be dispensable for polarity establishment although they are present at the apical membrane (72) (73) (16). However, when CRB-1 and EAT-20 are knocked down together with the basolateral protein LET-413 and alpha-catenin HMP-1, polarity is affected, indicating they have accessory roles (73) (74). The *Drosophila* basolateral complex Scribble/Discs

Large/Lethal giant larvae is essential in polarity establishment. In *C. elegans*, however, the main polarity determinant in the epidermis appears to be the basolateral protein LET-413 (66) (75). LET-413 is uniformly expressed in the early embryo but becomes localised to the basolateral membrane in differentiated epithelium (Figure 1-2A) (75). In a *let-413* mutant, CeAJ components are laterally localised and fail to coalesce into mature junctions (76) (66). The apical marker CHE-14 also appears to be mislocalised along the lateral membrane, suggesting that LET-413 maintains polarity by preventing mislocalisation of apical markers (66). The N-terminal leucine-rich repeats region of LET-413 shares similarity with a Ras-activating protein SUR-8, suggesting that LET-413 may also be controlled by small GTPases (75). Loss of either inositol-triphosphate receptor ITR-1 or inositol polyphosphate 5-phosphatase IPP-5 has been shown to partially suppress *let-413* mutations, indicating that LET-413 is calcium sensitive (77). The exact molecular mechanism for LET-413 mediated coalescence of apical junction proteins remains unclear. ITR-1 has been shown to interact with non-muscle myosin II heavy chain (NMY-2) and is required for migration of ventral epidermis during ventral closure, suggesting it may also have a role in organizing junction proteins to their proper localisations (78) (79). As mentioned earlier, polarity is re-established in later developmental stage when new junctions are formed between migrating epithelia. Such processes require an interplay between the actin cytoskeleton which drives the migration and the junction components. Indeed, early studies observed that the CCC is mobilised along protrusions formed by actin filament to prime new junction formation at the ventral midline (Figure 1-2B) (58). Regulators of actin dynamics appear to affect new junction formation as the depletion of UNC-34/Enabled, which

promotes actin polymerization, results in enhanced defects in a weak HMP-1/α-catenin mutant due to reduced actin binding activity (59) (60).

1.3.2.2 AP polarity establishment in *C. elegans* epithelial tubes.

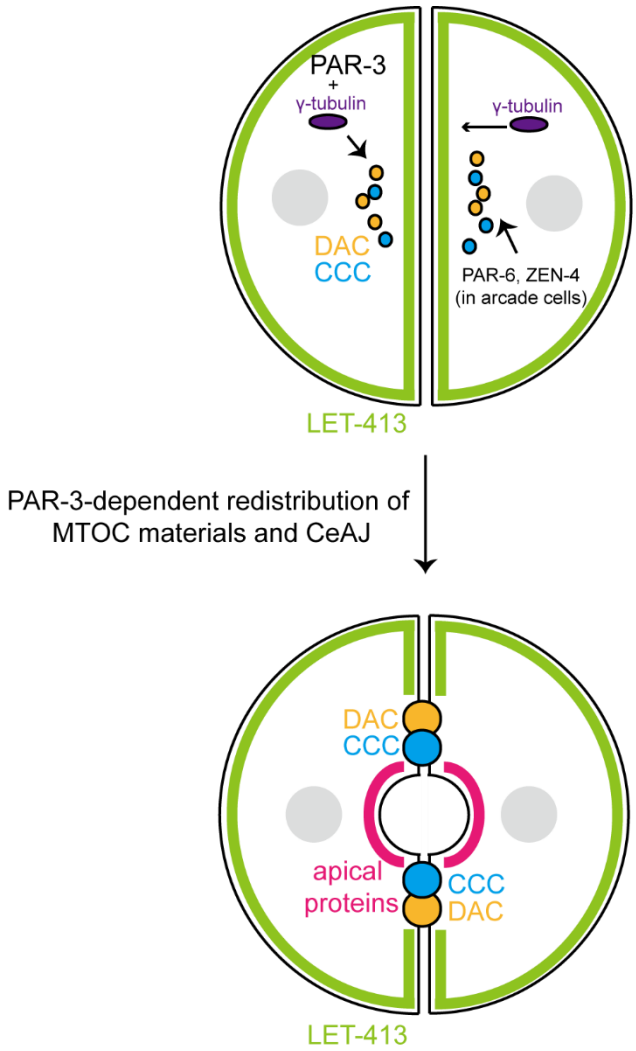

C. elegans epithelial tubes.

Figure 1-3 Polarity establishment in *C. elegans* epithelial tubes.

Polarisation of epithelial tubes, specifically in the intestine, requires handing over of MTOC materials (γ-tubulin) from close proximity of nuclei to the apical surface in a PAR-3-dependent process. In arcade cells, PAR-6 and ZEN-4 are required for polarisation. Modified based on (16)

The main epithelial tube in *C. elegans* is the intestine, it is therefore the main subject of discussion here. The intestine is one of the major organs in *C. elegans* and it is responsible for digestion of food, nutrient exchange, synthesis and storage of macromolecules (80). The *C. elegans* intestine develops from the single E blastomere cell (81) (82). The E blastomere undergoes 4-rounds of cell division to form the 16-cell intestinal primordium, which consists of two rows of cells (63). It is at this stage that the intestine precursor cells start to become polarised and change their shape to form the intestinal lumen (63).

Polarity begins to establish in intestinal epithelium when CeAJ components form puncta like structures and migrate towards the midline and start to assemble junctions (Figure 1-3) (63). PAR-3 also moves along in this process (69). PAR-3 appears to be the primary polarity determinant in this case as in the absence of PAR-3, PAR-6, PKC-3 and CCC components fail to localise to the apical domain while the basolateral markers spread around the cells (69). The mechanism by which PAR-3 determines polarity seems to be associated with the microtubule organising centre (MTOC), as the core centrosome protein γ-tubulin CeGRIP also moves apically during polarity establishment in intestinal epithelium in a PAR-3-dependent manner (Figure 1-3) (70). Furthermore, when centrosomal materials are removed by laser ablation, junctions cannot form properly (70). PAR-3 is also important in polarity establishment in other tubular epithelium. RNAi knockdown of *par-3* in larvae affects polarity in the distal spermatheca (83). Studies in arcade cells, which links the pharynx and the rostral epidermis, suggest that a complex formed during cytokinesis called centralspindlin (84), composed of the conventional kinesin ZEN-4 and the Rho GAP CYK-4, is required for the epithelization of arcade cells during their mesenchymal-epithelial transition (MET) (85) (86). CeAJ and PAR-

3/PKC-3 fail to assemble at apical membrane in *zen-4* or *cyk-4* mutants (86). A recent study showed that PAR-6 is also required for epithelial polarisation of arcade cells, as apical marker ERM-1, CeAJ components HMR-1 and AJM-1 fail to localise to apical membrane in more than 50% of mutant arcade cells (87).

1.3.3 Maintenance of epithelial polarity in *C. elegans* epidermis and epithelial tubes.

Since epithelial morphogenesis is a highly dynamic process, junctions are under constant stress when epithelial tissues are adopting different shapes. It is therefore important that there are mechanisms to maintain junctions after polarity is established in order to prevent the tears and breakage of cells (16). UNC-94/Tropomodulin, an actin pointed-end capping protein, works with HMP-1/α-catenin to maintain a continuous ring of junction. Loss of UNC-94 causes fragmented junctions and defects in the ability of the actin filament to anchor to the apical membrane (88). A mechanism is proposed in which UNC-94 stabilises long actin filaments so that they can act like a root to prevent tearing (88). Interestingly, UNC-94 is mainly expressed in lateral seam cells, even though its requirement is reflected in non-seam cells. The lack of UNC-94 detection in non-seam epithelia might be due to the highly dynamic nature of the epithelial cells (16).

In recent years, studies have identified glycosphingolipids (GSL) biosynthesis and clathrin-dependent polarised trafficking as two other processes involved in polarity maintenance (89) (90) (91). An RNAi screening looking for regulators involved in tubulogenesis identified several genes which are capable of encoding enzymes of the GSL biosynthesis pathway and it also identified the clathrin heavy chain CHC-1 and subunits of AP-1 as regulators for apical polarised transport (89) (91). Depletion of these genes caused partial loss of polarity, which is

indicated by mislocalisation of apical proteins such as PAR-6, formation of lateral lumens at later developmental stage, and loss of RAB-11^{+} recycling endosomes (89) (90) (91). Interestingly, a recent study has linked the polarity protein PAR-5 to the RAB-11^{+} recycling endosome. Depletion of *par-5* by RNAi in *C. elegans* larvae causes the normally apically localised RAB-11+ endosomes to localise to the basolateral domain in the larval intestine in a process requiring kinesin-1 and actin regulators (92). Since the combined effect of losing components in the GSL pathway and the clathrin-dependent pathway is stronger than when each is affected individually, it has been proposed that AP-1/Clathrin act in a direct apical sorting pathway together with a sphingolipid-dependent sorting pathway (91). The link between these pathways and RAB-11 suggests that they might work towards the recycling endosomes to maintain polarity (16).

A separate trafficking pathway has also been shown to be important in maintaining the positions of CeAJ in the intestinal lumen, which involves actin regulator Arp2/3 complex, TOCA1/2, is a Cdc-42 small GTPase effector, and apical marker ERM-1 (93) (94) (95) (96). Loss of these components cause reduction of the DAC complex, polarity defects, a reduced level of F-actin accumulation at the apical domain, and a wider intestinal lumen (93) (94) (95) (96). Studies in *Drosophila* indicate that the TOCA-1 homologue CIP4 works together with polarity regulators Cdc42/Par6 to control endocytosis of E-cadherin (97). Therefore, dissecting the relationship between these components and intestinal endocytosis is key to understanding the polarity maintenance process. TOCAs can bind to the WAVE complex to activate the ARP2/3 complex (94). When WAVE is depleted, the apical DAC is reduced while apical ERM-1 levels are increased, resulting in a wider lumen (95) (96). Consistent with this finding, when ERM-1 is depleted, the intestinal lumen

also narrows (95), indicating that WAVE, TOCA1/2 and Arp2/3 together act as negative regulators of the apical marker ERM-1 in an endocytosis-dependent manner.

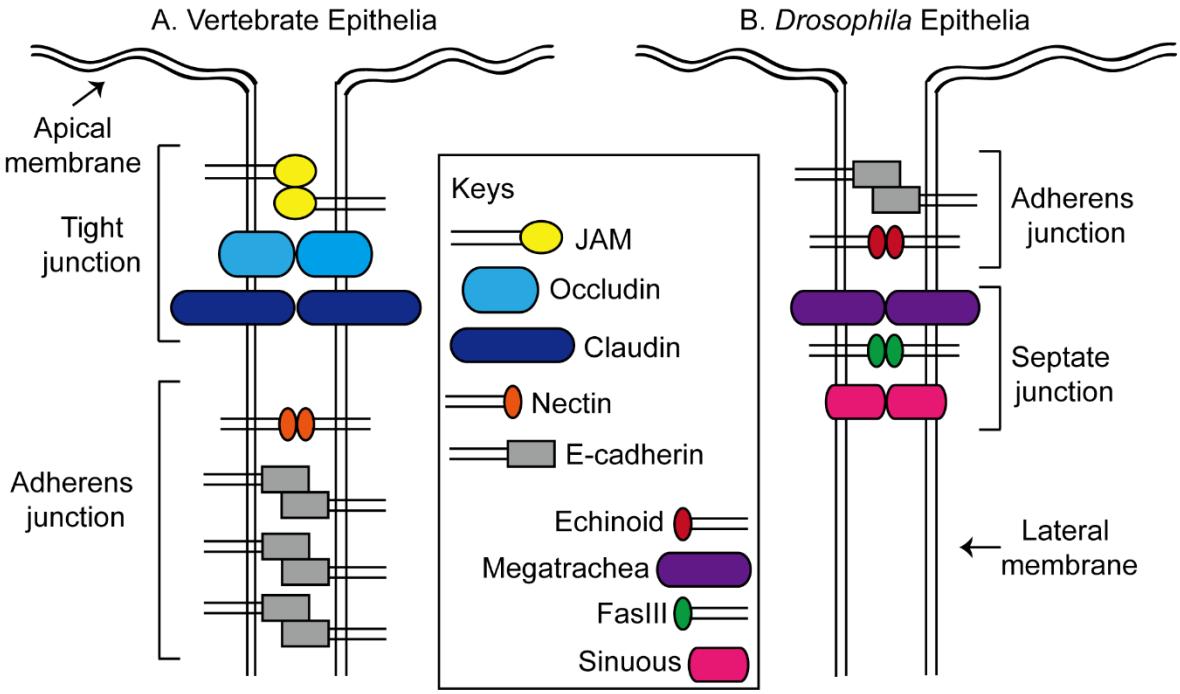

Figure 1-4 Organisation of junctional adhesion complexes in vertebrate and *Drosophila* epithelia

A. At vertebrate epithelial junction, tight junctions composed of JAMs (junctional adhesion molecules), Occludins and Claudins are localised to the apical domain of epithelia. Adherens junctions made of Nectin and E-cadherins are localised to the lateral membrane domains. **B.** At *Drosophila* epithelial junctions, adherens junctions made of E-cadherins and Nectins equivalent Echinoid are localised to the apical membrane domain. Tight junctions equivalent septate junctions composed of Megatrachea, FasIII and Sinuous are localised slightly basolateral to the adherens junctions. Intracellular interacting partners are omitted from the figure for simplicity purpose. Modified based on (98)

1.4 *C. elegans* apical junctions (CeAJ) structure and functions.

Epithelial cells differ from other polarised cells in that they have specialised junctions between neighbouring cells, which are essential for the organization of epithelial tissues, maintaining epithelial polarity (as discussed in the previous section) and downstream signalling transduction as they form a hub to mediate protein-protein interactions (99). In vertebrate and *Drosophila* epithelia, two electron-dense complexes can be detected by transmission electron microscopy at the epithelial junctions: tight junction (also known as ZO, short for *zonula occludens*) and adherens junctions (also known as ZA, short for *zonula adherens*) in vertebrates; adherens and septate junctions in *Drosophila* (100) (Figure 1-4).

In vertebrate epithelia, tight junctions are comprised of the adhesion molecules Occludins, Junctional Adhesion Molecules (JAM) and Claudins; together these proteins act as the paracellular gate to prevent mixing of proteins between the apical and basolateral membrane domains (101). Tight junctions are localised to the apical membrane (101). Adherens junctions are localised along the lateral membrane domain and contain the homophilic adhesion molecule E-cadherin and its interacting components α-catenin and β-catenin (99). Along the lateral membrane domain, nectins and their intracellular adaptor proteins Afadin/AF-6 form a second group of homophillic adhesion complexes (102) (Figure 1-4A).

In *Drosophila* epithelia, by contrast, adherens junctions containing homophilic adhesion Cadherin-Catenin complex and the Nectin complex equivalent Echinoid-Canoe complex are localised to the apical membrane domain, whereas septate junctions, the tight junctions equivalent, contain the transmembrane components Megatrachea, FasIII and Sinuous, and are located more basolaterally (103) (Figure 1-4B).

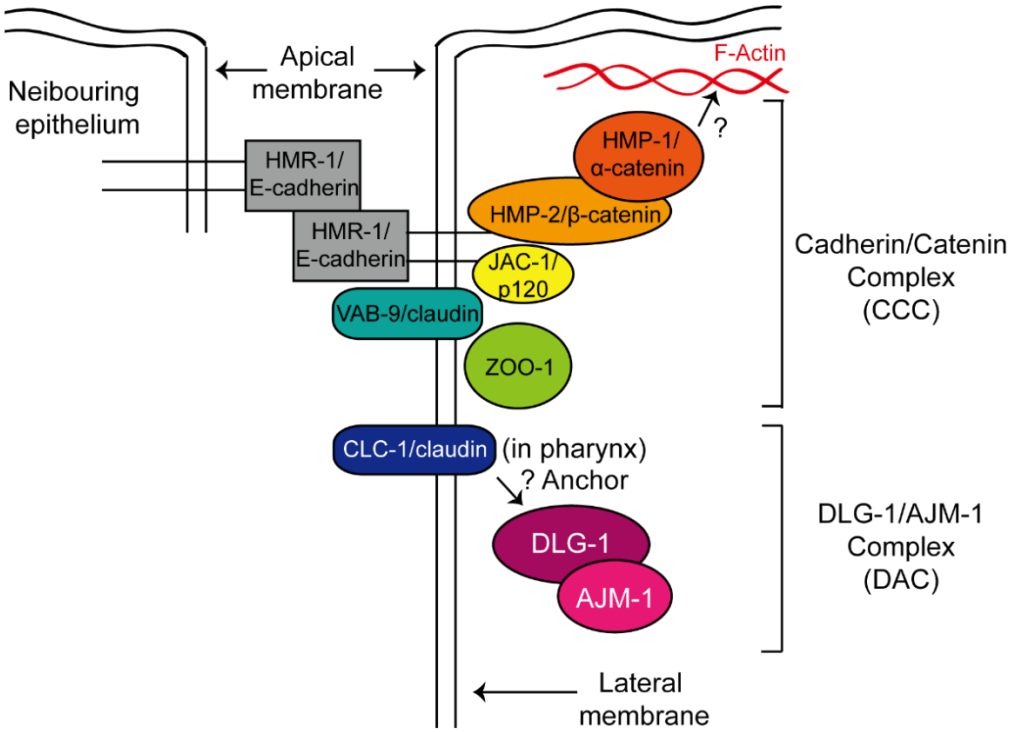

Figure 1-5 Organisation of junctional adhesion complexes in *C. elegans* epithelia.

C. elegans apical junction (CeAJ) is made up of two complexes namely Cadherin/Catenin Complex (CCC) and DLG-1/AJM-1 Complex (DAC). CCC contains the E-cadherin homologue HMR-1 which is possibly capable of forming homophilic bond with neighbouring HMR-1/E-cadherin through its extracellular domain (details see text). HMR-1/E-cadherin recruits the classic HMP-2/β-catenin and HMP-1/α-catenin contains HMP-2/β-catenin and actin binding domain. HMP-1/α-catenin contains HMP-2/β-catenin and actin binding domains and is important in anchoring F-actin to the apical membrane, however the exact mechanism of F-actin binding remains unknown. HMR-1/E-cadherin can also recruit the p120 homologue JAC-1 to the juxta membrane space. There are two *C. elegans*-specific CCC components, claudin homologue VAB-9 and MAGuK homologue ZOO-1. DAC contains the *Drosophila* Discs large homologue DLG-1 and its interacting nematode-specific coiled-coil protein AJM-1. It is still unknown how DLG-1/AJM-1 are anchored to the membrane however in *C. elegans* pharynx, a claudin homologue CLC-1 might confer this function. SMAC complex is not included in the figure as its localisation is still debatable. Only one side of the junctional complexes were depicted in the figure for simplicity purpose. Modified based on (16)

In *C. elegans*, however, only one single electron-dense complex was observed by transmission electron microscopy (14). Despite this observation, there are actually two functionally distinctive complexes present in CeAJ - CCC (Catenin/Cadherin Complex) and DAC (DLG-1/AJM-1 Complex) (104). CCC is localised closer to the apical membrane of *C. elegans* epithelia whereas the localisation of DAC is slightly more basolateral (Figure 1-5), and is more similar in organization to the *Drosophila* AJ (16). Therefore, CCC and DAC together adopt the roles for adhesion and paracellular gate function of their vertebrate and *Drosophila* counterparts (16).

Major CCC components, including a classic E-cadherin homologue HMR-1, and two classic catenin homologues HMP-1/α-catenin and HMP-2/β-catenin were all identified initially through genetic screen for embryonic morphogenetic defects (62). The molecular properties of HMR-1/E-cadherin, HMP-1/ α-catenin and HMP-2/β-catenin are essentially similar to their vertebrate and *Drosophila* homologues, but they also have worm-specific features (104). HMR-1/E-cadherin is a transmembrane protein, which is possibly capable of forming homophillic bonds with neighbouring cadherin through its extracellular domain in a Ca^{2+}-dependent manner based on studies of the *Drosophila* counterpart Shotgun/E-cadherin (105) (106) and is capable of interacting via its cytoplasmic tail with HMP-2/β-catenin, and JAC-1, the only p-120 homologue in *C. elegans* (107) (108). HMP-2/β-catenin co-localises with HMR-1/E-cadherin in early blastomeres and at CeAJ (62). The loss of HMR-1/E-cadherin causes redistribution of HMP-2/β-catenin in the cytoplasm (62). HMP-1/α-catenin co-localises with HMR-1/E-cadherin and HMP-2/β-catenin and requires both proteins for its proper localisation (62). Biochemical analysis has revealed that HMP-1 is a bona fide α-catenin with a C-terminal actin binding domain and also a

HMP-2/β-catenin binding domain (108). However, unlike vertebrate α-catenin, *C. elegans* HMP-1/α-catenin cannot form detectable homodimers *in vitro* and despite having an actin binding domain, does not bind actin *in vitro* (108) (109). It was further revealed that HMP-1/α-catenin actin binding domain is auto-inhibitory, and it may require other proteins for its actin binding function (108). Interestingly, removal of either F-actin binding domain or HMP-2/β-catenin binding domain disrupts *C. elegans* development, which means HMP-1 must somehow be able to bind with F-actin and HMP-2/β-catenin *in vivo* (108). HMP-1/α-catenin also does not recruit actin binding protein vinculin, which is absent in *C. elegans.* In vertebrates, vinculin binds to α-catenin in a force-dependent manner (108) (110). HMP-2 is one of the four *C. elegans* β-catenin homologues with functions largely in cell adhesion, although like its vertebrates counterpart, recent studies have linked HMP-2 to the Wnt signalling pathway during early embryonic cell fate specification (111) (112). The *C. elegans* JAC-1 is the only p120 homologue that co-localises with the cadherin-catenin complex during elongation (107). Unlike vertebrate p120, which is required for stabilization of E-cadherin, loss of JAC-1/p120 causes only mild HMR-1/E-cadherin defects and does not affect *C. elegans* epithelial development (107). However, depletion of JAC-1 in a weak *hmr-1* mutant causes morphogenetic defects, indicating it has a supporting role in adhesion (107). The CCC contains two other proteins that are unique to *C. elegans*: VAB-9 and ZOO-1. VAB-9 is a distant tight junction molecule claudin superfamily member and is closest to human brain cell membrane protein 1 (BCMP1) (113) (114). VAB-9 requires HMR-1/E-cadherin for its proper localisation and co-localises with the cadherin-catenin complex (114). *vab-9* mutants exhibit morphogenetic defects in the epidermis during elongation and mutations in *vab-9* enhance the mutant phenotypes caused by AJ proteins loss,

indicating that *vab-9* might work downstream of *hmr-1* to maintain adhesion (114). ZOO-1 is a homologue of the *zonula occludens* membrane-associated guanylate kinase (MAGuK) protein and its recruitment to CCC requires VAB-9 (115). ZOO-1 co-localises with VAB-9 and other CCC components and requires HMR-1/E-cadherin and VAB-9 for its proper localisation (115). *zoo-1* RNAi knockdown shows similar defects to *vab-9* mutations and enhances weak *hmp-1* and *hmp-2* mutant phenotypes. However, *zoo-1*(RNAi) does not enhance the phenotype of a *vab-9* null mutant, indicating that *zoo-1* most likely functions downstream of *vab-9* in cell adhesion (115). Although VAB-9 and ZOO-1 appear to be related to vertebrate tight junction components, they are not essential for paracellular gate function (114) (115). As mentioned in section 1.3.2, mutations in any single CCC component does not affect polarity nor adhesion during early epidermis and intestine development (62), however, they appear to have more significant roles during ventral closure, when new junctions are formed between migrating epithelia as mutations in *hmr-1*, *hmp-1* and *hmp-2* in ventral epithelia cause no junction formation even though cells are able to migrate towards the ventral midline .

The DAC is defined by two main protein components, a membrane-associated *Drosophila* MAGuK homologue scaffolding protein DLG-1 and a coiled-coil protein AJM-1 which is nematode-specific (64) (116) (65) (66). Removal of DLG-1 causes the single electron dense complex to disappear and immuno-gold staining experiments placed AJM-1 at the electron dense area while removal of AJM-1 causes bubble-like separations between junctions, indicating they correspond to the single electron dense complex observed (65) (66). These two proteins interact *in vitro* and are dependent on each other for proper localisation *in vivo* since AJM-1 becomes puncta-like in the absence of DLG-1 (65) (66) (74). DLG-1 shares strong

similarity with the *Drosohphila* Discs large, which is required for septate junction formation (16). Large vacuoles are detected in *ajm-1* and *dlg-1* mutants, suggesting defects in the paracellular gate function, indicating that AJM-1 and DLG-1 could perform the role of a septate junction (65). It is still unclear how AJM-1 and DLG-1 are anchored to the membrane, but recent studies showed that the *C. elegans* claudin homologues CLC-1 or CLC-2 are needed in the pharynx for the paracellular gate function, because a low molecular weight fluorescent dye is able to diffuse freely between pharyngeal cells when CLC-1 levels are reduced (117). Also, CLC-1 co-localises with AJM-1 in the pharynx (117). Therefore CLC-1 is likely to be the anchor for AJM-1 and DLG-1 in the pharynx, although there is no direct evidence to support this hypothesis (117). The DAC appears to be dispensable for epithelial adhesion as loss of AJM-1/DLG-1 does not cause major adhesion defects (65) (66). However, when CCC components and DAC components are removed at the same time, CeAJ can no longer be maintained causing cells to round up, suggesting they work together in maintaining cell adhesion (114) (74).

Apart from CCC and DAC, a third potential CeAJ complex has emerged through recent studies, which is composed of SAX-7, a transmembrane L1CAM homologue, MAGI-1, another MAGuK homologue and AFD-1, an Afadin homologue (118) (119). SAX-7 localises to epithelial cell-cell junction and mutations in *sax-7* result in highly penetrant adhesion defects (119). SAX-7 interacts with both MAGI-1 and AFD-1, which makes it the transmembrane anchor of this potential complex. MAGI-1 also localises to the apical domain of epithelia (119). Mutations in *sax-7* and *magi-1* can both enhance the mutant phenotypes of the other CeAJ components, indicating they could act as a third adhesion complex in mediating adhesion between epithelial cells (118) (119). The role of the SAX-7/MAGI-1/AFD-1 complex

(SMAC) has been proposed to maintain the separation between CCC and DAC, because loss of MAGI-1 causes the CCC and DAC to overlap (119). However, the exact location of the SMAC is still debated (118) (119).

1.5 *C. elegans* hemidesmosome (CeHD) structure and functions compared with its mammalian equivalent.

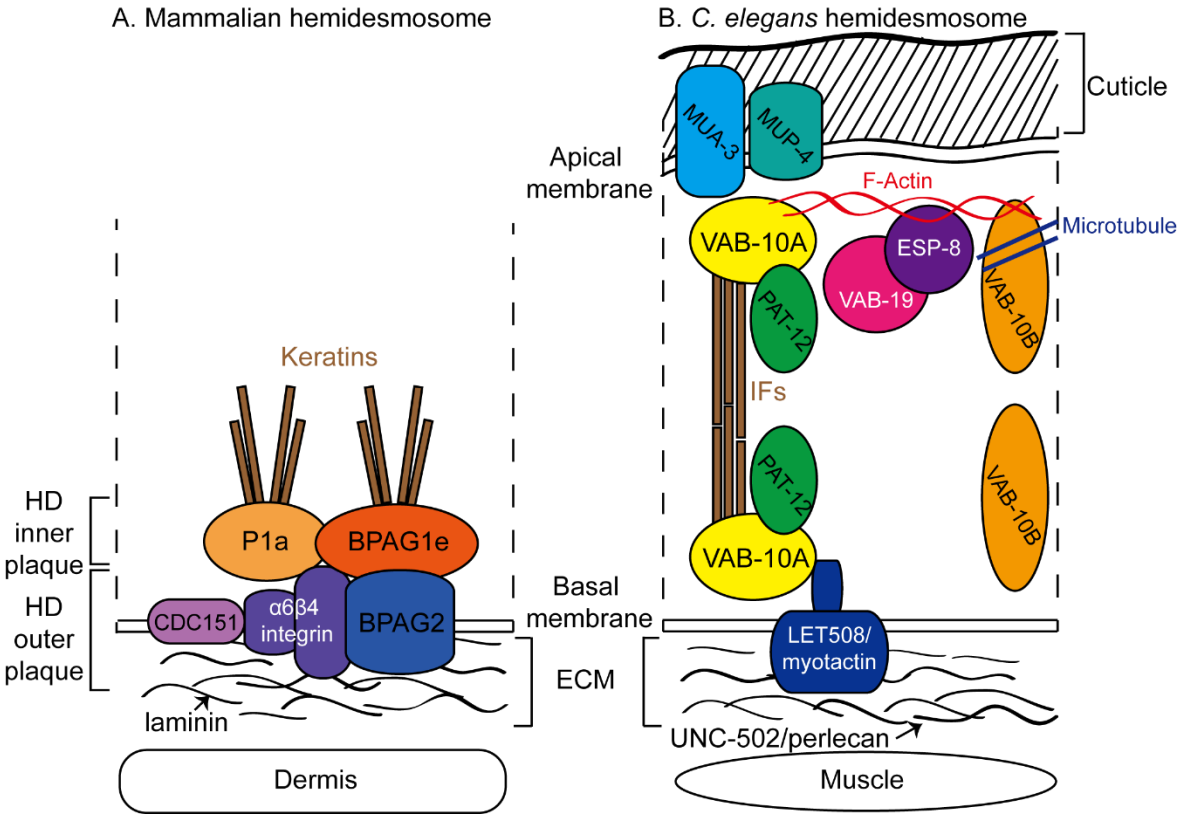

Figure 1-6 Organisation of hemidesmosome complexes in mammalian and *C. elegans* epithelia.

A. Mammalian hemidesmosome I (HD I) are made of two HD plaques namely the HD inner plaque which contains plectin P1a and BPAG1e, which interact with mammalian IF keratins, and the HD outer plaque which contains transmembrane proteins CDC515, α6β4 integrin and BPAG2. α6β4 integrin can interact with laminin in the extracellular matrix (ECM). Mammalian HDs are found exclusively adjacent to the basal membrane and link the basal epidermis and the dermis underneath through ECM. **B.** *C. elegans* hemidesmosomes (CeHD) contain core component VAB-10A, a plectin and BPAG1e homologue which is capable of organising IFs possibly through the help of a nematode-specific protein PAT-12. VAB-10A contains actin binding domain so it could interact with F-actin to stablise the CeHD. CeHDs extend from the apical membrane to the basal membrane. At the apical membrane, VAB-10A is likely anchored by transmembrane proteins MUA-3/MUP-4 whereas at the basal membrane it is likely anchored by transmembrane protein

LET508/myotactin. In the ECM LET508/myotactin interacts with UNC-52/perlecan. There are two additional CeHD components which are VAB-19, an ankryin repeat-containing protein, and ESP-8, an actin-capping protein which is capable of binding to VAB-19. Another VAB-10 isoform VAB-10B, which has no overlapping function with VAB-10A is thought to maintain the CeHDs possibly through interactins with F-actin since it also contains actin binding domain and also with MT binding domain. CeHD links the epidermis to the cuticle on the apical side and to the muscles on the basal side. Modified from (120)

Adhesion complexes at cellular junctions maintain strong contacts between neighbouring epithelial cells. Within epithelia, an adhesion complex called the hemidesmosome (HD) links epithelia to the extracellular matrix (ECM) (121). HDs are essential structures in epithelial tissues, such as the epidermis and the intestine, because they provide mechanical resistance and also act to transduce mechanical signals (121). Defects in hemidesmosomes can result in diseases such as skin blistering epidermolysis bullosa (EB), carcinoma invasion and defects in wound-healing (122) (123) (124). Mammalian basal epidermal HDs, usually referred to as type I HDs (125), contain 5 main components, α6β4 integrin, plectin isoform 1a (P1a), tetraspanin CD151, bullous pemphigoid antigen (BPAG) 1e and BPAG2 (126). Together α6β4 integrin, CDC151 and BPAG2 form a transmembrane outer complex called HD outer plaque that links to the HD inner plaque composed of P1a and BPAG1e at intracellular juxtamembrane space (Figure 1-6A) (127). The HD outer plaque, specifically α6β4 integrin, binds to laminin in the ECM (128) while HD inner plaque associates with intermediate filament (IF) cytoskeleton assembled from keratins K5 and K14 (127). Together this transmembrane complex helps to maintain the integrity of epithelial tissues (121).

In *C. elegans*, a similar structure exists which acts as an *in vivo* model. The bulk of knowledge about mammalian HD comes from in vitro studies using keratinocyte cell cultures (127). This structure was originally called the fibrous organelle (FO). However, because it is composed of similar molecular components and because it shares ultrastructural and functional similarities with the mammalian HD, it is now referred to as the *C. elegans* hemidesmosome (CeHD) (23). CeHDs were detected by transmission electron microscopy as regularly spaced electron densities throughout apical and basal membranes of dorsal and ventral epidermis

(129). Unlike mammalian type I HD which is localised to the basal membrane, CeHD has two HD facing structures, which extend from the apical membrane of the epithelia to the basal membrane (Figure 1-6B) (129). The core component of the CeHD is VAB-10A, a plakin family member homologous to both P1a and BPAG1e (129). *vab-10* mutants were identified in genetic screens for embryonic morphogenetic defects and VAB-10A is one of the two major isoforms encoded by the *vab-10* gene (129). VAB-10A is functionally similar to P1a and BPAG1e, because it co-localises with IFs and contains a putative IF-binding domain (129). Loss of VAB-10A causes IF bundling and detachment of muscle from the epidermis, suggesting it plays a role in anchoring IFs and maintaining epidermis-muscle attachments (129). VAB-10A appears to be the essential component in CeHD assembly, because loss of VAB-10A prevents other CeHD components from anchoring to their appropriate locations (129). VAB-10A also contains an actin binding domain, which has been demonstrated to bind actin autonomously *in vivo* (Figure 1-7). Hence, VAB-10A might function in stabilizing CeHDs by interacting with F-actin (Figure 1-6B) (129).

The keratin cytoskeleton equivalents in *C. elegans* are the IFB-1/IFA-3 and IFB-1/IFA-2 intermediate filaments (130). The apical membrane anchor of VAB-10A is likely to be the transmembrane proteins MUA-3 and MUP-4 (131) (132), and the basal membrane anchor is predicted to be LET-508/myotactin (133). MUA-3 and MUP-4 are single transmembrane proteins which are weakly homologous to the vertebrate tendon components named matrilins (131) (132). LET-508/myotactin is a large single transmembrane protein, which has the potential to physically interact with the muscle membrane through the ECM (133). LET-508 appears to be as essential to CeHD integrity as VAB-10A, because depletion of LET-508 also results

in detachment of muscle from epidermis (133). The two transmembrane complexes formed at apical and basal membranes of the epithelia are linked together through IFs, which establish the two HD facing structures (Figure 1-6B) (23). On the apical side, CeHD links the dorsal and ventral epidermis to the cuticle ECM through a yet unknown molecule(s). On the basal side, CeHD links the epidermis to the muscle-epidermis interface ECM protein UNC-52, which is a perlecan homologue (134). Additional CeHD components have been identified in recent years. VAB-19, an ankyrin repeat-containing protein homologous to the mammalian tumor suppressor Kant, co-localises with CeHD components (135). VAB-19 is crucial during CeHD re-organization as remodelling of CeHD becomes defective in cryo-sensitive *vab-19* mutants (135). A VAB-19 binding partner ESP-8, which is an actin-capping protein, was identified in yeast-two hybrid screening (136). Imaging studies in pharyngeal marginal cells have provided evidence that VAB-19 and ESP-8 are likely to associate primarily with apical side of CeHD , although the the nature of their attachment to the CeHD remains unknown (136).

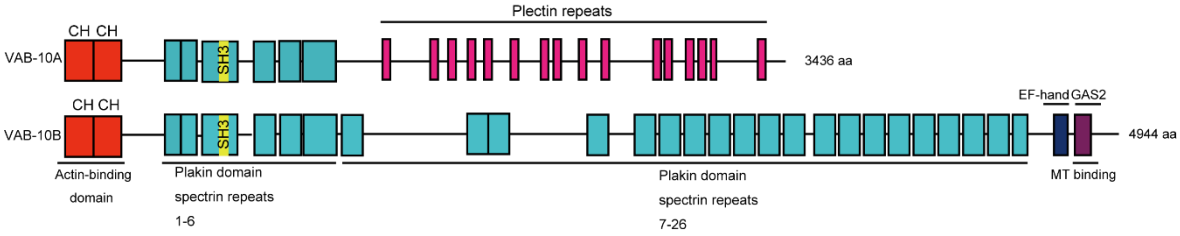

Figure 1-7 Schematic diagram of the VAB-10A and VAB-10B isoforms.

The common region of the two proteins encodes two CH (calpin homology) domains, which are predicted to bind actin. Also common between the two isoforms are 6 spectrin repeats with the third one containing SH3 domain (yellow). VAB-10A specific region contain 16 plectin repeats. VAB-10B specific region contains 20 spectrin repeats, EF-hand and a GAS2 domain which is capable of MT binding. Modified based on (137)

The nematode-specific protein PAT-12, which was identified through a yeast-two hybrid screen, is another protein that has been shown to interact directly with the VAB-10 central common region (VAB-10A and VAB-10B) (138). It was proposed that maintenance of CeHD depends on VAB-10B, the other major isoform encoded by the *vab-10* gene. Loss of VAB-10B causes progressive loss of CeHD (129). VAB-10B is a vertebrate microtubule actin cross-linking factor (MACF) homologue, which shares no overlapping function with the CeHD core component VAB-10A, despite being encoded by the same gene (129) (Figure 1-7). Antibodies have been raised that have led to detecting VAB-10B in the dorsal and ventral epidermis, pharynx, intestine and muscle (16). VAB-10B contain both actin and microtubule binding domains and is speculated to maintain the CeHD by interacting with these cytoskeletal components (137). A *vab-10b* specific mutation causes defects in intestinal lumen and muscle fibre organisation (129). VAB-10B has also been implicated in playing roles in nonepithelial cells because a unique nonsense mutation was identified that caused defects in distal tip cell (DTC) migration (139). Other ECM proteins with important roles in maintaining the CeHD, include the F-spondin homologue SPON-1 and PXN-2. Loss of SPON-1 causes muscle detachment from the epidermis during embryonic elongation (140), and the ECM-modifying enzyme peroxidasin homologue PXN-2 is essential for muscle-epidermis attachment during embryonic development (141). Laminin might also be required because a mutation in a α-laminin subunit causes cell adhesion defects (142).

Just as the CeAJ undergoes remodelling during morphogenetic processes, such as ventral closure, the CeHD also undergoes remodelling and reorganisation during epidermal morphogenesis. During elongation of the worm, a bean shaped embryo is extended into a four-fold worm shaped larva. Elongation of the *C. elegans*

embryo beyond the two-fold stage requires input from muscle. The CeHD is likely to be the mediator because remodelling of the CeHD fails in strong muscle mutants (21). Indeed, recent genetic screens have identified genes required for CeHD maturation during elongation, which also function in a mechanical signalling pathway (120). In this pathway, muscle twitching is sensed by a yet unidentified CeHD component, and is transduced into a biochemical signalling pathway involving the Rac-Guanine exchange factor PIX-1, its adaptor protein GIT-1, and the p21-activating kinase PAK-1 (21). It was proposed that PAK-1 might phosphorylate IFA-3 directly or indirectly through additional pathway to promote recruitment of IFA-3 to CeHD (21). Mutations in any of the components in this pathway combined with a weak *vab-10a* mutation causes IFA-3 recruitment defects (21). CeHD remodelling also depends on other factors, including the relative level of CeHD proteins, specifically LET-805/myotactin and UNC-52/perlecan. Increasing LET-805/myotactin levels while decreasing UNC-52/perlecan levels in a weak *vab-10a* mutant also causes disruption to the CeHD ultrastructure and the rate of elongation. It was further observed that CeHD defects are partially suppressed in animals with elongation defects.

1.6 Cytoskeleton dynamics during *C. elegans* epithelial morphogenesis

The cytoskeleton is the basic building blocks of all cells. In epithelial cells, they not only contribute to structural integrity but their ability to constantly assemble and disassemble help to regulate important cellular processes such as cell migration, trafficking and positioning of organelles (16). The previous sections have focused on the basic features of epithelial cells such as AP polarity, the structure of the adhesion complexes, and the dynamic nature of these features during epithelial morphogenesis. However, the way in which epithelial cells achieve dynamic

changes of polarity and adhesion crucially depends on the interplay between the protein complexes discussed previously with the cytoskeleton (16) with cytoskeletal regulators being the master orchestrators behind the scene.

1.6.1 Role of the actomyosin network during *C. elegans* embryonic ventral closure and elongation

A *C. elegans* embryo develops from a bean shaped stage (usually referred to as the 'lima bean' stage), and elongates to four times its initial length while reducing its initial circumference twice to form a worm shaped larva, the worm then hatches and enters the L1 larval stage (143). After gastrulation, neuroblasts move to close the cleft caused by the ingression of precursor cells, which form internal tissues such as body wall muscles and later the pharynx and the intestine, and become the underlying substrate for the migrating ventral epidermis (82). Actin in migrating ventral epidermal cells form protrusions of filopodia and along with them bring the junctional proteins towards the edge of cells in order to establish new junctions at the ventral midline during ventral closure (58). After the ventral epidermis is sealed and the embryo becomes the lima bean stage, it then goes through elongation along the anterior-posterior axis, during which time the embryo changes into a long worm shape without changing cell number (143) (82). This change of shape is mainly achieved by the driving force provided by the subcellular cortex localised actomyosin network in the *C. elegans* epidermis consisting of actin, non-muscle myosin II and also the junction complexes, which help to anchor the actomyosin network to the subcellular cortex of the epidermis (Figure 1-8) (16). The roles of actin and the actomyosin network and their regulators during epithelial morphogenesis differ in ventral closure and in elongation.

Elongation after the 2-fold stage requires the cytoskeleton in the dorsal and ventral epidermis together with the underlying muscle fibres with the CeHD linking these two tissues and possibly transducing contraction forces from the body wall muscle to the epidermis (Figure 1-8) (144).

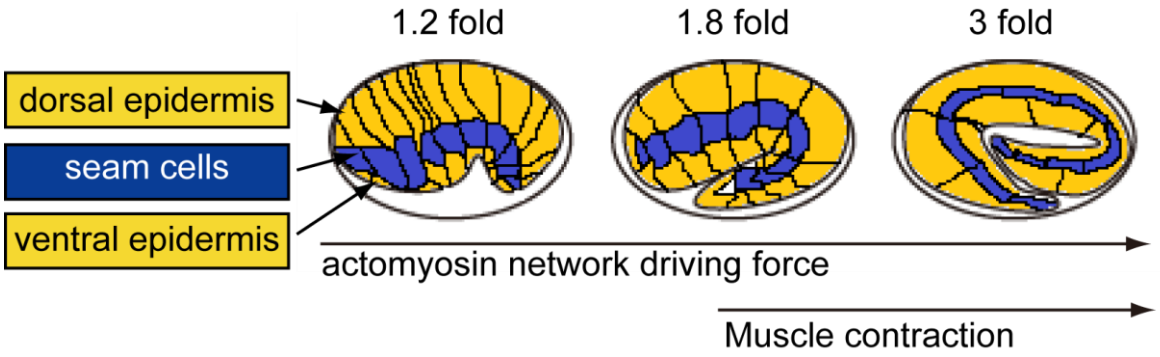

Figure 1-8 Schematic showing changes of dorsal ventral and lateral epidermis during elongation.

The actomyosin network is the main driving force before the 2-fold stage. After the 2-fold stage, muscle contraction is essential for elongation to take place. Modified based on (145)

Actin is important for ventral closure during early embryonic development, as cytochalasin D blocks ventral closure by disrupting the actin in the two leading anterior ventral epidermal cells (146). Laser ablation experiments in which these two cells are disrupted causes ventral closure failure as well, suggesting these cells are essential for the initiation stage of enclosure (146). Laser ablation of a large number of the posterior ventral cells also causes defects in enclosure (146).

Guidance cues in neuroblasts activate ligand binding receptors in the membrane of the leading ventral epidermal cells including UNC-40/Netrin receptor, SAX-3/Slit receptor and VAB-1/Ephrin receptor (147). UNC-40 activates the small GTPase Rac CED-10 (147), which then activates the Arp2/3 complex likely through the Wave/Scar protein GEX-1/WVE-1 to promote the polymerization of actin (148). CED-10 is localised to the cortex of the epidermal cells close to the CeAJ, and a *ced-10* mutant mother produces progeny that are largely unable to go through ventral closure (148). SAX-3 promotes the assembly of the Scar/Wave and the Arp2/3 complexes, leading to accumulation of branched actin at the ventral epidermis (147). The ephrin receptor VAB-1 controls the subcellular localisation of the Scar/Wave complex (147). Mutations affecting these receptors result in embryos that undergo normal ventral closure, but rupture during elongation (147).

Other proteins that are important in controlling actin dynamics during ventral closure include the WASP family proteins WSP-1 and UNC-34/Enabled. Simultaneous loss of WSP-1 and UNC-34 results in ventral closure defects; both proteins are likely to exert their effect on the Arp2/3 complex to indirectly control the polymerisation of the actin filaments at the leading edge of epidermal cells (59). Mutations affecting Scar/Wave or Arp2/3 complex components cause a reduction in the accumulation of actin at the ventral end of the epidermis and a failure to initiate

migration (149) (93) (147). After the two leading ventral cells migrate towards each other and establish new junctions between them, an actin-rich border is established in the posterior ventral cells, which form a ‘ventral pocket’ (146). Coordinated contraction in the ventral pocket formed by the posterior epidermal cells encloses the posterior part of the embryo possibly through a purse-string mechanism mediated by actin filaments (146). It is not yet known how the enclosure of the posterior part is achieved, although NMY-2 (non-muscle myosin II heavy chain 2) is enriched at the border of the ventral pocket cells and is also detected in the underlying neuroblasts (150). It seems that maintaining distance between migratory ventral epidermal cells is also important, because mutations affecting secreted MAB-20/Semaphorin, which in other systems normally mediate repulsive guidance cues, causes ectopic contacts to be formed between migratory posterior ventral epidermal cells (151).

After the bean shaped embryo is formed, the epidermis provides the main driving force for elongation before the 2-fold stage, involving both actin and microtubule dynamics (62, 143, 146, 152). Embryos treated with cytochalasin D stop elongation reversibly, indicating that actin plays a crucial role for elongation (143). Actin forms highly organised circumferential F-actin bundles (CFB), which are found in the dorsal, ventral and lateral epidermis subcellular cortex and tightly anchored to the CeAJ in dorsal and ventral epidermis (62). In the lateral epidermis (seam cells) CFBs are also present, but appear disordered and not as tightly anchored to the CeAJ (153). The mechanism by which F-actin achieves the circumferential bundling arrangement in the dorsal and ventral epidermis is not yet understood. Actin appears unordered before and after elongation, so CFBs only form transiently (62). The force required for contraction is generated by the CFBs and associated non-

muscle myosin II motors through hydrolysis of ATP in the lateral epidermis (154). This force is transmitted to the dorsal and ventral epidermis possibly through the CFBs and CeAJ (154). Non-muscle myosin II in *C. elegans* is composed of two heavy chains NMY-1 and NMY-2, which have partially redundant functions (155). NMY-2 is a crucial player during early embryonic polarity establishment and also for cytokinesis (31). While phosphorylation of myosin heavy chains of nonmuscle myosin II regulate actomyosin contraction in mammals, they appear less essential for *C. elegans* epithelial actin dynamics (155). There are two regulatory myosin light chains MLC-4 and MLC-5 which have phosphorylation sites upon which small GTPases phosphorylate and control the contractility (153). Regulatory light chains control actomyosin contractions by keeping the non-muscle myosin II motors in a closed confirmation (inactive) when they are not phosphorylated and in functional (active) confirmation upon phosphorylation (153). A Rho-binding kinase LET-502 and a myosin phosphatase MEL-11 act antagonistically on the regulatory light chains of non-muscle myosin II motors to control the contraction process (153, 156). Loss of LET-502 results in elongation defects whereas loss of MEL-11 results in rupture of embryos due to hypertension (156). Null mutants of *let-502* and *mel-11* suppress each other (156), hence LET-502 promotes contraction whereas MEL-11 promotes relaxation (156). The target for MEL-11 and LET-502 is MLC-4, one of the regulatory myosin light chain in the non-muscle myosin II complex (153). MLC-4 is mainly detected in the lateral epidermis (seam cells) during elongation. Phosphorylation of MLC-4/regulatory myosin light chain is essential for elongation, as a mutated version which was unable to be phosphorylated failed to rescue *mlc-4* mutants having elongation defects (153). Two other kinases also act in parallel to LET-502, the p21-activated kinase homologue PAK-1 and the myotonic dystrophy

kinase-related Cdc42-binding kinase homolog MRCK-1. Genetic analysis revealed that PAK-1 acts in parallel with LET-502 whereas MRCK-1 is more likely to acts upstream of LET-502 (153).

1.6.2 Anchoring of actin filaments to junction complexes during *C. elegans* ventral closure and elongation.

Since the epidermis is under tension during ventral closure and elongation, actin filaments need to be properly anchored to the CeAJ and CeHD to maintain the shape of epithelial cells (16). Several CeAJ and CeHD components are essential for actin anchoring: Loss of maternal and zygotic HMP-1 causes severe enclosure failure while mutations in zygotic *hmp*-1(encodes α-catenin/HMP-1) and *hmp-2* (encodes β-catenin/HMP-2) cause elongation defects in which embryos undergo enclosure but form abnormal bulges while elongating (62). CFBs also become visibly detached from the junctions in these mutants (62). In a weak *hmp-1* mutant, loss of other CCC components JAC-1/p120, UNC-94/tropomodulin, actin capping protein, and the junction proteins VAB-9/claudin, ZOO-1 and the SMAC component MAGI-1 all enhance the elongation defects, suggesting that they are important in anchoring F-actin (107) (88) (114) (119) (115). The CeHD components required for maintaining the CFB include actin binding proteins VAB-10 (both A and B isoforms) and ESP-8 (129) . Apical protein ERM-1 appears to be essential for the anchoring of actin in the intestine epithelia together with spectrin SMA-1/β_H-spectrin (157) (158). ERM-1 is important in maintaining apicobasal polarity in the intestine as *erm-1*(RNAi) depletion causes extreme narrowing of the intestine lumen, which is possibly due to a failure of actin anchoring so the intestinal lumen has lost its shape (158).

1.6.3 Function of membrane associated spectrin network during *C. elegans* elongation

There are three major spectrins in *C. elegans*, SPC-1/α-spectrin, SMA-1/β_H-spectrin and UNC-70/β_G-spectrin (16). Spectrins are cytoskeleton linkers that anchor actin filaments to the apical membrane and are essential for elongation. Loss of SPC-1/α-spectrin causes embryos to arrest mid-elongation (159). SMA-1 is localised at the apical membrane of the dorsal and lateral epidermis (160). Disruption of the *sma-1* gene causes an elongation defect in which the worms elongate very slowly and fail to grow to appropriate size, hence the name *sma* (meaning small) (160). Actin in the lateral epidermis (seam cells) also becomes disorganised in *sma-1* null mutant (160). Together SPC-1 and SMA-1 are important in stabilizing CFBs at the apical membrane of the lateral epidermis (seam cells) during elongation (160) (159). UNC-70 does not appear to be as essential as SMA-1 but it showed redundant SMA-1 function in *sma-1* null mutants (161).

1.6.4 Role of noncentrosomal microtubules in *C. elegans* epithelia

Microtubules (MTs) are composed of α-tubulin and β-tubulin which form a polarised cytoskeleton which usually exist as parallel filaments. An individual monomer has plus and minus ends and can only be nucleated from the minus end to plus end. In *C. elegans*, microtubule filaments are generated from 11 protofilaments (162). The polarised property of MTs enable them to transport proteins to different subcellular compartments in a directional manner, and this function is crucial in polarity establishment in early embryo as discussed in section 1.3.1 (98). The minus ends of each individual MT filament are capped by protein complexes, which are essential in controlling the nucleation of MTs. The main complex, which controls the dynamics of MTs by helping to initiate the nucleation

process, is the γ-tubulin ring complex (γ-TuRC) (163). There are two types of MTs in most cell types, the centrosomal MTs, which are nucleated from the centrosomes comprised with a pair of centrioles and pericentriolar materials (PCM) and are important in mitotic spindle assembly to ensure proper segregation of chromosomes during cell cycle, and noncentrosomal MTs, which are organised along the apical-basal axis of the epithelial cell in parallel arrays (163). In *C. elegans*, the organisation of noncentrosomal MTs require the re-localisation of γ-TuRC to the cell surface (162). In the epidermis, they are re-located from the centrosomes towards the apical membrane of the cells along the CeHD junctions or the CeAJ (164) (165), whereas in the intestine γ-tubulin and other proteins move to the apical surface of the intestinal lumen in a PAR-3 dependent manner (70).

MTs are important for elongation because embryos treated with the microtubule inhibitor nocodazole undergo a reversible block in elongation (143). During epithelial cell migration and morphogenesis, their nuclei need to be anchored at the correct position. This is achieved by the KASH (Klarscicht, ANC-1 and Syne-homology) and SUN (Sad-1 and UNC-84) proteins (166). These two proteins build a bridge called LINC (linker of nucleoskeleton and cytoskeleton), which recruits MTs to the outer nuclear surface and moves nuclei along MTs (167). The driving force responsible for moving nuclei to the plus end of the MT filament is provided by KLC-1/kinesin-1, whereas minus-end dynein motors fine tunes the movement (167). Both of these motors are recruited by the KASH protein UNC-83 and SUN. MTs are also intertwined with actin filaments, and have been implicated to participate in the same nuclear migration process (167). The mechanisms controlling the dynamics of microtubules in epithelia are very poorly understood. Studies indicate that the small GTPase EVL-20 and the spectroplakin VAB-10B might have a role in controlling

microtubule dynamics in epithelial cells but their roles have not yet been characterised (168) (139).

1.7 WD40 domain and WD40 protein functions

The WD40 domain is a structural motif, which is usually composed of 40 amino acids (169). The name of the motif comes from the fact that it contains a WD dipeptide at the C-terminus of the motif. Another signature of a WD40 domain is the presence of a variable region 11-24 residues followed by key signature sequence features: a glycine-histidine (GH) dipeptide away from the N-terminus (169) (Figure 1-9A). Found between the GH and WD dipeptides is a conserved core, which is capable of forming a propeller like platform or scaffold where proteins can bind stably or reversibly. Each propeller is made up of four β sheets running anti-parallel with each other (169) (Figure 1-9B). A classic example of WD40 containing protein is the β-transducin, which contains one 7-blade propeller and functions as a scaffold to mediate signal transduction (170) (Figure 1-9B). WD40 proteins are named for a group of proteins containing various number of WD40 domains and they have a wide variety of functions such as signal transduction, mRNA processing, chemotaxis cytoskeleton assembly and cell cycle control (171). In *Drosophila*, two WD40 proteins have been shown to be cytoskeleton regulators, one of them is the tumor suppressor Lgl protein, able to bind with nonmuscle myosin II heavy chain (172), the other one is Fritz, a WD40 protein specifically involved in planer cell polarity in *Drosophila* wing epithelia (173). Most WD40 proteins which have been studied so far have 7-blade propeller structure, although in rare cases, different numbers of blades could be observed such as 6 or 5. In some WD40 proteins, two 7-blade propeller domains can be linked through a coiled-coiled domain and they function stoichiometrically as negative regulators for certain cellular processes (169). This is

because the relative stable structure of WD40 repeats provide stable binding surface for interacting proteins (169). One such example is Tomosyn, involved in neutrotransmitter vesicle fusion at the synaptic membrane. Tomosyn acts as a negative regulator of the SNARE protein Syntaxin through its N-terminal WD40 domain (174).

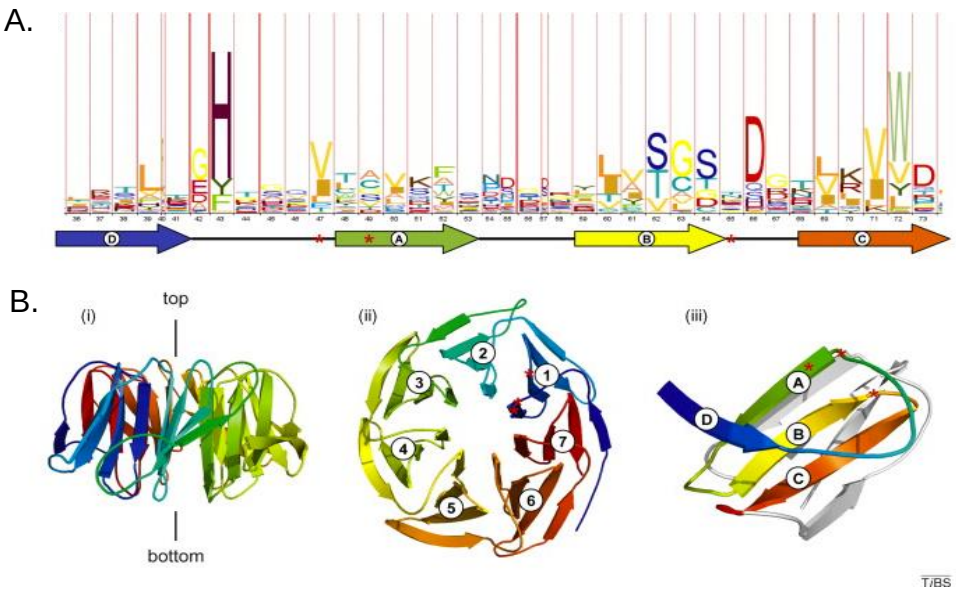

Figure 1-9 Amino acid signature and crystal structure of WD40 domain.

A. Amino acid signatures of the WD40 domain, which is characterised by (a) a variable region of 11–24 residues followed by key signature sequence features: a glycine-histidine (GH) dipeptide at the end of strand D (coloured blue), three small amino acids at the C-terminal end of strand B (coloured yellow) and a tryptophan-aspartate (WD) dipeptide at the end of strand C (coloured orange). **B.** Crystal structure of WD40 domain formed by 7-blade β sheet with colour coding corresponding to the strands shown in A. Adapted from (169)

1.8 Background to the Identification of the *lawd-1* gene

lawd-1 was isolated in a genetic screen as a homozygous viable mutant with a notched head and epithelial morphogenetic defects similar to that of *vab-1* and *vab-2* (175, 176). A smaller number of animals also showed generalised body morphogenetic defects, such as protrusions and indentations on various body parts (section 3.1, Figure 3-2E). The original mutant allele was named *cr7*. Subsequently, fosmid clones were tested for their ability to elicit rescue of the *cr7* mutant phenotype by germ line microinjection. The clones used were H24G06 and WRM0637dG12. The overlapping regions of two fosmids contain the full genomic sequence of *lawd-1*. The molecular basis of the *cr7* mutation was then determined by sequencing the H24G06.1 region of the fosmid H24G06. The *cr7* mutation was found to disrupt an alternative exon in the *H24G06.1* gene, which is located on LGV (Linkage Group V/Chromosome V) (PEK, unpublished work). A single base change was identified, and an alternative exon found close to the 3' end (Figure 1-10C) of the gene. The base change created a nonsense change in an alternative exon leading to premature termination of this alternative transcript.

Genetic analysis indicated that when *cr7* was placed in *trans* to a deficiency, the resulting lethality was more severe than that observed with the original *cr7* homozygote, suggesting that *cr7* was a non-null allele of *lawd-1*. cDNA clones were identified corresponding to at least 7 transcripts, which encode for multiple protein isoforms (PEK, unpublished work) (Figure 1-10A). Some isoforms were predicted to carry a dual N-terminal WD40 domain with at least 14 WD40 repeats (Figure 1-10B). While mapping *lawd-1*, it was also discovered that *cr7* is synthetic lethal with *sma-1*, which encodes β-H spectrin, an important cytoskeleton component of the epithelial cells (160).

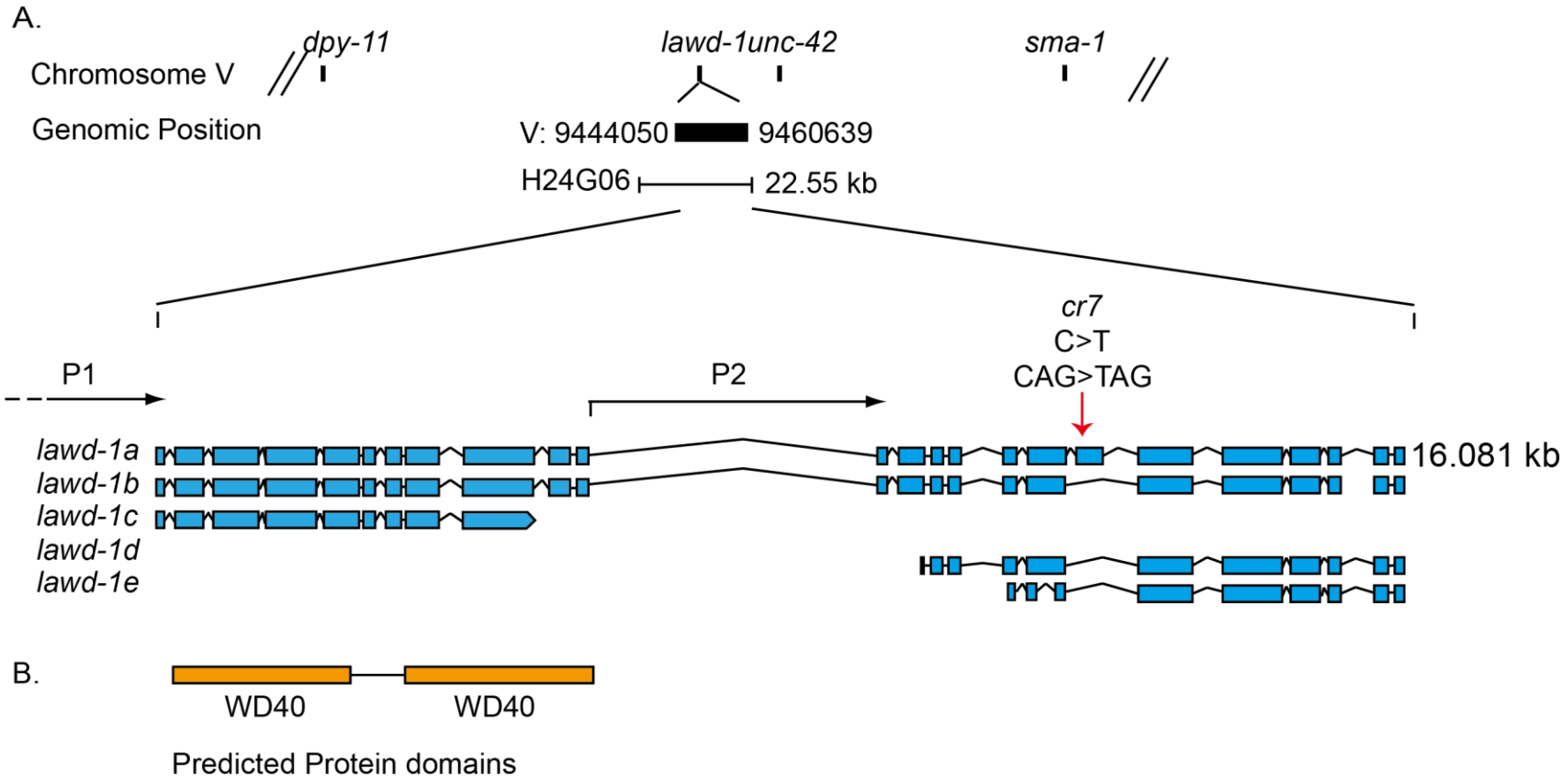
A.
Chromosome V
dpy-11
lawd-1unc-42
sma-1
Genomic Position
V: 9444050
9460639
H24G06
22.55 kb
cr7
C>T
CAG>TAG
P1
P2
lawd-1a
lawd-1b
lawd-1c
lawd-1d
lawd-1e
16.081 kb
B.
WD40
WD40
Predicted Protein domains
C.
Alternative exon 18
...intron...
_AC ACA GAT AAA
cr7
C>T
CAA CCA CAG AAA CTT CGG
TTT ACG ACC ACC GTT CAA
ACG CGC GAG ATA TCT CTT
GAT GAT GAA GTT GTC A

Figure 1-10 Genetic organisation of *lawd-1* gene and the position of *lawd-1* mutation *cr7*.

A. *lawd-1* is located on chromosome V as indicated on the black line which represents partial chromosome V and the relative positions of neighbouring genes are marked. *lawd-1* gene is completely covered by the fosmid H24G06 and its genomic position and relative size compared with the fosmid is indicated by the black block above. Predicted alternatively spliced variants of the *lawd-1* gene are shown based on the existence of fully and partially confirmed cDNA clones (Some cloned by Patricia Kuwabara, some are shown by RNA-seq and cDNA sequencing of Yuji Kohara's library). There are two *lawd-1* promoters which are P1 and P2. P2 is an intragenic promoter. The longest *lawd-1*a transcript is 4.984 kbp and is encoded by a genomic region of 16.081 kbp. The mutation *cr7* is indicated by the red arrow. The brackets show the region of the gene deleted by mutation. **B.** The 5' end of the longest *lawd-1* transcripts is predicted to encode two WD40 domains each consisting of 7 WD40 repeats. **C.** *cr7* encodes a premature stop codon in the alternative exon 18 of *lawd-1a*.

1.9 Objectives of this thesis

Given that a lot is still unknown about the precise mechanism underlying the dynamic changes of cytoskeletons and their interactions with the junction complexes, and given that LAWD-1 isoforms are predicted to form potential WD40 domain which is capable of mediating multi-protein interaction, it was hypothesised that LAWD-1 might act as a protein-protein interacting mediator in epithelial cells during embryonic development and in epithelial tissue development in larva. The present study characterised *lawd-1* gene with genetic and molecular techniques and aimed to achieve the following objectives:

1. To characterise the *lawd-1* locus using genetic techniques
2. To examine the intracellular expression pattern of LAWD-1 isoforms.
3. To identify and validate LAWD-1 interacting proteins using proteomics.
4. To verify any potential interacting partners using co-immunoprecipitation.

Chapter 2 **Materials and methods**

2.1 Materials

2.1.1 Consumables and lab equipments

-20 ºC freezers (Thermo Cryotechnics)

-80 ºC freezers (New Brunswick)

Amersham Hyperfilm ECL (GE Health)

Biolistic Macrocarriers (BIO-RAD)

Biolistic PDS-1000/He particle delivery system (BIO-RAD)

Borosilicate glass capillaries (Clark Electromedical Instruments)

Cryo 1 ºC freezing container (NALGENE™)

Cryotubes (Nunc™)

^{137}Cs irradiation source RX30/50 (Gravatom Industries)

Dark reader™ (Clare Chemical)

Dissecting microscope (Leica)

DNA electrophoresis chamber (BIO-RAD)

DNA electrophoresis power supply (Amersham Pharmacia Biotech)

Eppendorf 5415D centrifuge (Eppendorf)

Eppendorf 5810R centrifuge (Eppendorf)

Flaming/Brown micropipette puller (Shutter Instrument Co.)

Gene Pulser® Cuvette (BIO-RAD)

Heat block (Techne dri-block),

Heat/stir stand (Stuart)

Hepta Adapter (BIO-RAD)

Hepta Stop Screen (BIO-RAD)

Micropulser™(BIO-RAD)

Microwave (Panasonic)

Mini PROTEAN® blotter (BIO-RAD)

Mini PROTEAN® electrophoresis system (BIO-RAD)

Nitrocellulose membrane (Whatman)

Omega Media autoclave (Prestige Medical)

PCR machine (PTC-225 MJ Research)

perimetric GP pump (Jencons Scientific)

Rupture Discs 1350 psi (BIO-RAD)

Shaker incubator (Innova®)

Silicon tubing to use with perimetric GP pump (Jencons Scientific)

Sorvall GSA centrifuge (Thermo)

Spectrophotometer (CECIL)

Sterile 10 cm plates (Sarstedt Petri Dishes)

Sterile 5 cm plates (Gosselin™ Petri Dishes)

UV transilluminator system (SynGene)

Vacuum pump (Fisher Scientific)

Vortex Genie™-2 (Scientific Industries)

Water bath (Grant instrument)

Worm incubators (LMS)

2.1.2 Chemicals and reagents

1 mM gold beads (BIO-RAD)

2-Deoxy-D-galactose (ALDRICH)

2-Mercaptoethanol (SIGMA)

2x Rapid ligase buffer (Promega)

30% Acrylamide/Bis Solution 29:1 (BIO-RAD)

5% non-fat milk formula (MARVEL)

Acetic acid (AnalaR®)

Agar (MELFORD)

Agarose (Seakem®)

Antibiotics: ampicillin (SIGMA), kanamycin (MERCK), hygromycin (InvitroGen) chloramphenicol (SIGMA), tetracyclin (SIGMA)

APS (SIGMA)

Boric acid (SIGMA)

Bromophenol blue (BDH Laboratory supplies)

Butan-1-ol (Fisher Scientific)

$CaCl_2$ (SIGMA)

Cholesterol (SIGMA)

$CuSO_4.5H_2O$ (ALDRICH)

D-(+)-galactose (SIGMA)

dATP, dGTP,dCTP, dTTP (BIO-RAD)

d-biotin (BIO-RAD)

DNA ladder (Promega)

DTT (MELFORD)

EDTA (SIGMA)

EGTA (SIGMA)

Ethidium bromide (BIO-RAD)

EtOH (Sigma-Aldrich)

$FeSO_4.7H_2O$ (ALDRICH)

Gelatin (BDH Chemicals)

Glucose (AlanaR®)

Glycerol (Fisher Scientific)

Glycine (SIGMA)

Glycogen (Promega)

GoTaq 10X PCR buffer (Promega)

HCl (Fisher Scientific)

HEPES (SIGMA)

IPTG (APOLLO SCIENTIFIC LTD.)

Isopropanol (Kluka)

K_2HPO_4 (Fisher Scientific)

KCl (SIGMA)

KH_2PO_4 (Fisher Scientific)

KOH (Fisher Scientific)

L-arabinose (Sigma)

LB powder (Fisher Scientific)

Liquid N_2 (University of Bristol)

L-leucine (Sigma)

$MgCl_2$ (BDH laboratory supplies)

$MgSO_4$ (AnalaR®)

$MnCl_2.4H_2O$ (SIGMA)

Na_2HPO_4 (Fisher Scientific)

NaCl (Fisher Scientific)

NAD (SIGMA)

NaH_2PO_4 (Fisher Scientific)

NaOCl solution with 12%-15% available chlorine (ACROS ORGANICS)

NaOH (AnalaR®)

NP-40 Alternative (CALBIOCHEM)

PBS tablets (MELFORD)

PEPES (SIGMA)

Peptone (BD Bacto™)

Phenol: chloroform (SIGMA)

Phusion 5X HF buffer (Finzyme)

PMSF (SIGMA)

Ponceau S (Sigma, P3504)

Potassium acetate (AnalaR®)

Potassium citrate (SIGMA)

Precision plus all blue standards (BIO-RAD)

Protease inhibitor cocktail tablet (Roche)

Proteinase K (SIGMA)

SDS (BDH laboratory supplies)

Sodium acetate (AnalaR®)

Spermidine (Sigma)

Sucrose (AnalaR®)

SYBR-Gold nucleic acid gel stain (Invitrogen)

TEMED (SIGMA)

Tris (SIGMA)

Triton-100 (Fisher Scientific)

Tween-20 (MELFORD)

X-gal (APOLLO SCIENTIFIC LTD.)

$ZnSO_4.7H_2O$ (SIGMA)

2.1.3 *C. elegans* strains

See Table 2-1. for the list of strains.

2.1.4 DNA constructs

See Table 2-2. for the list of constructs generated.

Commercial plasmids:

pRF4 (*rol-6*), pPD49.26 (basic Fire vector backbone with multiple cloning sites), pPD93.97 (*myo-2::gfp*), pPD118.33 (*myo-3::gfp*)

Plasmids gifted:

pBALU1 (recombineering *gfp*), pBALU20 (recombineering *mCherry*), pIC26 (tev-S-tag *gfp*), pAA65 (tev-S-tag *mCherry*), pCFJ151 (*Cb-unc-119*), pMA122 (*peel-1* negative selection), pJL43 (Mos-1 transposase)

CRISPR clones: pIR1283 (hygR), pIR1287 (hygR), pJA58 (*dpy-10* sgRNA), pDD162 (Cas-9 nuclease), sgRNA-pU6::*klp-12*, pMB70 (sgRNA-pU6 empty vector)

Commercial fosmid:

WRM0627dG12 (contains *lawd-1* full genomic sequence)

2.1.5 Primers

See Table 2-3 for the list of primers used in this project.

2.1.6 Media

Bacterial media:

1.6% LB agar (1 L): 25 g LB powder and 16 g agar were autoclaved in 1 L milliQ water.

Galactose minimal agar (1 L): 15 g agar was autoclaved in 780 mL milliQ H_2O. After cooling down to 55˚C, 200 mL M63 medium, 1 mL 1 M $MgSO_4.7H_2O$, 10 ml 20% galactose, 5 mL 0.2 mg/mL d-biotin, 4.5 mL 10 mg/mL L-leucine (dissolved at 50 °C) and 250 μl 50 mg/mL chloramphenicol in EtOH were mixed respectively into the solution.

Deoxygalactose minimal agar (1 L): 15 g agar was autoclaved in 780 mL milliQ H_2O. After cooling down to 55˚C, 200 mL M63 medium, 1 mL 1 M $MgSO_4.7H_2O$, 10 ml 20% 2-deoxy-galactose, 5 mL 0.2 mg/mL d-biotin, 4.5 mL 10 mg/mL L-leucine (dissolved at 50 °C) and 250 μl 50 mg/mL chloramphenicol in EtOH were mixed respectively into the solution.

MacConkey indicator agar with 1% galactose (1 L): 5 g of MacConkey agar (BD Difco, #281810) was autoclaved in 232.5 mL milliQ H_2O. After cooling to 55˚C, 62.5 μl 50 mg/mL chloramphenicol was added, followed by 12.5 mL 20% galactose to make the final galactose concentration to 1%.

LB (1 L): 25 g LB powder was dissolved in 1 L milliQ water and autoclaved before use.

C. elegans media:

NGM (1 L): 3 g NaCl, 2.5 g peptone and 19 g agar were autoclaved in 980 mL of milliQ water, after cooling down to 55˚C, 1 mL 5 mg/ml Cholesterol in 96% EtOH, 1 mL 1M $CaCl_2$, 1 mL 1M $MgSO_4$ and 25 mL 1M KH_2PO_4, pH 6.0 were added with sterile technique to make 1L of media. Approximately 100 plates were made from 1L of media.

S-basal complete (500 mL): 1.5 mL 1M $MgSO_4$, 1.5 mL 1M $CaCl_2.6H_2O$, 5 mL 100x Trace Metals solution and 5 mL 1 M Potassium Citrate pH 6.0 were added with sterile technique to 500 mL of S-basal media (S-basal media recipe was listed below)

2.1.7 Buffers and solutions

10x TAE (1 L): 242 g TRIS-base, 57.1 mL acetic acid, 0.5 M EDTA pH 8.0, 100 mL 0.5M EDTA pH8.0 were added to 700 mL milliQ water to dissolve, after everything was dissolved, milliQ water was added to make the final volume to 1 L and the resulting buffer was autoclaved.

10x TBE (1 L): 109 g TRIS-base, 55.6 g boric acid and 40 mL 0.5 M EDTA pH 8.0 were added to 700 mL milliQ water to dissolve, after everything was dissolved, milliQ water was added to make the final volume to 1 L and the resulting buffer was autoclaved.

1x H100 + 10% glycerol worm lysis buffer (100 mL): The following reagents were mixed with milliQ water. HEPES pH 7.4 was added to the final concentration of 50 mM. EGTA was added to the final concentration of 1 mM. $MgCl_2$ and KCl were added to the final concentrations of 1 mM and 100 mM respectively. Glycerol were added to 10% final w/v concentration and NP-40 was added to 0.05% w/v

concentration. 1x protease inhibitor cocktail was added to the solution just prior to use, with PMSF and DTT added to 1 mM and 0.5 mM respectively.

2x SDS sample buffer (10 ml): 2.5 mL 0.5 M TRIS-HCl pH 6.8, 2 mL glycerol, 4 mL 10% SDS and 0.02 g bromophenol blue were mixed together with milliQ water to a final volume of 9 mL, 10% 2-Mecaptoethanol was added just prior to use the buffer.

2x worm bleach solution: NaOH and NaClO were added to milliQ water to the final concentrations of 1N and 40% respectively.

2x worm freezing buffer: the following reagents were mixed with milliQ water. NaCl was added to the final concentration of 0.1 M, KH_2PO_4 was added to the final concentration of 50 mM. Glycerol was added to the final w/v concentration of 30%. NaOH was added to 1N and $MgSO_4$ was added to the final concentration of 0.3 mM.

5x isothermal reaction buffer: the following reagents were mixed with milliQ water. PEG-8000 was added to the final w/v concentration of 25%. Tris-HCl pH 7.5 was added to the final concentration of 500 mM. $MgCl_2$ was added to the final concentration of 50 mM. DTT was added to the final concentration of 50 mM. dATP, dTTP, dCTP and dGTP were added to the final concentration of 1 mL respectively. NAD was added to the final concentration of 50 mM.

6x ficoll buffer: the following reagents were mixed with milliQ water. 15% Ficoll 400 was added to the final w/v concentration of 15%. Bromophenol blue and Xylene Cyanol were added to the final w/v concentration of 0.025% respectively.

$CaCl_2$ Competent cell buffer (250 mL): 15 mL 1M $CaCl_2$, 37.5 mL glycerol, 2.5 mL 1 M PEPES were mixed with milliQ water to the final volume and the resulting solution was autoclaved before use.

GTE solution: the following reagents were mixed with milliQ water. Glucose was added to the final concentration of 50 mM. Tris-HCl pH 7.4 was added to the final concentration of 25 mM and EDTA was added to the final concentration of 10 mM.

M63 media (1 L): 10 g $(NH_4)_2SO_4$, 68 g KH_2PO_4 and 2.5 mg $FeSO_4.7H_2O$ were mixed with milliQ water, KOH was then used to adjust the pH of the solution to 7 followed by milliQ water to make up the volume to 1 L. The solution was then autoclaved before use.

M9 buffer (1 L) 6 g Na_2HPO_4, 3 g KH_2PO_4, 5 g NaCl and 1 mL 1M $MgSO_4$ were mixed with milliQ water to the final volume of 1 L. The solution was then autoclaved before use.

Miniprep solution 3 (100 mL): 60 mL of 5M potassium acetate, 11.5 mL acetic acid and 28.5 mL milliQ water were mixed and autoclaved.

S-basal (1 L): 5.9 g NaCl, 50 mL 1M KH_2PO_4, pH 6.0, 1 mL 5 mg/ml cholesterol in 96% EtOH were mixed with milliQ water to the final volume. The solution was then autoclaved before use.

SDS PAGE running buffer (10x 1L): 30.3 g TRIS-base, 144g Glycine and 10 g SDS were mixed with milliQ water to the final volume.

Single worm lysis buffer (100 mL): 0.37g KCl, 1 mL 1M Tris-HCl pH 8.3, 0.25 mL 1 M $MgCl_2$, 0.45 mL NP-40, 0.45 mL Tween-20 and 1 mL 1% gelatin were mixed with milliQ water to the final volume.

Tris-EDTA (TE) 1 L: 10 mL 1M Tris-HCl pH 8.0 and 1 mL 0.1M EDTA were mixed with milliQ water to volume. The solution was then autoclaved before use.

Trace metals solution: the following reagents were mixed with milliQ water. disodium EDTA was added to 5 mM final concentration, $FeSO_4.7H_2O$ was added to 2.5 mM final concentration, $MnCl_2.4H_2O$ was added to 1mM final concentration, $ZnSO_4.7H_2O$ was added to 1 mM final concentration and $CuSO_4.5H_2O$ was added to 1 mM final concentration.

Western blot stripping buffer: the following reagents were mixed with milliQ water. 2-Mecaptoethanol was added to 100 mM final concentration, SDS was added to 2% w/v final concentration and Tris-HCL pH 6.7 was added to 62.5 mM final concentration.

Western blot transfer buffer (10x 1L): 30.3 g TRIS-base, 144g glycine were mixed with milliQ water to the final volume.

Western blot transfer buffer (1x 1 L): 1 mL 10% SDS, 150 mL EtOH were mixed with 100 mL 10x transfer buffer and milliQ water to the final volume.

2.1.8 Solid materials

1% TAE gel (100 mL): 1g of agarose was mixed with 100 mL TAE buffer and the mixture was then heated up to mix and stored at 55 °C.

1% TBE gel (100 mL): 1g of agarose was mixed with 100 mL TBE buffer and the mixture was then heated up to mix and stored at 55 °C.

7% SDS PAGE gel (6 mL): 1.4 mL 30% Acrylamide/Bis Solution 29:1, 1.5 mL 1.5M Tris pH 8.8 and 3.1 mL milliQ water were mixed together and the resulting solution was then poured between glass plates to set.

2.1.9 Enzymes

CIP phosphatase (Roche)

GoTaq polymerase (Promega)

Phusion polymerase (Finzyme)

Restriction enzymes used (supplied with NEB buffers 1-4 and 100x BSA):

BamHI, BglII, BsaI, DpnI, EagI, EcoRI, EcoRV, HindIII, KpnI, NheI, PstI, SmaI SpeI, XbaI, XhoI.

RNAse A (SIGMA)

T4 ligase (Promega)

T5 exonuclease (Thermoscience)

Taq ligase (Thermoscience)

2.1.10 Antibodies

Primary antibodies:

Anti-GFP antibodies (mouse):

Jackson Immuno Research B-1; Covance; Roche.

Anti mRFP antibody (rabbit):

MBL Japan

Gifted anti-VAB-10N antibody (rabbit) ((139)

Anti-tubulin antibody (mouse)

Sigma

Secondary antibodies:

Goat-anti-rabbit (Jackson Immuno Research)

Goat-anti-mouse (Jackson Immuno Research)

2.1.11 Manufactured kits

Chemiluminescence Detection Kit (Roche)

Coomassie (Bradford) Kit (Fisher Scientific)

GRP-trap (Chromotek)

Molecular biology kits:

mRFP-trap (Chromotek)

Promega PureYield plasmid extraction kit

Protein kits:

QIAgen gel purification

QIAgen plasmid purification

Silver Stain Kit (Thermo Science)

2.2 Methods

2.2.1 General *C. elegans* methods

2.2.1.1 Strain maintenance on solid media

C. elegans worms were cultured on NGM single peptone plate at 20 °C as described before (1). NGM plates were made by autoclaving 1 L of the media and then dispensed sterilely into 5 cm plates. Plates were seeded with OP50 *E. coli* as source of food for the worms (1). Worms were passaged onto new plates regularly by either chunking a piece of agar with a metal loop from a starved plate and transferred onto new plates or by picking single worms with a platinum wire pick and transferred onto new plates to maintain health (177).

2.2.1.2 Decontamination of small *C. elegans* culture on NGM plates

5 µl of sodium hypochlorite (12-15% available chlorine) and 5 µl of 2N NaOH were mixed and then pipetted onto the edge of a clean and OP50 seeded plate. 12 gravid adults were picked from the contaminated plate into the bleach mixture. The gravid adults would dissolve leaving only embryos to hatch. After a 2-3 days the grown worms hatched from the remained embryos were picked onto new plates (177).

2.2.1.3 Bleaching to obtain synchronised culture

> 1 mL of packed gravid adults were collected in a 15 mL falcon tube using cold M9 buffer (22 mM KH_2PO_4, 42mM Na_2HPO_4, 217 mM NaCl, 1mM $MgSO_4$) from either large double peptone plates or a liquid culture. Worms were washed three times with cold M9 buffer by centrifuging at 1200 RPM for 2 min at 4 °C in between washes. 6 mL 2x bleach solution (1N NaOH, 40% NaClO) was added to worms re-suspended in 6 mL of cold M9. The falcon tube was vigorously inverted for up to 4 min. Progress was checked by putting a drop of the mixture under a dissecting microscope to see how many adults were dissolved. When roughly 90% of the gravid adults were dissolved, the mixture was centrifuged at 1500 RPM for 1 min at 4 °C. Supernatant was removed as soon as possible and the embryo pellet was re-suspended in 12 mL cold M9 buffer. The pellet was washed three times with cold M9 buffer by centrifuging at 1500 RPM for 1 min at 4 °C. The washed embryos were finally re-suspended in 10 mL of M9 and 5 mL each was distributed onto two large unseeded NGM single peptone plates (10 cm). Plates were rocked on a shaker overnight at 20 °C for the embryos to hatch. Hatched L1 larvae were collected and washed three times with M9 buffer before distributed onto OP50 seeded NGM plates (177).

2.2.1.4 Freezing and thawing strains

C. elegans worms can be frozen and stored in liquid N_2 indefinitely (1). Worms were washed off 3 x 5 cm nearly starved plates with 1.5 mL M9 each into a 15 mL falcon tube, the majority of the worms should be L1 stage for successful thawing. Worms were centrifuged at 1200 RPM for 2 min at 4 °C and then the worm pellet was re-suspended in a mixture of 1 mL M9 buffer and 1 mL 2x freezing buffer (0.1 M NaCl, 50 mM KH_2PO_4 30% glycerol, 1N NaOH, 0.3 mM $MgSO_4$). 0.6 mL of the mixture was dispensed into each of the three freezing vials and the freezing vials were placed into an isopropanol freezing container. The container was placed in the - 80°C freezer for 24 hours before the individual vials were transferred into liquid N_2 tank (177).

2.2.1.5 Large scale liquid culture

A single *E. coli* NA22 colony was inoculated in 10 mL of LB media overnight in a universal culture vial and the total 10 mL of culture was subsequently used to inoculate a 1L overnight culture. The 1L overnight culture was pelleted in two sterile 500 mL bottles by centrifuging 10 min at 4000 RPM at 4 ºC in a SLC-3000 rotor. The bacteria pellet was then re-suspended in 500 mL S-basal complete medium (256 mM NaCl, 50 mM KH_2PO_4, 5 µg/mL cholesterol, 50 µM disodium EDTA, 25 µM $FeSO_4.7H_2O$, 10 µM $MnCl_2.4H_2O$, 10 µM $ZnSO_4.7H_2O$, 10 µM $CuSO_4.5H_2O$ 3 mM $MgSO_4$, 3 mM NaOAc, pH 6.0) (178). On the same day, worms from 10 NGM plates which were just about to starve were rinsed off with 1.5 mL cold sterile M9 buffer per plate into a 15 mL falcon tubes. Worms were pelleted at 1200 RPM at 4 ºC and washed twice with 15 mL cold sterile M9 buffer. After the final wash, worms were re-suspended in 5 mL cold sterile M9 buffer and transferred into the 500 mL S-basal complete medium supplied with re-suspended NA22 pellet in a 1 L flask. The liquid

culture was placed in a shaker at 20 ºC and 200 RPM for 3-4 days. The progress of the culture was checked by pipetting some of the liquid culture out onto a glass slide and observing the growth under a dissecting microscope. When most of the worms were of the desired stage, usually meaning the majority of the worms are adults, the liquid culture was poured into a pre-cooled 500 mL glass cylinder and worms were allowed to settle. After 2-4 hours of settling, the supernatant was removed until $<$ 50 mL of culture remained in the cylinder. The remaining worm culture was poured into a 50 mL falcon tube and centrifuged at 1200 RPM for 2 min at 4 °C. Cold M9 were used to rinse the cylinder to collect any remaining worms. After two washes with cold M9 buffer, worms were transferred from the 50 mL falcon tube into a 15 mL falcon tube, usually 4-6 mL of packed worms were obtained from a 500 mL liquid culture (Slightly modified from (177)).

2.2.1.6 Setting up crosses

Genetic crosses were set up by placing 4 L4 stage hermaphrodite worms with 12 L4 stage males onto an OP50 seeded plate. Replicates of plates were usually set up. Mating plates were kept at 20 °C and cross progeny were observed after 2 days. L4 stage cross progeny were observed after 5 days at 20 °C (179).

2.2.1.7 Mapping

Genetic crosses were set up using either of the mapping strains MT465, MT464 with N2 males (180). The F1 heterozygotes males obtained from the first cross were then mated with the integrated strain. ~50 homozygotes worms of each phenotype were picked (for MT465 the F2 phenotypes would include: *Dpy* (I); *Bli* (II); *Unc* (III) and for MT464 the F2 phenotypes would include: *Unc* (IV); *Dpy* (V); *Lon* (X)) and the absence of the fluorescent marker from each phenotype was examined. The absence of the fluorescent marker from any chromosome linked

phenotype indicated that the integrated fluorescence marker would be on the same chromosome of the one marked by one of the mutant alleles carried in MT464 or MT465.

2.2.1.8 Phenotypic analysis

The penetrance of the *lawd-1* mutant phenotype was determined by picking 5 individual L4 worms onto separate OP50 seeded NGM plate and transferring them onto new OP50 seeded NGM plate every 24 hrs for a duration of 4 days. The number of wild type larvae, arrested Vab (Variable abnormal morphology) larvae, viable Vab adult and dead eggs were scored after 48 hrs of each transfer and the percentage embryonic lethality, larval lethality, Vab adult and non-Vab adult were determined (175).

2.2.1.9 Genotypic analysis using single worm PCR

Single worms were individually picked into PCR tube with 2.5 µl single worm lysis buffer (50mM KCl, 10 mM Tris, 2.5 mM $MgCl_2$, 0.45% Nonidet P-40, 0.45% Tween 20, 0.01% (w/v) gelatin) completed with Proteinase K (181). Worms were then incubated at -80 °C for 1 hr and then with a drop of mineral oil on top of the buffer in each tube, were lysed for 1 hr at 60 °C followed by 20 min at 95 °C in the PCR machine. A 25 µl total PCR reaction was prepared for each tube based on manufacturer's instruction (GoTaq) and a 35 cycle PCR reaction was performed with the general setting of: 1 cycle at 95 °C for 3 min; 95 °C 40 sec, 60 °C 40 sec, and 72 °C 1min/kb 35 cycles; 72 °C for 10 min and finally hold at 15 °C.

2.2.2 *C. elegans* transgenesis methods

2.2.2.1 Generating transgenic animals: Germline Microinjection

Microinjection introduces DNA into *C. elegans* worms (182). Briefly, single young adult N2 worm was placed in mineral oil dropped on a 0.8% agarose coverslip glass pad (dimensions 22mm x 50 mm). The agarose pad was then transferred onto a microinjection stage coupled with a capillary needle pre-filled with desired DNA mixture fitted onto a Zeiss microscope. Under a 40x inverted air lens, the glass capillary was gently pushed into the germline of the worm and the DNA mixture was pushed by gas into the germline. A drop of M9 buffer was immediately added onto the agarose pad after injection to prevent the worm from drying out and the slide was put aside. After 1 hour of recovery, the worm was gently lifted from the M9 buffer with a pick and placed onto an OP50 seeded NGM plate. Injected worms were allowed to lay F1 progeny and the successful transgenic F1s were singled onto individual plates to allow F2 progeny to be produced. A transgenic line was obtained when F2 and successive progeny all carry the transgene as extrachromosomal arrays (183).

2.2.2.2 Generating integrated transgenic lines: Gamma irradiation

50 L4 stage transgenic worms with the transgene transmission frequency lower than 40% were placed onto a 5 cm NGM plate with the lid removed. Worms were irradiated at a distance 30 cm away from the ^{137}Cs irradiation source for a total of 4800 Rds (4000 sec in a source containing chamber at 1.2 Rd/sec). The irradiated worms were allowed to recover overnight at 20 °C before being moved to individual plates with 4 worms on each plate. When plenty of F1 progeny came out, 250 of which were singled onto individual plate to allow to lay eggs (184). Each individual plate was scored of F2 transgenic transmission frequency when F1 has laid most of

its eggs. Based on Mendel's rule, a 75% transmission frequency indicates a possible heterozygote F1. These lines were kept and further investigated by putting 12 single F2 onto individual plate and then looking for a line that had 100% transmission frequency.

2.2.2.3 Generating single copy integrated transgenic lines: Hepta adapter biolistics

6 plates of starved *unc-119* (*ed3*) animals were used to start a liquid culture and approximately 4-6 ml of worms obtained were spotted on 2 cold and dry unseeded 10 cm double peptone NGM plates with 0.5 mL packed worms on each (enough for two rounds of shooting). Fosmid DNA containing *Cb_unc-119* rescuing marker was prepared with gold beads in advance in 100% EtOH to a final concentration of 1 mg/mL and a final volume of 96 µl. 6 µl of the prepared DNA gold mixture was pipetted onto each biolistics macrocarrier (A total number of 7) fitted into a single hepta adapter and this adapter was fitted into the Helium primed Biolistic PDS-1000 Helium particle delivery system (BIO-RAD). One unseeded plate with a monolayer of worms on top was fixed to the bottom of the chamber and the DNA was shot into the worm through the high Helium pressure. After the bombardment, worms were allowed to recover for 30 min and then washed with M9 onto ~20 seeded plates to lay progeny. (185) Worms were scored beginning on the 7th day after the bombardment and those with the *unc-119* phenotype rescued were picked onto new plates and then the integrated fluorescent marker was mapped.

2.2.2.4 Generating single copy indigenous integrated transgenic lines: CRISPR-Cas9

2.2.2.4.1 CRISPR-Cas9 using hygromycin resistant selection marker

The 19 nt protospacer motif and Protosacer Adjacent Sequences (PAM) were chosen by putting up to 250 bp of sequence containing the desired modification site

into an established online database developed by Zhang lab (http://crispr.mit.edu/). The selected 19 nt protospacer motif sequence was then cloned into a kindly gifted sgRNA clone containing the *rpr-1* promoter and terminator (De Bono Lab, LMB). A repair template was made by Gibson Assembly, wherein a hygromycin resistant gene was flanked by homology arms which were 250 bp away from the modification site in order to create a deletion at 5' end of the gene. Microinjection was performed with 50 ng/µl Cas-9 vector (kind gift from De Bono Lab, LMB), 100 ng/µl sgRNA clone, 50 ng/µl repair template together with a mixture of selection marker vectors (10 ng/µl *phsp-16.41::peel-1*, 10 ng/µl *prab-3::mcherry*, 2.5 ng/µl *pmyo-2::mcherry* and 5 ng/µl *pmyo-3::mcherry*) which were used in a similar selection scheme as previously described in the Mos-1 mediated transgenesis method (186). One of the marker plasmids encodes for a heat induced toxin (*phsp-16.41::peel-1*) which would eliminate any F1 worms that carry the transgenes as extrachromosomal array. F1 worms which carry the fluorescent selection markers and survived the heat shock were picked onto individual plates and allowed to produce eggs, when most of the eggs hatched hygromycin B was added to a final concentration of 0.2-0.3 mg/mL. F2 worms that survived the hygromycin B treatment were then moved onto new plates which contain 0.2-0.3 mg/mL hygromycin. These worms were allowed to lay eggs for 2 days and single worm PCR and sequencing were then performed on them to confirm successful knockout (9). 12 F3s derived from positive F2 lines were isolated to confirm germline transmission and to isolate homozygous line.

2.2.2.4.2 Co-CRISPR with *dpy-10* (*nt64*) marker

The 19 nt protospacer motifs were chosen as described in section 2.2.2.4.1. This time they were cloned into vector pRB1017 which contained the polIII U6

promoter (11) and also a GG motif right adjacent to the PAM in the genome was preferably chosen as it was reported to enhance CRISPR efficiency (13). To create the deletion, two PAM sites which defined the part of the genome to be deleted were chosen so that a double CRISPR coupled with homologous repair would result in a double cut and customised knockout (12). A repair template for creating the deletion was made by cloning using Gibson Assembly with two 1 kb homology arms right adjacent to the two PAM sites chosen, a restriction site was also engineered in between the two homology arms to facilitate selection. A repair template for creating a C-terminal mRFP knock-in was made by PCR, wherein two 60 bp homology arms were designed in the primers which were used to amplify the mRFP gene. Co-CRISPR using ssODN to create *dpy-10* (*cn64*) mutation was performed as a co-selection strategy as previous report demonstrated high level of success (11). To make the deletion, microinjection was performed with 50 ng/µl pDD162 Cas-9 vector (10), 75 ng/µl sgRNA clone 1, 75 ng/µl sgRNA clone 2, dpy-10 sgRNA (Co-CRSPR) 30 ng/µl, 50 ng/µl repair template clone, 0.5 µM ssODN repair template *dpy-10* (*cn64*). To make the C-terminal mRFP knock-in, microinjection was performed with 50 ng/µl pDD162 Cas-9 vector (10), 100 ng/µl sgRNA clone, dpy-10 sgRNA (Co-CRISPR) 30 ng/µl, 50 ng/µl repair PCR template, 0.5 µM ssODN repair template *dpy-10* (*cn64*). Injected worms which segregated a lot of dpy-10 (cn64)/+ roller animals were referred to as the jackpot brood (12) and a large number of their F1 progeny were picked onto individual plates to allow to lay eggs for 2 days and single worm PCR followed by restriction digest and sequencing were performed on F1 parents to confirm success modifications. 12 F2s derived from positive F1 lines were isolated to confirm germline transmission and to isolate homozygous line.

2.2.3 C. *elegans* protein methods

2.2.3.1 Preparation of worm extracts

Small scale for western blot:

45 worms of adults were picked (more worms were picked in other stages in the developmental blot analysis shown in Figure 5-2) into an Eppendorf tube with 50 μl M9 buffer, a 10 μl mark was marked onto the tube beforehand. Worms were washed three times with 50 μl M9 buffer and pelleted on bench top centrifuge at 1200 RPM for 2 min. Supernatant was removed to the 10 μl marked line. 10 μl of 2x SDS sample buffer (125 mM Tris, 20% glycerol, 4% SDS, 0.08% bromophenol blue, 1.43 M 2-Mecaptoethanol) was added into the 10 μl worm containing tube and sample immediately boiled at 95 °C for 5 min and transferred onto ice afterwards (187).

Large scale for immunoprecipitation:

Large scale liquid culture prepared as previously described in 2.2.1.5 was split into several 15 mL falcon tubes with each containing 500 μl packed worms in the end after two M9 washes. 500 μl 1.5x cold H100 lysis buffer (75 mM HEPES, pH 7.4 1.5 mM EGTA 1.5 mM $MgCl_2$ 150 mM KCl 15% glycerol without NP40, with 2x protease inhibitor cocktail, 1mM PMSF, 0.5 mM DTT in final volume) (188) was added to the packed worms and after a few mixes by a pipette immediately dropped frozen into liquid nitrogen as worm beads. Worm beads were then grinded with mortar and pestle into fine powder and the power was collected into the falcon tube. The worm powder was stored at -80 °C for up to several months. To prepare the worm lysate, worm powder was thawed at room temperature until mostly melted and immediately transferred on ice. 1 mL of 1x cold H100 lysis buffer (50 mM HEPES,

pH 7.4 1 mM EGTA 1 mM $MgCl_2$ 100 mM KCl 10% glycerol with 0.05% NP-40, 1mM PMSF, 0.5 mM DTT, 1x protease inhibitor cocktail) was added into the thawed worm pellet and the mixture was transferred into a pre-cooled 2 mL Dounce homogeniser. The mixture was homogenised with 50 strokes and then transferred into a 2 mL eppendorf tube. Worm extract was centrifuged at maximum speed of a bench top centrifuge for 10 min at 4 °C. The supernatant was saved as whole worm lysate (188).

2.2.3.2 Polyacrylamide gel electrophoresis

Worm protein samples were denatured and separated by running into a 7% resolving gel prepared based on manufacturer's instruction (BIO-RAD). The resolving gel was made even and set by placing water-saturated butan-1-ol on top. About 1 mL of 4.75% stacking gel was placed on top after the resolving gel was set and butanol removed. Protein electrophoresis was performed in a mini-PROTEAN vertical electrophoresis system (BIO-RAD) at 100 V for about 2 hours.

2.2.3.3 Western blot

Protein gel was placed on top of a nitrocellulose membrane equilibrated with cold 1X western blot transfer buffer and placed between two sponges and two filter paper all saturated with cold western blot transfer buffer into a cassette. The cassette was then placed in a mini-PROTEAN blotter (BIO-RAD) and placed at 4 °C. The transfer was performed overnight at 40 mA constant current setting (189). The nitrocellulose membrane was washed with sterile water once after the transfer was finished.

2.2.3.4 Immunostaining

Western blot analysis was performed by blocking the membrane with PBS containing 5% non-fat milk and 0.1% Tween-20 for 30 min followed by incubation with primary antibody at the following concentrations: mouse anti-GFP antibody 1:1000 or rabbit anti-mRFP antibody 1:2000 for 1 hr at room temperature followed by secondary Horseradish Peroxidase (HRP) conjugated anti-rabbit antibody or anti-mouse antibody at 1:5000 for 1 hr at room temperature. When using anti-tubulin antibody, 1: 20k primary was used in the incubation followed by secondary Horseradish Peroxidase (HRP) conjugated anti-mouse antibody at 1:5000. 3 x 5 minutes of PBS-0.1% Tween-20 washes were performed in between each incubation step. Membrane was developed using BM Chemiluminescence Western Blotting Substrate and detected on film (189).

2.2.3.5 Immunoprecipitation using large scale worm extracts

Whole worm lysate was prepared as described in section 2.2.3.1. The lysate was spun at max speed in a bench top centrifuge for 10 min at 4 ºC (high speed supernatant/HSS). 100 µl of HSS were saved for western blot analysis (input). 1 ml of the HSS was mixed with 20 µl pre-equilibrated mRFP nanotrap (Chromotek) and incubated with constant mixing at 4 ºC for 1 hr. The mixture was then centrifuged at 2.500 xg for 2 min at 4 ºC. 50 µl of supernatant was mixed with 2x SDS sample buffer as the unbound sample. Beads were washed 3 times and then boiled in 50 µl 2x SDS sample buffer for 10 min at 95 ºC to elute immunoprecipitated samples (Methods described by Chromotek).

2.2.3.6 Silver stain

A thermoscience silver stain kit was used to perform staining. Silver staining was performed based on manufacturer's instructions (Thermo Science).

2.2.3.7 Mass spectrometry and data analysis

Data were analysed by Proteome Discoverer v. 2.1 software. Mascot search engine (Matrix Science) were used to perform searches against the NCBI (nr) database. Any candidates with a Mascot score greater than the default threshold were identified as significant ($p<0.05$). The candidates were clustered according to subcellular localization and/or function using GO (gene ontology) term annotation. A PSM ratio of 1.5 was set as the threshold to compare the abundance of a certain protein between the sample and control and a list of proteins were obtained based on this criterion (Personal communication with Marion van den Bosch).

2.2.4 Molecular biology methods

2.2.4.1 DNA separation using agarose gel electrophoresis

Agarose gel was prepared by mixing agarose with either 0.5x TRIS-borate-EDTA (TBE) buffer or 1X TRIS-acetate-EDTA (TAE) buffer to 1% (w/v), then the mixture was heated in a microwave and stored at 65 ºC. DNA samples were mixed with 6x ficoll dye and loaded into wells in solidified agarose gel submerged in either 0.5x TBE buffer (diagnosis) or 1x TAE buffer (purification, see DNA extraction and purification for details). Samples were then electrophoresed at 65V for 30 min alongside a DNA ladder (190). Gel was then stained in diluted ethidium bromide solution for at least 20 min before being visualised in a UV transilluminator system and captured as images using SynGene software.

2.2.4.2 Restriction digest of DNA

DNA was digested using Restriction endonucleases from New England Biolabs. Restriction digest was performed following manufacturer's instructions (NEB).

2.2.4.3 DNA extraction and purification

2.2.4.3.1 DNA plasmids purification

XL1-Blue strain carrying the desirable plasmid was grown on agar plate with appropriate antibiotics at 37 ºC overnight (see transformation below). A single colony from the plate was then used to inoculate 5 mL of LB media with the appropriate antibiotics overnight at 37 ºC. The bacterial culture was harvested on the next day into an Eppendorf tube by centrifuging for 30 sec at 9000 RPM on a bench top centrifuge and then treated using the Promega PureYield™ Plasmid Miniprep System based on manufacturer's instructions (Promega).

2.2.4.3.2 DNA fragments gel purification

PCR or restriction digest products were ethanol precipitated, re-suspended in 10 µl of TE and then mixed with 4 µl 6x ficoll lite dye. The samples were then loaded into solidified agarose gel submerged in 1x TAE buffer and electrophoresed at 55V for 1 hour in 1X TAE buffer (190). The gel was then stained in 1: 50,000 SybrGold for at least 30 min before being visualised on a dark reader. The correct DNA bands were excised using a razor blade and the DNA product purified using the Qiagen Gel Extraction kit based on manufacturer's instructions (QIAGEN).

2.2.4.4 Polymerase Chain Reaction (Phusion)

A typical PCR reaction was performed by preparing a PCR reaction mix with primers to a final concentration of 0.2 µM, 0.5 µl Phusion Polymerase, 0.1 µM of each dNTPs, 50-100 ng of template and water to a final volume of 50 µl. This reaction mix was quickly transferred to a PCR machine. A typical PCR reaction of 35 cycles was performed with the following settings: 1 cycle at 98 °C for 30 sec; 98 °C 10 sec, 60 °C 40 sec, and 72 °C 30 sec/kb 35 cycles; 72 °C for 10 min and finally hold at 15 °C (Methods described by Finzyme).

2.2.4.5 Cloning

2.2.4.5.1 Standard cloning procedure

De-phosphorylation of vector

Restriction digested vector was checked using TBE gel electrophoresis for successful digest and 10x of intestine alkaline phosphatase CIP buffer was added to a final concentration of 1x and 1 unit/50 µl CIP phosphatase was also added. The mixture was incubated at 37 °C for 30 min and then phenol extracted.

Ligation

1 µl of purified insert and 1 µl of purified vector were mixed with 2 µl of 2.5x Promega rapid ligation buffer and 0.5 µl T4 ligase. The mixture was incubated at room temperature for 2 hrs before being transformed into $CaCl_2$ competent cells (Methods described by Promega).

2.2.4.5.2 Blunt-end cloning

1 µl of EcoRV digested vector pBluescript/pBSKSII(+) (Stratagene) was used most of the time) and 1 µl EcoRV insert were gel purified and mixed with 2 µl of 2.5x Promega rapid ligation buffer and 0.5 µl T4 ligase. The mix was then treated like general ligation reaction and transformed into $CaCl_2$ competent cells. If pBSKSII(+) was used as vector, a blue/white selection was then performed to isolated successfully transformed colonies.

2.2.4.5.3 Recombineering

A rescuing copy of the *Cbr-unc-119::FRT*galKFRT** cassette was first recombineered into the fosmid backbone of WRM0637dG12 (http://www.lifesciences.sourcebioscience.com) for use as a biolistic co-transformation marker. Subsequently, fluorescent reporter cassettes expressing the

selectable marker *galK* flanked by *FRT/Flp* recombination sites were amplified from either pBALU1 (*gfp*) or pBALU20 (*mCherry*) and electroporated into the SW105 bacteria host for recombineering immediately upstream of the *lawd-1* stop codon (191). DNA from successfully recombineered fosmids was isolated and transformed into the EPI300 strain for maintenance and large-scale DNA preparation using QIAprep® Spin mini kit. Fosmid DNA was amplified in EPI300 using 10% L-arabinose solution (Methods described by Epicentre).

2.2.4.5.4 Gibson assembly

10-100ng of purified PCR fragments containing homologous overlaps to each other were added to make up a 5 µl DNA mix. This was then added to a 15 µl 1.33X Gibson assembly on ice before being incubated for 1 hr at 50 ºC in a PCR machine (192). 5 µl and 2 µl aliquots were transformed separately into XL-1 blue competent cells (Based on methods described by Promega).

2.2.4.6 $CaCl_2$ competent cells preparation

Tiny XL-1 blue frozen aliquot was picked by a toothpick and streaked onto Kanamycin resistant agar plate. On the next day, a single colony was used to inoculate 5 mL LB media and the culture was grown in the shaking incubator at 37 °C overnight. On the next day, 4 mL of the overnight culture was added to 420 mL of LB and the culture was placed in a shaking incubator at 37°C until OD_{590} reached 0.375. The culture was then split into 8 pre-cooled falcon tubes on ice and left for 5-10 min. Cells were then spun down at 4000 rpm for 7 minutes at 4°C. The pellets were washed three times with ice cold $CaCl_2$ solution before finally re-suspended in 4 mL of $CaCl_2$ solution per tube. Cells were then aliquoted into Eppendorf tubes and stored at – 80˚C.

2.2.4.7 Bacterial transformation into $CaCl_2$ competent cells

100 µl aliquot of XL-1 blue competent cells was hand thawed and immediately placed on ice. This was then mixed with 5 µl of ligation product or 1 µl of plasmid in TE and then transferred into pre-cooled glass test tubes and kept on ice for 10 minutes. The cells were then heat shocked for 2 minutes at 42 ºC, placed back on ice before adding 250 µl of LB without antibiotics and incubated at 37 ºC for 1 hr. Transformation mixture was spread on agar plates with appropriate antibiotics and incubated at 37 ºC overnight.

2.2.5 Imaging

2.2.5.1 Widefield imaging

Worms were anesthetised using tricane (10 mg/mL) and tetramisole (100 mg/mL) and mounted on 3% agarose pads. Differential Interference Contrast (DIC) and epifluorescence images were obtained with a Zeiss Axioskop 2 microscope fitted with an Exi Aqua Bio-imaging Microscopy Camera driven by Image-Pro® Plus 7.0 software. Confocal images were obtained using Leica SP5-AOBS confocal laser scanning microscope attached to a Leica DM I6000 inverted epifluorescence microscope.

2.2.5.2 Confocal imaging and imaging analysis

Confocal images were obtained using Leica SP5-AOBS confocal laser scanning microscope attached to a Leica DM I6000 inverted epifluorescence microscope. Images were analysed in Adobe photoshop and Image J.

Lab name	**Strain name**	**Genotype**
xPK1010	CB270	*unc-42(e270)* V
xPK1003	MT464	*unc-5(e53)* IV; *dpy-11(e224)* V; *lon-2(e678)* X
xPK1009	MT465	*dpy-5(e61)* I; *bli-2(e768)* II; *unc-32(e189)* III
PK2050	JR667	*wIs51[SCMp::gfp + unc-119(+)]*
PK2061		*hmp-1::gfp*
PK2291	DR108	*dpy-11(e224)*; *unc-42(e270)* V
PK2772	ML1651	*mcIs46*[*dlg-1::rfp; unc-119*(+)]
PK2773	FZ223	*dlg-1::gfp + rol-6 (su1006)*
PK3013		*lawd-1(tm4605)*
PK3099-1	ML1150	*mlc-4(or253)*/ *qC1*[*dpy-19(e1259); glp-1(q339)*] III; *mcEx401*.
PK3021	CB1951	*unc-42(e270)*; *sma-1(e30)* V
PK3052	ML1735	*mcIs50*[*lin-26p::vab-10 (actin-binding domain)::gfp*; *myo-2p::gfp*; *pBluescript*]
PK3053	ML916	*mcIs40*[*lin-26p::ABDvab-10::mCherry + myo-2p::gfp*]
PK3059	AZ220	*sr4::gfp* (*partial sma-1*) (193)
PK3060		*zhIs396*[*pdlg-1::lifeact::gfp::unc-54 3'utr; plin-48::gfp*]
PK3061		*crIs12*[*lawd-1::gfp::unc-119*]
PK3062		*crIs12*[*lawd-1::gfp::unc-119*] (outcrossed)
PK3063		*crIs11*[*lawd-1::mCherry::unc-119 (pMQfos3)+ rol-6 (su1006)*]
PK3064		*crIs11*[*lawd-1::mCherry::unc-119 (pMQfos3) + rol-6 (su1006)*] (outcrossed)
PK3065		*crIs11*[*lawd-1::mCherry::unc-119 (pMQfos3) + rol-6 (su1006)*]; *hmp-1::gfp* (het)
PK3066		*crIs11*[*lawd-1::mCherry::unc-119 (pMQfos3) + rol-6 (su1006)*]; *syIs78*[*ajm-1::gfp + unc-119*(+)]; *unc-119(ed3)* III
PK3067		*crIs11*[*lawd-1::mCherry::unc-119 (pMQfos3) + rol-6 (su1006)*]; *dlg-1::gfp + rol-6 (su1006)*
PK3068		*crEX463*[*lawd-1p1::nls::gfp + rol-6 (su1006)*]

Lab name	**Strain name**	**Genotype**
PK3069		*crEX465*[(*sur-5p::mCherry::tev-s-tag::unc-54* 3' utr) + *rol-6 (su1006)*]
PK3070		*crIs13*[(*sur-5p::mCherry::tev-s-tag::unc-54* 3' utr) + *rol-6 (su1006)*] (outcrossed)
PK3071		*crIs13*[(*sur-5p::mCherry::tev-s-tag::unc-54* 3' utr) + *rol-6 (su1006)*]
PK3072		*lawd-1(tm4605)*; *myo-2p::gfp*
PK3073		*pxn-2(e1210)*
PK3076		*lawd-1(cr7)*
PK3077		*unc-119*
PK3088	BC1381	*dpy-18(e364)/eT1* III; *unc-46(e177) sDf29/eT1* V.
PK3089	BC2511	*dpy-18(e364)/eT1* III; *unc-60(e677) dpy-11(e224) sDf35/eT1* V.
PK3090	EG8920	*oxTi979*[*eft-3p::gfp::2xNLS::tbb-2* 3'utr + *HygroR*] I; *unc-119(ed3)* III.
PK3091	EG8926	*oxTi987*[*eft-3p::gfp::2xNLS::tbb-2* 3'utr + *HygroR*] V; *unc-119(ed3)* III
PK3092	LP162	*nmy-2*(*cp13* [*nmy-2::gfp* + *LoxP*]) I.
PK3093	MT13172	*mys-1(n4075)* V/*nT1* [*qIs51*] (IV;V).
PK3099-2	FT250	*unc-119(ed3)* III; *xnIs96*[*pJN455*(*hmr-1p::hmr-1::gfp::unc-54* 3'utr) + *unc-119*(+)]
PK3101	EU573	*orEx2*[*mlc-4p::mlc-4 genomic coding::gfp::unc-54* 3'utr + *rol-6 (su1006)*]
PK3105	JUP30	*unc119(ed3)*; *Is*[*plin-26::Lifeact::gfp::unc-54* 3'utr; *Cb-unc119*(+)]
PK3106	JUP38	*unc119(ed3)*; *Is*[*plin-26::Lifeact::mCherry::unc-54* 3′utr; *Cb-unc119*(+)]
PK3112	HS1215	*unc-76(e911)* V; *osEx211*[*apr-1::gfp* + *unc-76*(+)]
PK2050	JR667	*wIs51*[*SMCp::gfp* + *unc-119*(+)]; *unc-119 (ed3)* III
PK3147	CB1951	*unc-42(e270)*; *sma-1(e30)* V

Lab name	**Strain name**	**Genotype**
PK3152	VC601	*vab-10(ok817)* I/*hT2* [*bli-4(e937) let-? qIs48*] (I;III)
PK3158	FX17383	*lawd-1(tm6954)/nT1*
PK3196	MZE98	*unc-119(ed3)* III; *cbgIs98*[*pPept-1:gfp::rab-11.1*;*unc-119*(+)]
PK3197	JH2825	*axIs1943*[(*pFM050*)*mCherry::mlc-4* + *unc-119*(+)]
PK3198	SU295	*jcIs25*[(*pEP130(jac-1::gfp)* + *rol-6(su1006)*]
PK3199	EU1444	*orIs17*[*dhc-1p::gfp::dhc-1* + *unc-119*(+)]
PK3200	PS3729	*syIs78*[*ajm-1::gfp* + *unc-119*(+)]; *unc-119(ed3)* III
PK3201		*crIs11*[*lawd-1::mCherry::unc-119(pMQfos3)*]; *nmy-2*(*cp13*[*nmy-2::gfp* + *LoxP*])
PK3202		*crIs11*[*lawd-1::mCherry::unc-119(pMQfos3)*]; *unc119(ed3)*; *Is[plin-26::Lifeact::gfp::unc54* 3'utr *; Cb-unc119]*
PK3203		*crIs11*[*lawd-1::mCherry::unc-119* (pMQfos3)]; *zhIs396*[*pdlg-1::lifeact::gfp::unc-54* 3'utr, plin-48::gfp]
PK3204		*crIs11*[*lawd-1::mCherry::unc-119 (pMQfos3)*]; *wIs51* [*SCMp::gfp* + *unc-119*(+)]
PK3205		*crIs11*[*lawd-1::mCherry::unc-119 (pMQfos3)*]; *unc-119(ed3)* III; *cbgIs98*[*pPept-1:gfp::rab-11.1*; *unc-119*(+)]
PK3206		*lawd-1(cr7)*; *crIs11*[*lawd-1::mCherry::unc-119 (pMQfos3)*]
PK3207		*lawd-1(tm4605)*; *crIs11*[*lawd-1::mCherry::unc-119 (pMQfos3)*]
PK3208		*lawd-1(tm4605)*; *hmp-1::gfp*
PK3209		*lawd-1(tm4605)*; *dlg-1p::lifeact::gfp*
PK3230	PHX222	*syb222* [*lawd-1::mCh*(*knock-in*)]
PK3213	RT311	*pwIs69*[*vha6p::gfp::rab-11* + *unc-119*(+)]

Table 2-1 List of strains used in the project.

Name	Genotype/Composition	Note
pMQfos1	*lawd-1::unc-119*	
pMQfos2	*lawd-1::gfp::unc-119*	
pMQfos3	*lawd-1::mCherry::unc-119*	
pMQfos4	*lawd-1::gfp::tev-s-tag::unc-119*	
pMQfos5	*lawd-1::mCherry::tev-s-tag::unc-119*	
pMQ1	tev-S-tag in pBSKSII(+)	
pMQ2	*gfp::galK::tev-S-tag*	
pMQ3	*mCherry::galK::tev-S-tag*	
pMQ4	*unc-54* 3' utr in pBSKSII(+) EagI ends	
pMQ5	*gfp::tev-S-tag::unc-54* 3'utr	
pMQ6	*sur-5p::gfp::tev-S-tag::unc-54* 3'utr	
pMQ7	*mCherry::tev-S-tag::unc-54* 3' utr	
pMQ8	*sur-5p::mCherry::tev-S-tag::unc-54* 3' utr	
pMQ9	*sur-5p::gfp::tev-S-tag::unc-54 3'utr::Cbr_unc-119_MosSci*	
pMQ10	*sur-5p::mCherry::tev-S-tag::unc-54 3'utr::Cbr_unc-119_MosSci*	
pMQ11	*ajm-1p* in pBSKSII(+) with PstI ends	
pMQ12	*dpy-7p* in pBSKSII(+) PstI ends	
pMQ13	*ajm-1p::lifeact::gfp::unc-54* 3' utr::*Cbr_unc-119*	
pMQ14	*dpy-7p::lifeact::gfp::unc-54* 3' utr::*Cbr_unc-119*	
pMQ15	*lawd-1 5' end(exon-1b partial)::sfgfp::tbb-2 3' utr::lawd-1* 5'end (exon 1b partial)	
pMQ16	Target sequence: GACAGCACGTTAATATCCAT	sgRNA for *lawd-1* CRISPR indel (gfp)
pMQ17	*lawd-1 5' end(exon-1)::prps-0::hygR::unc-54* 3' utr::*lawd-1* 5' end(exon 1)	
pMQ22	Target sequence: TGTGTAGCTGTTACATCTTG	sgRNA for *lawd-1* CRISPR 5' del
pMQ23	Target sequence: GATTATTAAACTTCGATCAG	sgRNA for *lawd-1* CRISPR 5' del
pMQ24	Target sequence: CCAATATTCTTAGCTTCTGG	sgRNA for *lawd-1* CRISPR 5' del

pMQ25	Target sequence: CCTCTGAGTTGATCTTGAGG	sgRNA for *lawd-1* CRISPR 3' del
pMQ27	Target sequenceTGAGTCAGGCATAGGGTAGG	sgRNA for *lawd-1* CRISPR 3' del
pMQ28	Target sequence: GCTTCGACTGCGGAGTGAGG	sgRNA for *lawd-1* CRISPR 3' del
pMQ29	5'l*awd-1*UHA::HindIII::*lawd-1*DHA	repair template for *lawd-1* 5' CRISPR del
pMQ30	3'*lawd-1*UHA::EcoRI::*lawd-1*DHA	repair template for *lawd-1* 3' CRISPR del
pMQ31	Target sequence: GTTTTCACTGTCTGGATGAG	sgRNA for *lawd-1* C-term CRISPR mRFP ins
pMQ32	Target sequence: GGGATGAGAGGTTCTCTTTG	sgRNA for *lawd-1* C-term CRISPR mRFP ins
pMQ33	mRFP with 60 bp *lawd-1* homology arms in pBSKSII (+)	repair template for *lawd-1* C-term CRISPR mRFP ins
pMQ34	*lawd-1* UHA(600 bp)::mRFP::*lawd-1* DHA (600 bp)	repair template for *lawd-1* C-term CRISPR mRFP ins
pMQ35	*lawd-1* p1 in bluescript	
pMQ37	*lawd-1* UHA(600 bp)::mRFP::*lawd-1* DHA (600 bp)	repair template for *lawd-1* C-term CRISPR mRFP ins
pMQ38	Target sequence: TGTGTAGCTGTTACATCTTG	
pMQ39	Target sequence: CTGATCGAAGTTTAATAATC	

Table 2-2 List of plasmids generated for this project.

PK1057	TCCTCCCTTGCAATGGGTAG
PK1058	CTGACGTCTCCGAAACACAG
PK1059	CTCCGCCAGTTACGTCTCTG
PK1134	GTCATGCACAACAAAGCCGAC
PK1136	CCCTATAGTGAGTCGTATTA
PK1138	CATGAACTGGACCCGATCGT
PK1139	[AAGGCGCGAATATTTACGGAATCCTCAAAGAGAACCTCTC ATCCAGACAG]gggaagttcctatactttctagagaata
PK1140	[ACAAATATGTTTTCTATCACAGATTTTATAATTGGAGGATCA CAGTGTTT] TCActtgtacagctcgtccatgccgcc
PK1148	TTTCCTGTCACACCACACTC
PK1149	CTCGAGTATCAAGCTTATCG
PK1164	ATGTCAGGGCCAATGAACAG
PK1165	ATTGGTGCAGCAAACAGGCC
PK1173	tAAGCTTCTTCTCCTTCTTCCAATACGTTC
PK1174	tAAGCTTGATCAATACGTTTCAGTTTTTGAC
PK1175	aggatccCACATTTAAACTATTGAAATACGGAG
PK1176	tgagctCTGGATTAGATTTTTACTTGGAAC
PK1177	agctagcCACATTTAAACTATTGAAATACGGAG
PK1178	tggtacCTGGATTAGATTTTTACTTGGAAC
PK1184	GTGGTTGGACGAAGTGGAG
PK1185	GACAGAATAATCTAACAAGACC
PK1186	aggatccATGCAAAATGAAACACCTTCCT
PK1187	tctcgagTTAACTATCACCAACACGTGCGTA
PK1237	actgcagCCAGTTGCATATCGAATTGCC
PK1238	actgcagTTCGTCCTTGGTTCTGTAAAG
PK1239	tctgcagCTCATTCCACGATTTCTCGC
PK1240	tctgcagTCTGGAACAAAATGTAAGAATATTC
PK1261	gctgcaggaattcgatCGTTCTGTGTCATTCTGTC
PK1262	tttacgcatTACACATGTGAACTGTTGTTTC
PK1263	acatgtgtaATGCGTAAAGGCGAAGAG
PK1264	catttatcttaTTTGTACAGTTCATCCATACC
PK1265	ctgtacaaataaGATAAATGCAAAATCCTTTCAAG

PK1266	gctgatcgTGAGACTTTTTTCTTGGCG
PK1267	aaagtctcaCGATCAGCTATCCTAGCTG
PK1268	ggtatcgataagcttgatCAGTGAACACCCATGTCG
PK1173_M	GCGCGTCAAGTTGTGGACAGCACGTTAATATCCATGTTTTAGAGCTAGAA
PK1174_M	TTCTAGCTCTAAAACATGGATATTAACGTGCTGTCCACAACTTGACGCGC
PK1269	gcgcgtcaagttgtGACAGCACGTTAATATCCATGTTTTAGAGCTAGAA
PK1270	TTCTAGCTCTAAAACATGGATATTAACGTGCTGTCacaacttgacgcgc
PK1271	GCTTTGAAGGGACTCGAGCA
PK1272	GCCCAGGATATTGCCGTCTT
PK1273	TAAGGATGACGGCACGTACA
PK1274	GATGTTACCGTCACCATTCG
PK1285	ACCCGGGCACATTTAAACTATTGAAATACGGAG
PK1286	TCCCGGGTGGATTAGATTTTTACTTGGAAC
PK1287	gctgcaggaattcgatGCATCTTCTTCCATCACC
PK1288	catcttcatTGCTCGAGTCCCTTCAAAG
PK1289	ctcgagcaATGAAGATGAACGCAAGG
PK1290	cccacacaAGTTGAAACAGTTATGTTTGG
PK1291	actgtttcaactTGTGTGGGAAAACTATTCAG
PK1292	ggtatcgataagcttgatATGACCAGCAACCACAAATAAATC
PK1293	gcgcgtcaagttgtGGCCCGACTAAAAAACGTGGgttttagagctagaa
PK1294	ttctagctctaaaacCCACGTTTTTTAGTCGGGCCacaacttgacgcgc
PK1295	gctgcaggaattcgatCTGTTCGACACAACCACTG
PK1296	acggccgccatGCTAGCCAAGGGTCCTCC
PK1297	tggctagcATGGCGGCCGTAGGGTCC
PK1298	gaggccatAGCGGCCGCTTTTAGATCTCG
PK1299	cggccgctATGGCCTCCTCCGAGGAC
PK1300	ggtatcgataagcttgatGTTTGCGTATTGGGCGCTC
PK1301	GATACGTCCTCCGTGTCAAC
PK1302	GTCATGAGAGGCCCAGACGT

PK1509	gcgcgtcaagttgtGTGTGTAGCTGTTACATCTTGgttttagagctagaa
PK1510	ttctagctctaaaacCAAGATGTAACAGCTACACACacaacttgacgcgc
PK1511	gcgcgtcaagttgtGGATTATTAAACTTCGATCAGgttttagagctagaa
PK1512	ttctagctctaaaacCTGATCGAAGTTTAATAATCCacaacttgacgcgc
PK1513	gcgcgtcaagttgtGCCAATATTCTTAGCTTCTGGgttttagagctagaa
PK1514	ttctagctctaaaacCCAGAAGCTAAGAATATTGGCacaacttgacgcgc
PK1515	gcgcgtcaagttgtGCCTCTGAGTTGATCTTGAGGgttttagagctagaa
PK1516	ttctagctctaaaacCCTCAAGATCAACTCAGAGGCacaacttgacgcgc
PK1517	gcgcgtcaagttgtGAGACTGCGAATTGCGTTGAGgttttagagctagaa
PK1518	ttctagctctaaaacCTCAACGCAATTCGCAGTCTCacaacttgacgcgc
PK1519	gcgcgtcaagttgtGTGAGTCAGGCATAGGGTAGGgttttagagctaga a
PK1520	ttctagctctaaaacCCTACCCTATGCCTGACTCACacaacttgacgcgc
PK1521	gcgcgtcaagttgtGGCTTCGACTGCGGAGTGAGGgttttagagctaga a
PK1522	ttctagctctaaaacCCTCACTCCGCAGTCGAAGCCacaacttgacgcg c
PK1590	tcttGTTTTCACTGTCTGGATGAG
PK1591	aaacCTCATCCAGACAGTGAAAAC
PK1592	tcttGGGATGAGAGGTTCTCTTTG
PK1593	aaacCAAAGAGAACCTCTCATCCC
PK1594	TATACTCCAAAAGGCGCGAATATTTACGGAATaCTCAAAGA GAAtCTCTCATCCAGACAGatggcctcctccgaggacgt
PK1595	AATATTAACAAATATGTTTTCTATCACAGATTTTATAATTGGA GGATCACAGTGTTTTCAggcgccggtggagtggcggc
PK1598	GGACCCATACCAACTTATTC
PK1599	CGACTATCATCTTATCAGCAC
PK1619	TGTTCAATGGTCGGGACTTC
PK1620	GAACGTGGCAAATCAGTGCT
PK1646	CACCAAATTGTTTCACGCTTC
PK1647	CTCCGCTGATAGTTTCACTTC
PK1672	gctgcaggaattcgatGTGAATAGTGTCTGTTGTTAG
PK1673	tggagtataGTCATTGCCAACTGACAC

PK1674	gcaatgacTATACTCCAAAAGGCGCG
PK1675	tattcaaactAATATTAACAAATATGTTTTCTATCACAG
PK1676	ttgttaatattAGTTTGAATAACCATAAATATTCTGAAATAG
PK1677	ggtatcgataagcttgatCGTGAAATTAACATCCCG
PK1678	CAAGCTAAGAAACTGGTGAG
PK1679	GAGCCTCTTTACGGAATGC
PK1684	tcttGGGTCCTTGTGGGATATATC
PK1685	aaacGATATATCCCACAAGGACCC
PK1686	tcttGCGATGATGATGGTCCTTGT
PK1687	aaacACAAGGACCATCATCATCGC
PK1688	CAATTtCAGATATATtCCACAAGGACCATCATCATCGTCTTC AAAGatgagtaaaggagaagaac
PK1689	CATTCAAAAACATAGGAAAAAAAATTAAATCGAATCAATTAA ATCAtttgtatagttcatccatg
PK1690	gctgcaggaattcgatCCGATTATGAAGATTCGC
PK1691	ctgaaattgAATTTTTATTTTAAAATCGAAAATTTCAGG
PK1692	aaaataaaaattCAATTTCAGATATATTCCACAAGG
PK1693	aaaagtaaaatCATTCAAAAACATAGGAAAAAAAATTAAATC
PK1694	tttttgaatgATTTTACTTTTTTTTTTCTTAATTTTTTAATATGTACC C
PK1695	ggtatcgataagcttgatGTGCGAATTGGCTGGAATTTG
PK1696	GACTCGATGCGATCTTTCAC
PK1697	GAGCTCAGCAATGTATCCAG
PK1698	CTGAGACAAAGGTGACGAGC
PK1699	CATGATGCTGAGGTGCTGTG
PK1700	GAAGAGATGCTGAAGACACC
PK1701	GACCACTTCTTCAACCCACG
PK1702	GTGAATAGTGTCTGTTGTTAG
PK1703	CGTGAAATTAACATCCCG
PK1762	ccgggctgcaggaattcgatCTGTTCGACACAACCACTG
PK1763	tgggaaacatCTGGATTAGATTTTTACTTGGAAC
PK1764	tctaatccagATGTTTCCCATCTGGTTTAATTTTC
PK1765	cggaggaggccatATCACCAACACGTGCGTAG

PK1766	tgttggtgatATGGCCTCCTCCGAGGAC
PK1664	gatcttgcatTTAGGCGCCGGTGGAGTG
PK1665	cggcgcctaaATGCAAGATCCTTTCAAGC
PK1659	acggtatcgataagcttgatGAGACTTTTTTCTTGGCG
PK1767	CCTTCAAGCCCATCTTCCAC
PK1768	CCATGCAGTCTTGAACGTGG
PK1769	GTCGATAAGAGTCTTCAAGC
PK1770	GCATGAACTCCTTGATGACG
PK1771	GGACGAGTTCCTCCACAAAC
PK1772	CGATGGAGCACGTGGAATTC
PK1773	GGCGCGAATATTTACGGAATcCTCAAAGAGAAtCTCTCATC
PK1774	GATGAGAGaTTCTCTTTGAGgATTCCGTAAATATTCGCGCC
PK1775	ttcaggaggacccttggctagcgtcgacggtaccggtagaaaaaATGTTTCCC ATCTGGTTTAATTTTC
PK1776	cggaggaggccatATCACCAACACGTGCGTAG
PK1777	tgttggtgatATGGCCTCCTCCGAGGAC
PK1778	agcgaccggcgctcagttggAATTCGCTAGCTTAGGCGC
PK1779	GTCCAACATTCGTCGTTGGATATG
PK1780	CATATCCAACGACGAATGTTGGAC
PK1855	ACGGAATaCTCAAAGAGAAtC
PK1856	ACGGAATCCTCAAAGAGAAtC
PK1857	CCTCCAATTATAAAATCTGT
PK1861	tcttTGTGTAGCTGTTACATCTTG
PK1862	aaacCAAGATGTAACAGCTACACA
PK1863	tcttCTGATCGAAGTTTAATAATC
PK1864	aaacGATTATTAAACTTCGATCAG
PK1865	CACAAACGAAACAACAGTTCACATGTGTAGCTGTTACATCg gatccTTCTGGTGGAAGAGATCGATTTGTTCACGTATTTAGAA GA
PK1866	GCATTCACGCAATACAATCC
PK1867	ATAATTGGAGGATCACAGTG
PK1868	TACGGAATCCTCAAAGAGAAtC
PK1869	CACAGATTTTATAATTGGAGGATC

PK1870	GACGATACTTCTCTGGCTATGG
PK1871	GAAGGCATCGTCATGAGTG
PK1872	GCTCAACAGCATCACATGATAG
PK1873	GTGTACAGGTGAAGTTGACCG
PK1875	tcttAGTAAAAATCTAATCCAGAT
PK1876	aaacATCTGGATTAGATTTTTACT
PK1877	CACAAACGAAACAACAGTTCACATGTGTAGCTGTTACATCg ggatccTTCTGGTGGAAGAGATCGATTTGTTCACGTATTTAGA AGA

Table 2-3 List of primers used in this project.

Chapter 3 **Phenotypic analysis indicates *lawd-1* encodes an essential gene**

3.1 Phenotypic analyses of *lawd-1* mutants *cr7*, *tm4605*, and *tm6954*

The background information of how *cr7* mutation was identified genetically in previous work in the lab had been outlined in Chapter 1.8 Background to the identification of the *lawd-1* gene.

In order to determine whether *lawd-1* is an essential gene, a new mutant allele *tm4605* was acquired from Dr. Shohei Mitani. The reason for obtaining a new mutant was because when *cr7* was placed in *trans* to a deficiency (*sDf35* and *sDf29*), increased embryonic lethality was observed (PEK unpublished work) which indicated that it was unlikely to be a null allele (PEK unpublished work). *tm4605* is a *lawd-1* allele carrying a 651 bp deletion toward the 3' end of the gene (Figure 3-1A). Information reported on wormbase.org categorised *tm4605* as a null allele. However, after obtaining this mutant, it was placed in *trans* to a balancer *nT1* and instead it was found out that the deletion was homozygous viable.

A third deletion allele became available later in the project and it was again acquired from Dr. Shohei Mitani. This mutation was named *tm6954*, which carries a larger deletion of 1431 bp that partially overlaps the region removed by *tm4605* (Figure 3-1B). The strain obtained carried *tm6954 in trans* with the *nT1 (gfp)* balancer.

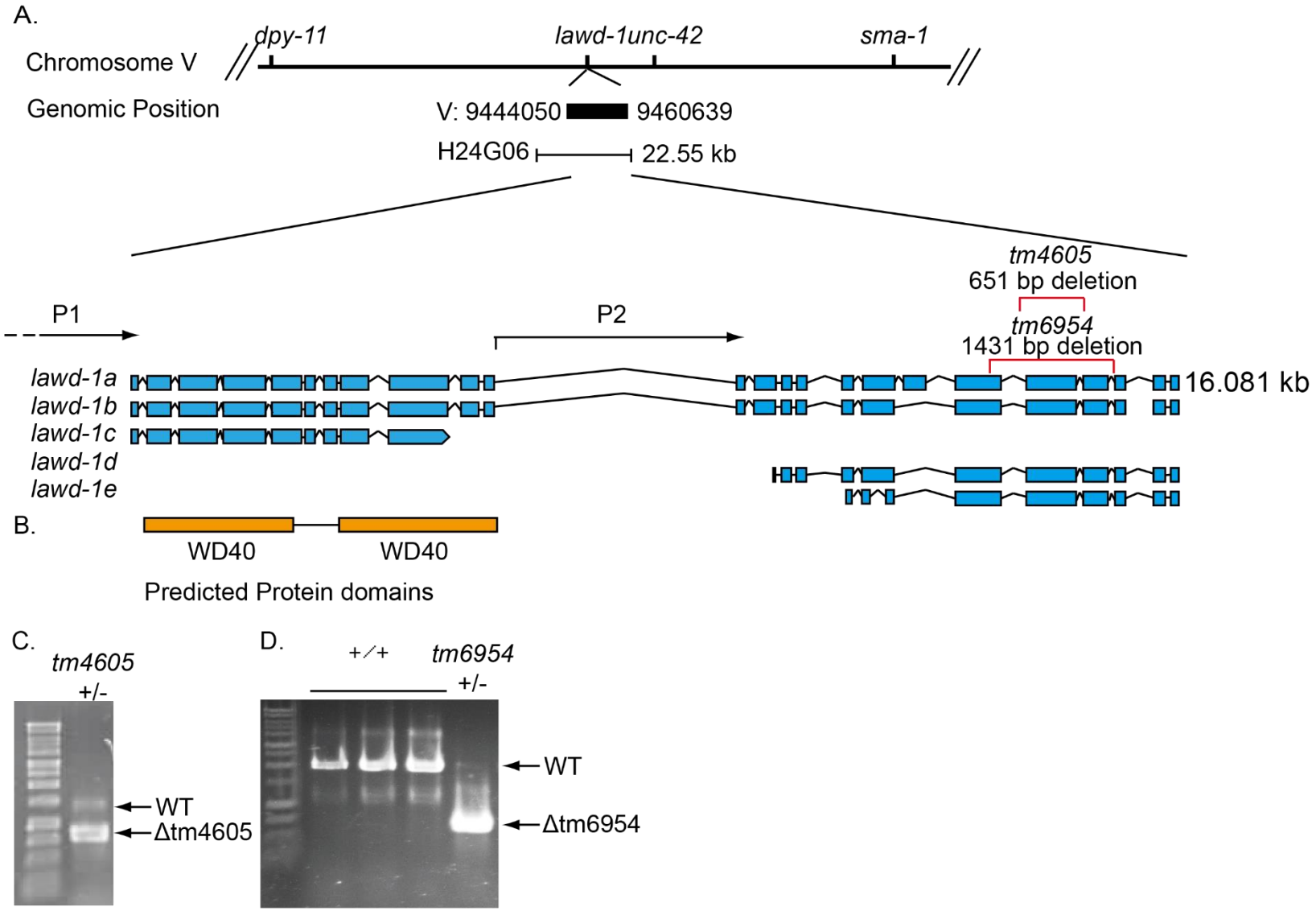
A.
Chromosome V
dpy-11
lawd-1
unc-42
sma-1
Genomic Position
V: 9444050
9460639
H24G06
22.55 kb
tm4605
651 bp deletion
tm6954
1431 bp deletion
P1
P2
lawd-1a
lawd-1b
lawd-1c
lawd-1d
lawd-1e
16.081 kb
B.
WD40
WD40
Predicted Protein domains
C.
tm4605
+/-
WT
Δtm4605
D.
+/+
tm6954
+/-
WT
Δtm6954

Figure 3-1 Genetic organisation of *lawd-1* gene and the position of *lawd-1* mutations.

A. See Figure 1-10 legend for the discovery of *lawd-1* gene and the *cr7* mutation. The mutations of *tm4605* and *tm6954* were shown as bracketed regions above the different *lawd-1* predicted transcripts. **B** The 5' end of the longest *lawd-1* transcripts is predicted to encode two WD40 domains each consisting of 7 WD40 repeats. **C.** Single worm PCR gel analysis using heterozygous *tm4605* animal indicates that it carries a deletion of 651 bp, corresponding to the lower band on the gel picture. **D.** Single worm PCR gel analysis using heterozygous *tm6954* animal indicates that it carries a deletion of 1431 bp, corresponding to the lower band on the gel picture.

The *cr7* mutant displays highly penetrant head morphogenetic defects (Figure 3-2E) with 80.4% ([148.8 Vab adults+12.3 arrested Vab larva]/200.3) of the total brood (N=5) showing this particular Vab phenotype, 74.3% of these animals developed into viable adults, whereas 6.1% of animals arrested during larval development. An additional 4.1% of *cr7* animals displayed embryonic lethality (Table 3-1).

After outcrossing the *tm4605* mutant 5 times to remove potential extragenic mutations, brood counts were carried out and the results indicated that although *tm4605* mutant is not a null allele since placing it in trans to a balancer *nT1* showed this mutant was heterozygous viable, *tm4605* animals have more severe morphogenetic defects than *cr7* animals (Figure 3-2B, F; Table 3-1). *tm4605* mutants not only had more severe morphogenetic defects, but they also displayed higher percentages of arrested larva and embryos when compared to *cr7* (Table 3-1). Only 26.4% of Vab *lawd-1* (*tm4605*) animals developed into viable adults, 37.9% of *tm4605* animals arrested during larval development and 10% arrested as embryos (Table 3-1). Brood sizes of individual *tm4605* animal (N>5) was highly variable, as indicated by the large standard error of the mean (Table 3-1).

tm6954 mutants also displayed high percentage of embryonic lethality (Figure 3-2C). *tm6954* mutant was outcrossed 5 times and characterised in the same way as the previous two mutants. Surprisingly, the observed number of lethal embryos was 70%, whereas the expected value was only 50% (Table 3-1). This could possibly be caused by the translocation balancer and because of this potential complication, the balancer was replaced with the LGV markers *dpy-11 unc-42,* which span the interval carrying the *lawd-1* gene. These two markers produce a

visible double-mutant phenotype, which is a combination of uncoordinated (Unc) and dumpy (Dpy). The resulting *tm6954/ dpy-11 unc-42* strain was characterised by counting broods. It was found that ~24% of progeny displayed embryonic lethality (Table 3-1), confirming that *lawd-1* has an essential role in development. The percentage of wild-type heterozygotes and recombinants were all categorised as non-Vab animals in Table 3-1 to avoid confusion. This strain also produced highly variably sized broods (N=5) indicated by the high standard error of the mean. It was also noted that the average brood size increased when the balancer for *tm6954* was changed from *nT1* to *dpy-11 unc-42* (Table 3-1), which supports the hypothesis that the *nT1* translocation balancer was itself contributing *in* trans to *tm6954* lethality.

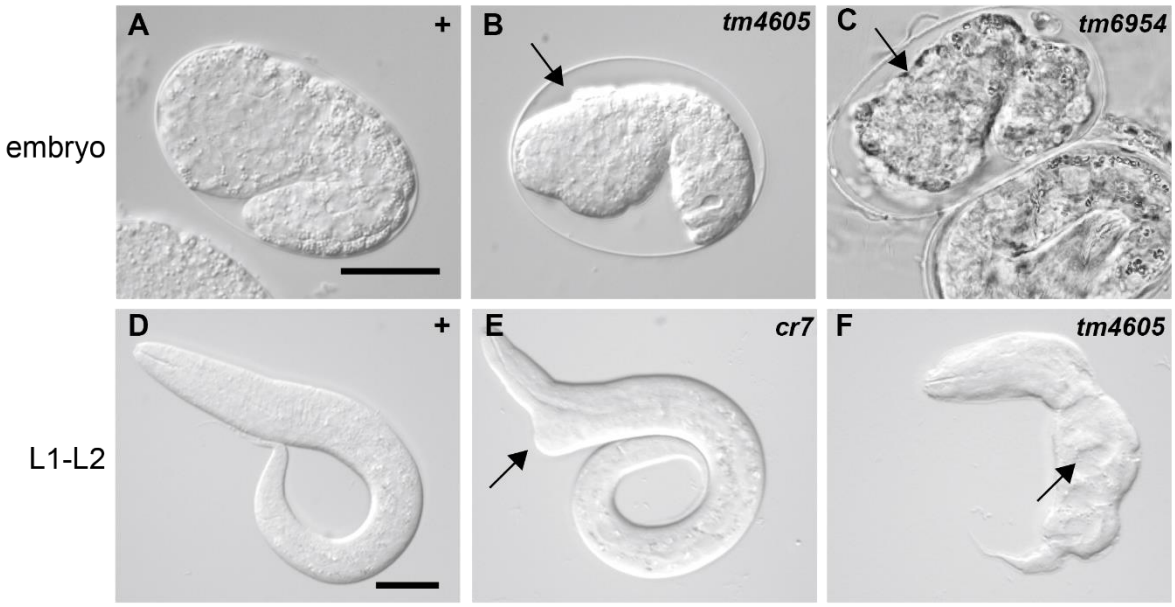

Figure 3-2 *lawd-1* mutants display Variable abnormal (Vab) body morphogenetic defects

Nomarski Differential Interference Contrast (DIC) images of wild type (N2) and three *lawd-1* mutants during embryonic development and early larval development stages. **A.** A Wild type 1.5 fold stage embryo. **B.** A *lawd-1* (*tm4605*) 1.5 fold stage embryo. The epidermis showed significant shrinkage compared with wild type as indicated by the arrow. Epidermis was also detached from the cuticle. **C.** A *lawd-1* (*tm6954*) 1.5 fold stage embryo. The epidermis showed significant shrinkage compared with wild type as indicated by the arrow. **D.** A wild type L1 stage larvae. **E.** *lawd-1* (*cr7*) L2 stage larvae with a notched head indicated by the arrow. **F.** A *lawd-1* (*tm4605*) arrested L1 stage animal. Animals also developed large intestinal vacuoles indicated by the arrow. Left – right = Anterior – posterior Scale bar = 20 µm

Alelle	**Brood size**	**Embryonic lethal**	**Larval lethal**	**Vab adult**	**Non-Vab adult**
+/+	217 ± 3.2	0	0	0	217 ± 3.2
cr7	200.3 ± 17.1	8.3 ± 1.9	12.3 ± 0.85	148.8 ± 12.4	31 ± 5.4
tm4605	222.8 ± 23.7	22.2 ± 6.3	84.5 ± 16.3	58.8 ± 3.8	57.3 ± 14.1
tm6954/nT1	138.2 ± 9.4	95.6 ± 7.8	0	0	40 ± 2.5
tm6954/dpy-11 unc42	216.8 ± 18.0	51.2 ± 6.1	0	0	165.6 ± 14.8

Table 3-1 Phenotypic analyses of 3 *lawd-1* mutants.

Brood counts of N2 (+/+), *lawd-1 (cr7), lawd-1 (tm4605), lawd-1(tm6954/nT1), lawd-1(tm6954/dpy-11 unc42)*. Phenotypes are categorised into four types namely embryonic lethal, larval lethal, Vab adult and Non-Vab adult. Animals were counted for each category with standard error of mean determined between plates (N=5). More than 1000 worms were counted from each strain.

3.2 *cr7* and *tm4605* mutants can be rescued by full length *lawd-1* genomic clone.

In order to prove that the Vab phenotypes were indeed caused by *cr7* and *tm4605* mutations, an integrated transgenic allele *crIs11* containing full genomic region of *lawd-1* gene tagged with mCherry (LAWD-1::mCh) was used to rescue the phenotypes. Details about cloning and making this transgenic line can be found in Chapter 4. Animals carrying this reporter were first mated with either *cr7* or *tm4605* animals. Subsequently, the strains were made homozygous for both the mutation and transgene insertion alleles. Broods for both rescued lines were then counted in the same way as previously described. Results indicate that both strains were successfully rescued by the transgenic allele *crIs11* (Table 3-2, Figure 3-3). This supports the observation that the Vab and lethal phenotypes were indeed caused by a mutation in *lawd-1*. However, the average brood size of the rescued *tm4605* animals was reduced compared to the original mutant, possibly because brood size varies greatly between animals as previously observed. Many unsuccessful attempts have been made to rescue *tm6954* animals with the *crIs11* transgene. The difficulty in mating appears to arise from the strong Rol (rolling) phenotype caused by expression of the co-transformation marker *rol-6* present in the *crIs11* transgene.

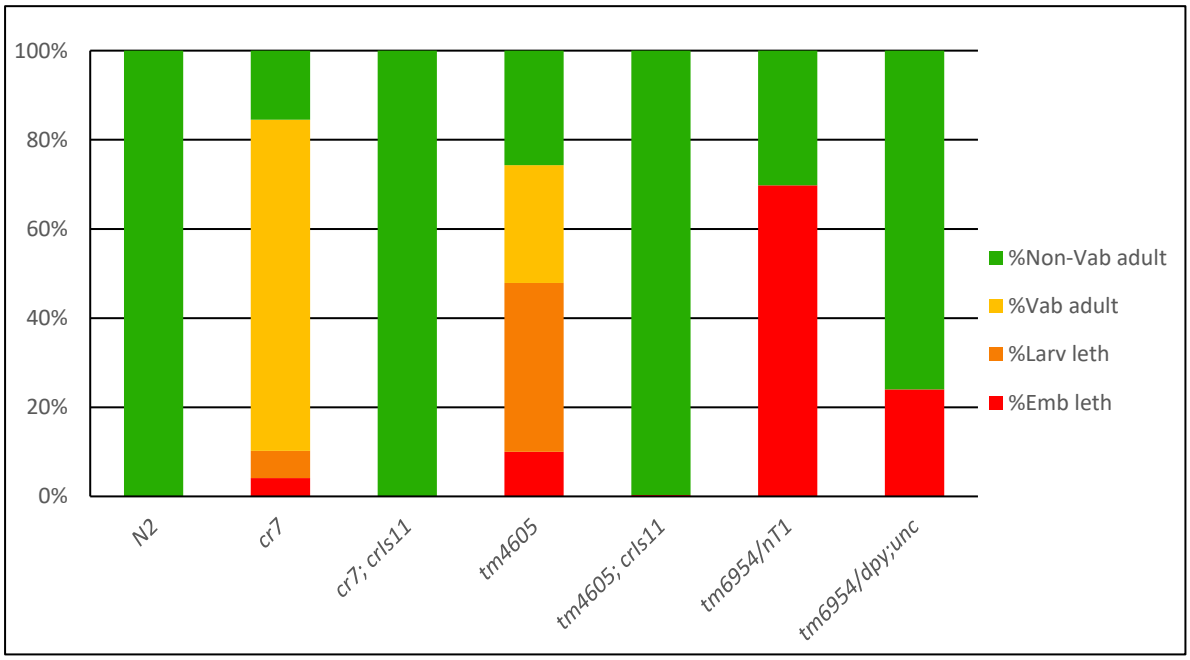

Figure 3-3 Percentage phenotypes of wild type, *lawd-1* mutants and *lawd-1* rescued lines.

Phenotypic analysis of table 3-1-1 and 3-2-1 represented in a graph form. Different colours indicate different phenotypes as explained in the graph. % Larv leth = % Larval lethality. % Emb leth = % Embryonic lethality. Average counts for each phenotype of each strain were used to construct the graph without showing the standard error of the mean.

Alelle	Brood size	Embryonic lethal	Larval lethal	Vab adult	Non-Vab adult
+/+	217±5.6	0	0	0	217±5.6
cr7;*crIs11*	209±5.5	0	0	0	209±5.5
tm4605;crIs11	160.5±45.9	0.5±0.5	0	0	160±36.3

Table 3-2 Transgenic rescue of three *lawd-1* mutants.

Brood counts of N2 (+/+), *lawd-1* (*cr7*)*;crIs11, and lawd-1* (*tm4605*)*;crIs11.* Phenotypes are categorised into four types namely embryonic lethal, larval lethal, Vab adult and Non-Vab adult. Animals were counted for each category with standard deviations determined between plates (N=5). More than 1000 worms were counted from each strain.

3.3 Discussion

Genetic and phenotypic analyses indicate that *lawd-1* is indeed an essential gene. *tm6954* is a deletion allele located close to the 3' end. Taken together with the evidence provided by the other deletion mutants *cr7* and *tm4605*, it appears that the C-terminus part of the protein is important for LAWD-1 function. As a mutant removing the 5' end encoding the WD40 is not yet available, it would be desirable to determine if disruption of the 5' end would cause similar phenotypes. The CRISPR-Cas9 technique was employed to make a 5' deletion mutant, however, the desired mutant was not generated at the end of the study. *tm6954* mutant showed embryonic lethality characterised by embryos arrested at around 1.5-fold stage (Figure 3-2). Although the *tm4605* mutant is viable, the significant percentage of embryos arrested also appear to be at around 1.5-fold stage (Figure 3-2). The embryos failed to elongate and also showed severe morphogenetic defects; therefore, it appears that *lawd-1* gene function might be important at this stage of embryonic development. It was discussed previously that an actomyosin network and microtubules are important for elongation before 2-fold stage whereas elongation beyond two fold stage not only require the actomyosin network but also muscle contraction (144). Co-ordination between the epithelia and the muscle cells is important to prevent detachment of epithelia from the underlying muscle which can cause rupture of embryos (147). The *C. elegans* hemidesmosome-like junctions (CeHD) can act as a mechanical transducer in the epithelia through ECM to muscle cells (129), therefore it will be useful to see if CeHD components are disrupted when *lawd-1* is mutated. This can be done through generation of double mutants.

When trying to rescue the null mutant *tm6954*, it was noted that the *tm6954*/+ males appeared much shorter compared with wild type animals and were not able to successfully mate even though there is only a single copy of the mutant allele. This short nature of the males is also an indication that there may be elongation issues with the mutant.

During genetic mapping of the *cr7* mutation, it was observed that when *cr7* was combined with *sma-1*, which encodes for *C. elegans* β-H-spectrin (160), synthetic lethality was observed (J. Hodgkin, unpublished), which is usually an indication that the two genes might be involved in similar processes or similar pathways. *sma-1* is an essential gene required for *C. elegans* embryonic elongation, a process which requires co-ordination of cytoskeleton assembly/disassembly in epithelial cells and also muscle movements as discussed in chapter 1. This interaction was not further explored in this study, it would be useful to build a double mutant of *sma-1* and the other viable *lawd-1* mutant *tm4605.*

Based on the information on wormbase.org, the closest *lawd-1* human homologue gene is *WDR62*. BLAST protein alignment using LAWD-1A and LAWD-1B predicted amino acid sequences both showed 29% similarity with 54% sequence covered (e-Value = 2e -83). *WDR62* was initially identified in genetic screen in patients with microcephaly (194). Studies have since shown that WDR62 is involved in JNK signalling pathway and mitotic spindle assembly (195) (196), although the precise role of WDR62 and the cause of the microcephaly disease is still unknown. Understanding the role of LAWD-1 might provide insight in the function of WDR62. A cDNA clone of WDR62 was available although no successful reporter was

generated from it in this project. It would be interesting to see in the future if WDR62 can be expressed in C. elegans given the protein sequence similarity.

Another human homologue identified in the wormbase.org database is WDR16. Little is known about this protein, but it was detected in the seminiferous tubules in the testes in human. It is explained in Chapter 4 that LAWD-1::mCh were also detected in tubular structures, therefore the tubular localisation of this homologue is an interesting correlation.

Chapter 4 The LAWD-1::mCh reporter is apically enriched in epithelial tissues and changes pattern in seam cells during embryonic elongation

4.1 LAWD-1::GFP and LAWD-1::mCh revealed that LAWD-1 is enriched in intestinal epithelia

Given that *lawd-1* mutants display morphogenetic defects, it was desirable to explore the expression pattern and subcellular localisation of LAWD-1 protein in epithelial tissues. It was anticipated that this would provide insights about the role of LAWD-1 during epithelial development. Two fluorescent reporter constructs were constructed using fosmid recombineering to accommodate the large size of the complete *lawd-1* genomic region (fosmid WRM0623dG12). This fosmid was engineered to carry either the *gfp* or *mCherry* gene sequence at the 3' end of *lawd-1* coding region. Several other tagged versions of *lawd-1* reporters were also made containing a LAP (Localisation and Affinity Purification) tag, but they were not used in the imaging studies presented in this chapter (See Table 2-1 and Table 2-2). To generate the expression fosmid, a *Cbr-unc-119* marker gene (Table 2-2) was constructed that was subsequently inserted into the fosmid backbone through recombineering to serve as a positive selection marker after biolistic bombardment. The next step involved inserting the appropriate fluorescent tags at the 3' end of the *lawd-1* gene. The C-terminus was the position selected to express the fluorescent tag, because it is present in all major LAWD-1 isoforms. Thus, it would permit detection of most LAWD-1 isoforms. A small number of fluorescent lines were obtained through biolistic bombardment, but all of the reporters were found to carry

extrachromosomal arrays. Hence, the fosmid reporters were then microinjected with the RoI (pRF4) co-transformation marker and several lines were obtained from each construct. One of each of the GFP and mRFP expressing transgenic lines was then subjected to gamma irradiation using ^{137}Cs to obtain chromosomally integrated versions of both reporters. Two of the strains obtained were used to analyse the intracellular localisation of LAWD-1::mCh (*crIs11*[*lawd-1::mCherry::unc-119* (pMQfos3) + *rol-6* (*su1006*)]) and LAWD-1::GFP (*crIs12*[*lawd-1::gfp::unc-119*]) (Table 2-1).

Initial fluorescent imaging studies revealed that LAWD-1::GFP (*crIs12*[*lawd-1::gfp::unc-119*]) and LAWD-1::mCh *crIs11*[*lawd-1::mCherry::unc-119* + *rol-6*]) could be detected in the developing intestine at the lima bean stage (Figure 4-1 E, M), and that fluorescence from these reporters could be detected throughout embryonic development. LAWD-1::mCh was most prominently detected in the developing intestine (Figure 4-1 F,G N,O). Around the 2-fold stage and slilghtly beyond, expression of both reporters were observed in the pharynx and in some hypodermal cells (Figure 4-1 H,P). The implications of these patterns will be discussed below in the context of their intracellular localisation compared to co-expressed markers.

The expression patterns of LAWD-1::GFP and LAWD-1::mCh in larval tissues were also examined. LAWD-1::mCh and LAWD-1::GFP were detected as diffuse signals in the seam cells of all larvae observed (Figure 4-2 H, N). Fluorescent signals were also observed in the intestine (Figure 4-2 G, M) and pharynx (Figure 4-2 E). Both reporters were also detected along the apical surface of the spermathecal lumen and also the vulva (Figure 4-2 F, L).

Several epithelial markers (HMP-1::GFP, DLG-1::GFP, lifeact::GFP) were used in subsequent analyses to further characterise the subcellular localisation of LAWD-1::mCh during epithelia development. As shown in Figure 4-1, both the LAWD-1::mCh and LAWD-1::GFP reporter strains produced similar temporal and spatial expression patterns. Thus, the LAWD-1::mCh reporter strain was used when constructing strains because most of the other protein markers being examined were available as GFP fusion proteins. The double fluorescent strains were made by crossing LAWD-1::mCh integrated strain into the reporter strain and the expression of both reporters were examined by confocal microscopy.

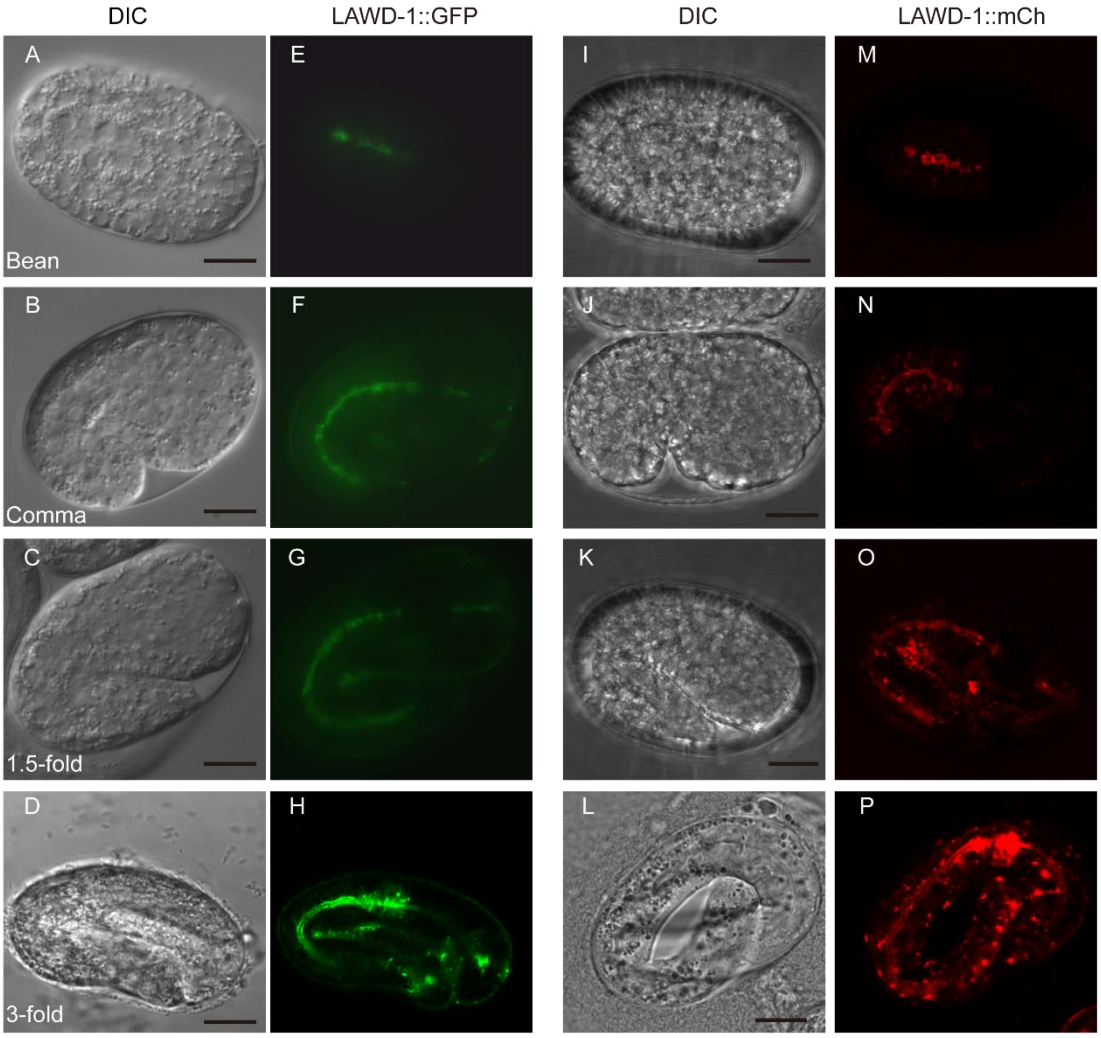

Figure 4-1 Similar patterns of expression observed with LAWD-1::GFP and LAWD-1::mCherry reporters during embryonic development.

A-D. Nomarski DIC images of *C. elegans* embryos carrying LAWD-1::GFP at the indicated stages on the left corner of each panel. **E-H.** Fluorescent microscopy of LAWD-1::GFP expression enriched in the developing intestine in the same embryos showing in A-D **. I-L.** Nomarski DIC images of *C. elegans* embryos carrying LAWD-1::mCherry at the indicated stages on the left corner of each panel**. M-P.** Fluorescent microscopy of LAWD-1::mCherry expression enriched in the developing intestine in the same embryos showing in I-L. Scale bar = 10 µm.

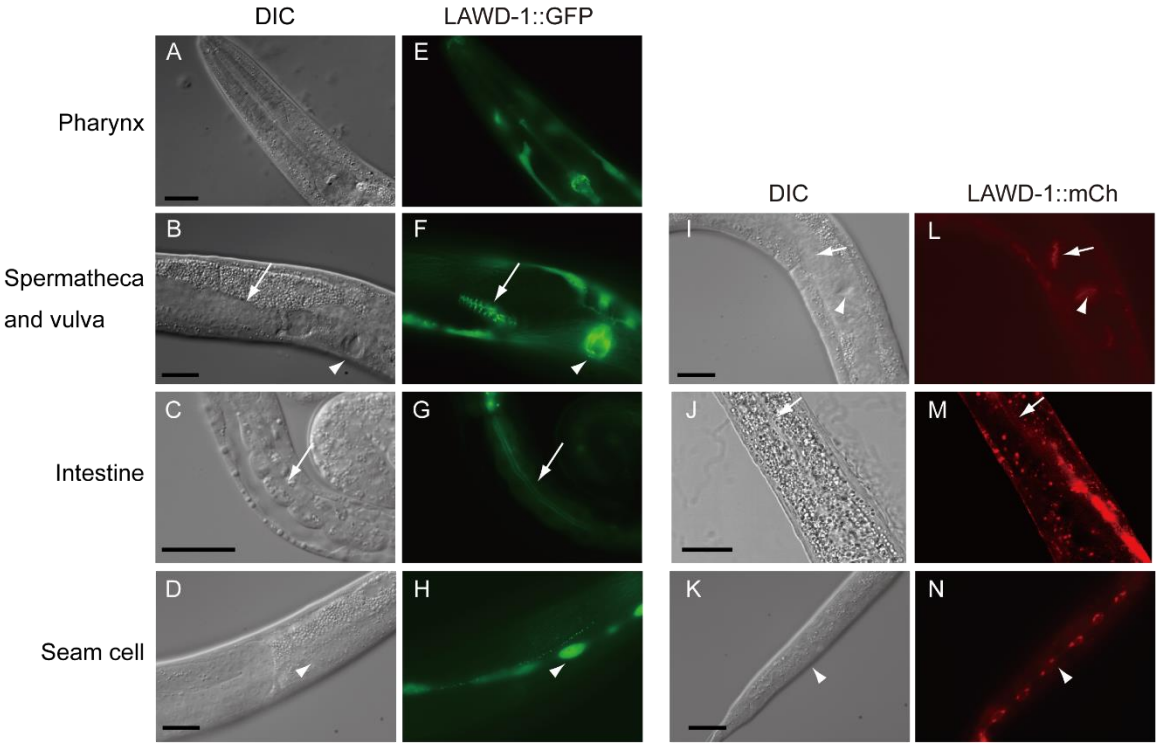

Figure 4-2 Expression of LAWD-1::GFP and LAWD-1::mCh in larval tissues.

A-D. Nomarski DIC images of *C. elegans* larva carrying LAWD-1::GFP. **E-H.** LAWD-1::GFP expression in the same focal plane as image in left panel. **E.** LAWD-1::GFP observed in pharynx in an L3 stage animal. **F.** LAWD-1::GFP observed in developing spermathecal lumen (arrow) and vulva (arrow head) in an L4 stage animal. **G.** LAWD-1::GFP observed in fully developed intestine in an L2 stage animal. **H.** LAWD-1::GFP observed in seam cells (arrow head) in an L3 stage animal. **I-K.** Nomarski DIC images of *C. elegans* larva carrying LAWD-1::mCh. **L-N.** LAWD-1::mCh expression in the same focal plane as image in left panel. **L.** LAWD-1::mCh observed in developing spermathecal lumen (arrow) and vulva (arrow head) in an L4 stage animal. **M.** LAWD-1::mCh observed in fully developed intestine in an L2 stage animal. **N.** LAWD-1::mCh observed in seam cells (arrow head) in an L3 stage animal. Scale bar = 20 µm.

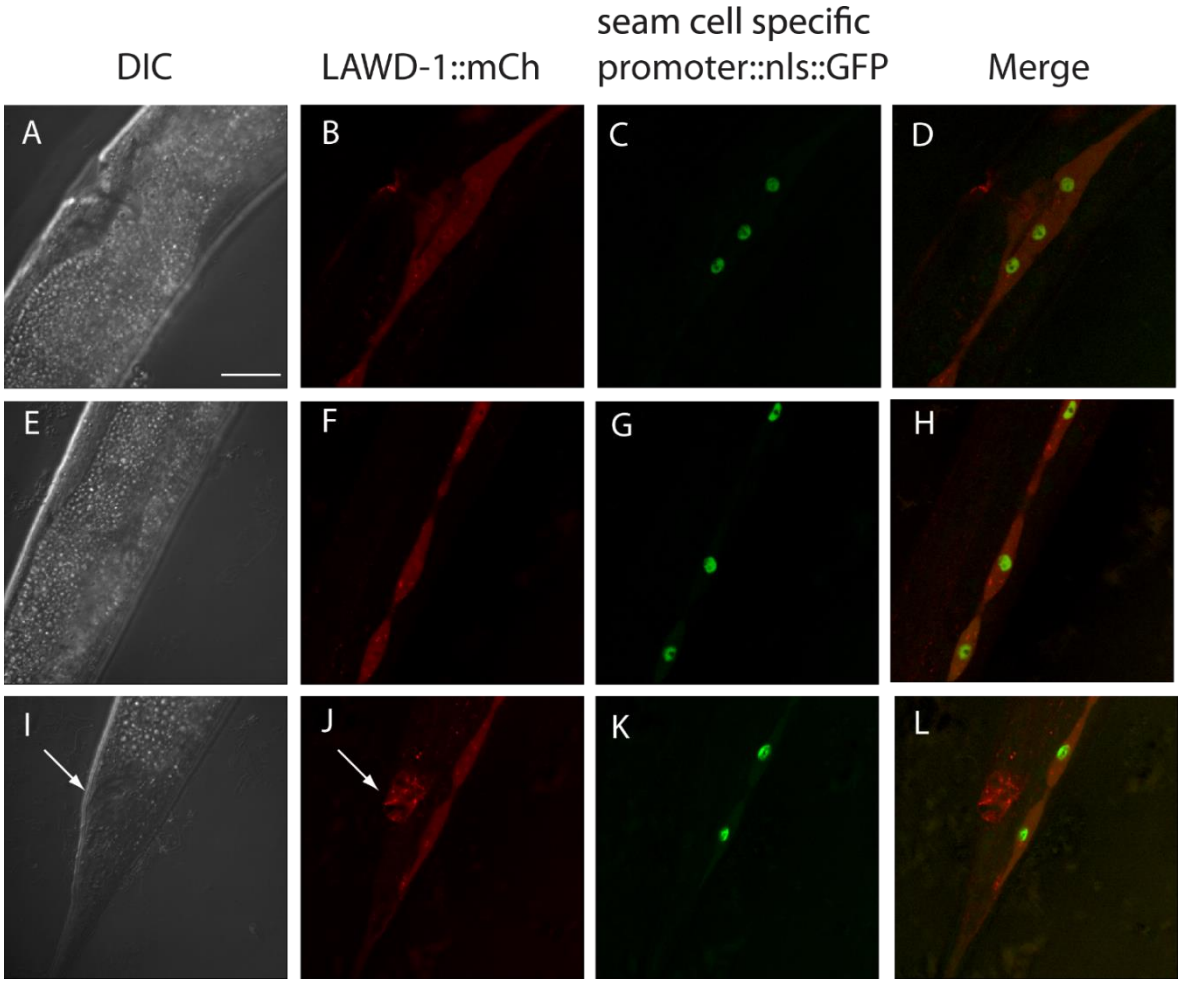

Figure 4-3 Co-expression of LAWD-1::mCh and smcp::nls::GFP in an L4 stage animal.

A, E, and I. Nomarski DIC image of sections of an L4 stage animal from anterior to posterior. **B, F, and J.** Expression of LAWD-1::mCh is detected in the cytosol of seam cells and rectum **J.** as indicated by arrows. **C, G, and K.** Expression of a GFP seam cell specific nuclear reporter confirms identification of LAWD-1::mCh expression in seam cells in **D, H, and L.** Scale bar = 20 µm.

4.2 LAWD-1::mCh and smcp::nls::GFP co-expression verified LAWD-1::mCh seam cell localisation in larva

To verify that hypodermal expression of LAWD-1::mCh was indeed confined to seam cells, the LAWD-1::mCh reporter strain was crossed with the smcp::nls::GFP reporter strain, which expresses GFP in the nuclei of the seam cells of larvae and adults. Confocal microscopy showed that LAWD-1::mCh was diffusely expressed in the seam cells of larvae (Figure 4-3 B, F, J), which were all marked by the presence of GFP expressing nuclei (Figure 4-3 D, H, L). It was not possible to verify LAWD-1::mCh seam cell expression in the embryo, possibly due to multicopy transgenic arrays not normally expressed in the germ line and early embryo because of silencing.

4.3 The intracellular localisation of LAWD-1::mCh

As introduced in Chapter 1.4, HMP-1 is the alpha catenin of the CeAJ CCC complex. HMP-1 is localised to the apical membrane of epithelia and acts as an apical membrane marker (62). A double fluorescent strain of LAWD-1::mCh and HMP-1::GFP made by crossing the two individual strains was analysed by confocal microscopy throughout embryonic development. As already reported, HMP-1::GFP was detected in all apical epithelia (Figure 4-4 C, G, K). LAWD-1::mCh appeared to partially co-localise with HMP-1::GFP in the developing intestine (Fig 4-4 D, H, L).

The LAWD-1::mCh reporter strain was next crossed with DLG-1::GFP reporter strain to generate a LAWD-1::mCh; DLG-1::GFP double fluorescent reporter strain. DLG-1 belongs to the CeAJ DAC complex and is localised at the basolateral membrane of epithelia (64). Confocal microscopic analysis of the double fluorescent strain expressing LAWD-1::mCh and DLG-1::GFP showed that DLG-

1::GFP was detected in all epithelia and formed a network of junction-like structures (Figure 4-5 C, G, K). Unlike with HMP-1::GFP, LAWD-1::mCh did not appear to co-localise with DLG-1::GFP (Figure 4-5 D, H, L). These results established that LAWD-1::mCh is apically enriched in the developing intestine epithelia.

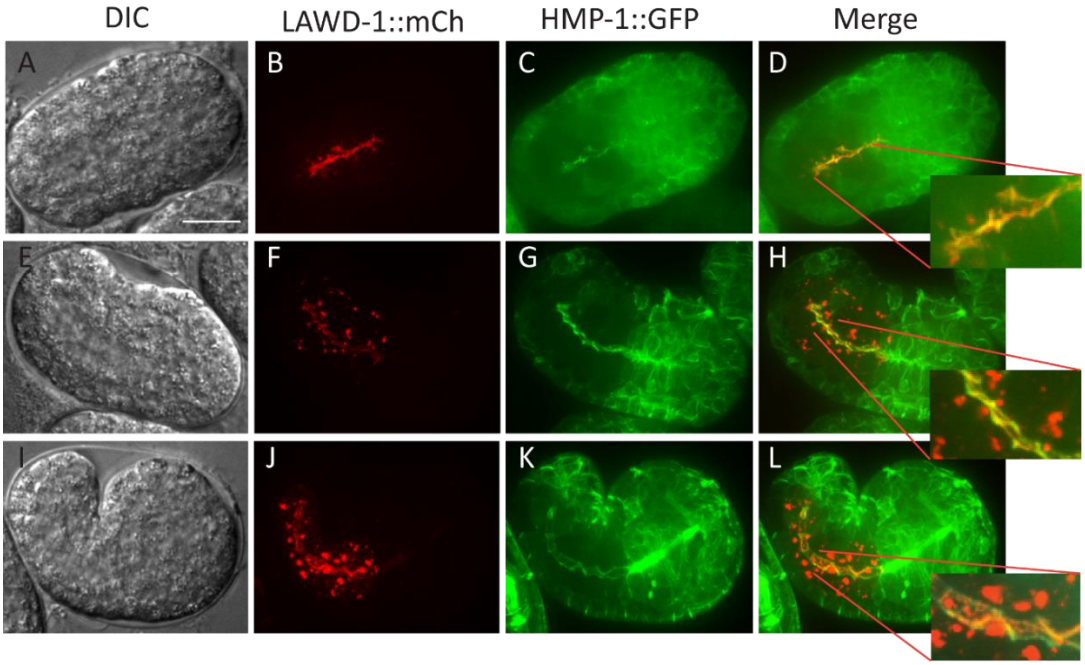

Figure 4-4 Co-expression of LAWD-1::mCh and HMP-1::GFP in the developing intestine of the embryo.

A, E, and I. Nomarski DIC micrographs of *C. elegans* embryos at bean stage, comma stage and 1.2-fold stage, respectively **B. F.** and **J.** LAWD-1::mCh expression corresponding to embryo in left panel revealed as puncta on the apical surface and cytosol of intestinal epithelial cells. **C, G,** and **K.** HMP-1::GFP expression in the same embryo on far left panel is shown as a marker for apical epithelia. **D, H,** and **L.** Co-expression of LAWD-1::mCh with HMP-1::GFP in developing intestinal epithelia reveals partial overlap in expression. Panel inserts magnify indicated regions of embryos. Scale bar = 10 µm.

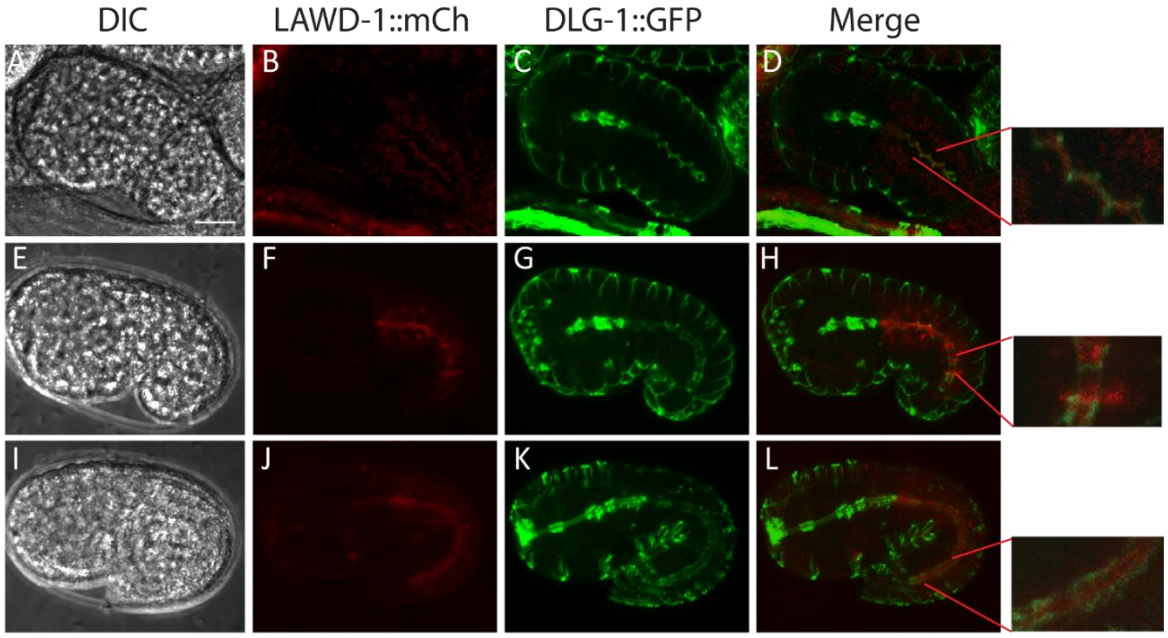

Figure 4-5 Co-expression of LAWD-1::mCh and DLG-1::GFP in the developing intestine of the embryo.

A, E, and I. Nomarski DIC images of *C. elegans* embryos at comma stage, 1.2-fold and 1.8- fold stages, respectively. **B, F, and J.** LAWD-1::mCh expression in embryos shown in left panels is observed as puncta on the apical surface and cytosol of intestinal epithelial cells. **C, G, and K.** DLG-1::GFP expression in the same embryo (left) is shown as a marker for the basolateral surface of epithelia . **D, H, and L.** Co-expression within the same embryo shows that LAWD-1::mCh does not co-localise with DLG-1. Panel inserts magnify indicated regions of embryos. Scale bar = 10 µm.

4.4 LAWD-1::mCh partially co-localises with F-actin in the subcellular cortex in intestine epithelia.

It is now possible to visualise actin in cells using non-invasive lifeact reporters. Lifeact consists of a short 17-aa motif fused to GFP, which is capable of binding to filamentous actin (F-actin) (197). Two lifeact strains were obtained as kind gifts from the labs of Alex Hajnal and Julie Plastino. The lifeact reporter obtained from the Hajnal lab is driven by a *dlg-1* promoter, which is expressed in all epithelia. The second reporter obtained from the Plastino lab is driven by a *lin-26* promoter, which is expressed specifically in the hypodermis. A double fluorescent strain of LAWD-1::mCh; *dlg-1p::lifeact::GFP* was built and used to analyse their co-expression in the developing embryonic intestine by confocal microscopy. The Lifeact::GFP reporter was capable of detecting F-actin in the subcellular cortex of all epithelia (Figure 4-6 C, G, K). In the developing intestine, LAWD-1::mCh appeared to partially co-localise with F-actin (Figure 4-6 D, H, L). The co-localisation of LAWD-1 and F-actin further supports previous observations indicating that LAWD-1::mCh is localised toward the apical and not the basolateral surface of intestinal epithelia.

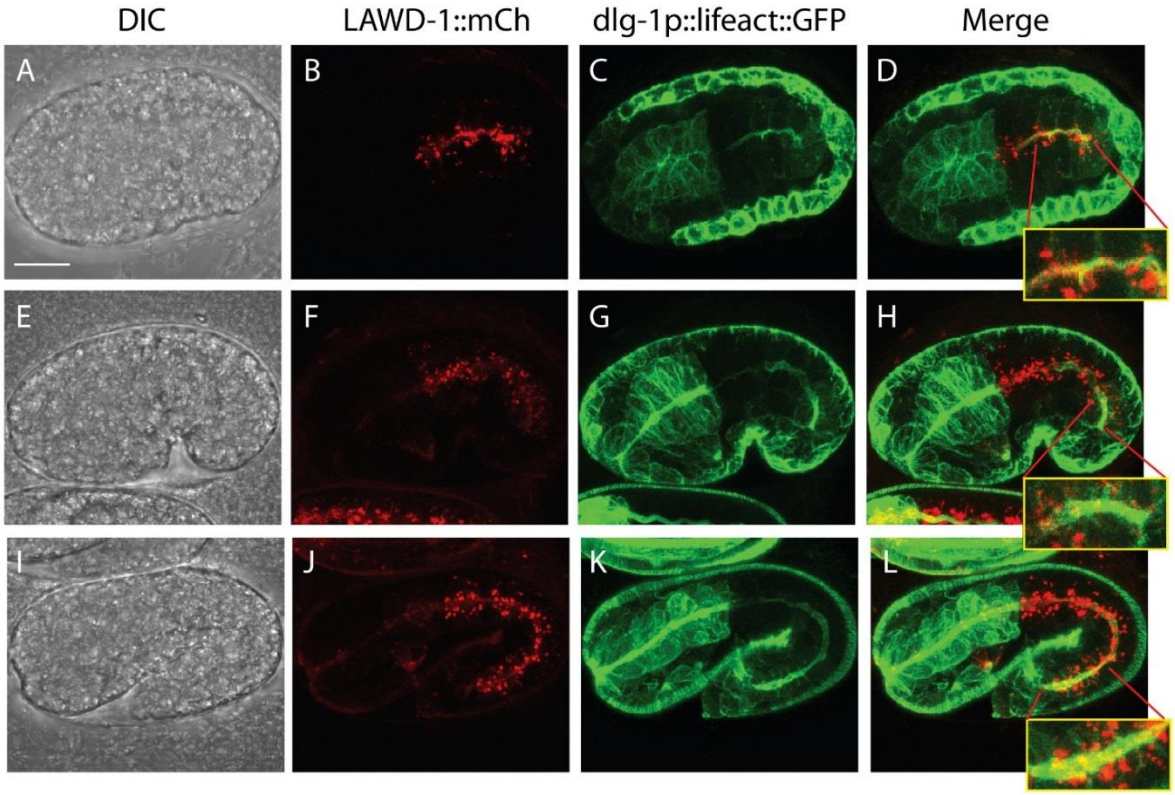

Figure 4-6 Co-expression of LAWD-1::mCh and dlg-1p::lifeact::GFP in the developing embryonic intestine.

A, E, and I. Nomarski DIC images of *C. elegans* embryos at bean stage, 1.2 fold and 1.8 fold stages, respectively. **B, F, and J.** LAWD-1::mCh expression in embryos shown in left panels is observed as puncta on the apical surface and cytosol of intestinal epithelial cells. **C, G, and K.** *dlg-1p::lifeact::GFP* expression in the same embryos (left) is included as a marker for filamentous actin in the sub-cellular cortex of apical epithelia. **D, H, and L.** Co-expression of LAWD-1::mCh and *dlg-1p::lifeact::GFP* in developing intestinal epithelia reveals partial overlap in expression. Panel inserts magnify indicated regions of embryos. Scale bar = 10 µm.

4.5 Co-expression of LAWD-1::mCh and NMY-2::GFP revealed changes of LAWD-1::mCh pattern in the developing seam cells during elongation.

It was initially observed that LAWD-1::mCh fluorescence could not be detected in the hypodermis of the embryo. Hypodermal expression of LAWD-1::mCh was only detected later during larval development in seam cells. The absence of hypodermal LAWD-1::mCh was surprising given that viable *lawd-1* display a notched head phenotype, and stronger mutants are embryonic lethal. In an effort to improve the ability to detect LAWD-1::mCh in the hypodermis of the embryo, a double fluorescent strain that had been previously built to co-express LAWD-1::mCh and NMY-2::GFP was re-examined. NMY-2 is the myosin heavy chain subunit of non-muscle myosin II, and a component of the actomyosin network. As such, it is also a suitable marker for the embryonic seam cell.

In the 1.5-fold stage embryo, it was possible to detect LAWD-1::mCh expression in seam cells for the first time, albeit very faintly, when viewed in the same plane as NMY-2::GFP. This observation prompted the collection of images beyond the 1.5-fold stage. It should also be noted that a change in confocal microscope conditions also improved the ability to detect LAWD-1::mCh.

Beyond 1.5-fold stage, NMY-2::GFP was detected in embryonic seam cells as a diffuse signal (Figure 4-7 K, Figure 4-8 C) that started to became organised into a discernible structures at the 2-fold stage (Figure 4-8 G). By the 3-fold stage, NMY-2::GFP was a component of a narrow band-like structure (Figure 4-8 K). The intracellular localisation and arrangement of NMY-2::GFP mirrored changes in the actomyosin network. LAWD-1::mCh was detected in seam cells first as puncta distributed throughout the cytosol (Figure 4-8 B). Similar to NMY-2, expression of

LAWD-1::mCh become more organised at the 2-fold stage (Figure 4-8F), but did not appear to co-localise with NMY-2::GFP. LAWD-1::mCh appeared to be intercalated between NMY-2::GFP, but not co-localised within a similar structure (Figure 4-8 H). By the 3-fold stage, LAWD-1::mCh also formed a band like structure marking the cell border of seam cells as shown by the evenly spaced lines perpendicular to the thin band (Figure 4-8 J). At the 3.5-fold, the structural organisation of both NMY-2::GFP and LAWD-1::mCh underwent a dynamic change. NMY-2::GFP was distributed in a more diffuse pattern (Figure 4-8 O), whereas LAWD-1::mCh not only appeared more diffuse, but also formed large in apposition to seam cell nuclei (Figure 4-8 N).

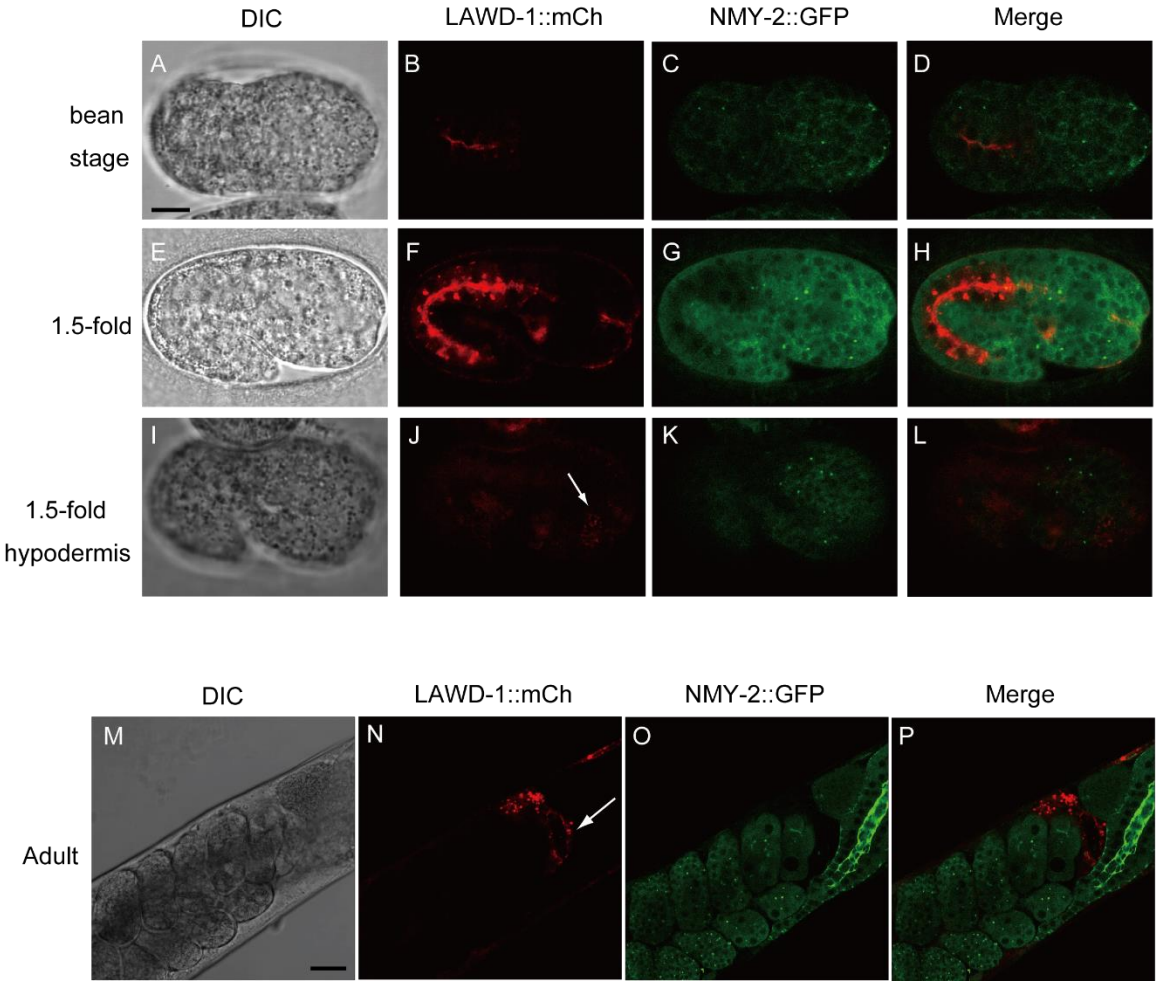

Figure 4-7 LAWD-1::mCh and NMY-2::GFP fail to co-localise in embryonic or post-embryonic intestinal cells.

A, E, I, and **M.** Nomarski DIC images of bean stage, 1.5-fold (2 focal planes) and adult animals embryo expressing LAWD-1::mCh and NMY-2::GFP. Panels on the right side of the DIC images show expression of LAWD-1::mCh **(B, F, J, N)** and NMY-2::GFP **(C, G, K, O)**, as indicated. Panels on far right show that these markers fail to co-localise in either embryonic or post-embryonic tissues **(D, H, L, P)**. **J-L.** LAWD-1::mCh is detected in the developing seam cell (arrow); however, it does co-localise with NMY-2::GFP. **N.** LAWD-1::mCh is detected in the vulva. Note that NMY-2::GFP is abundantly present in early embryos which are not hatched yet from the adult and also in the germline. Scale bar = 10 µm, except panels M-P where the scale bar = 20 µm.

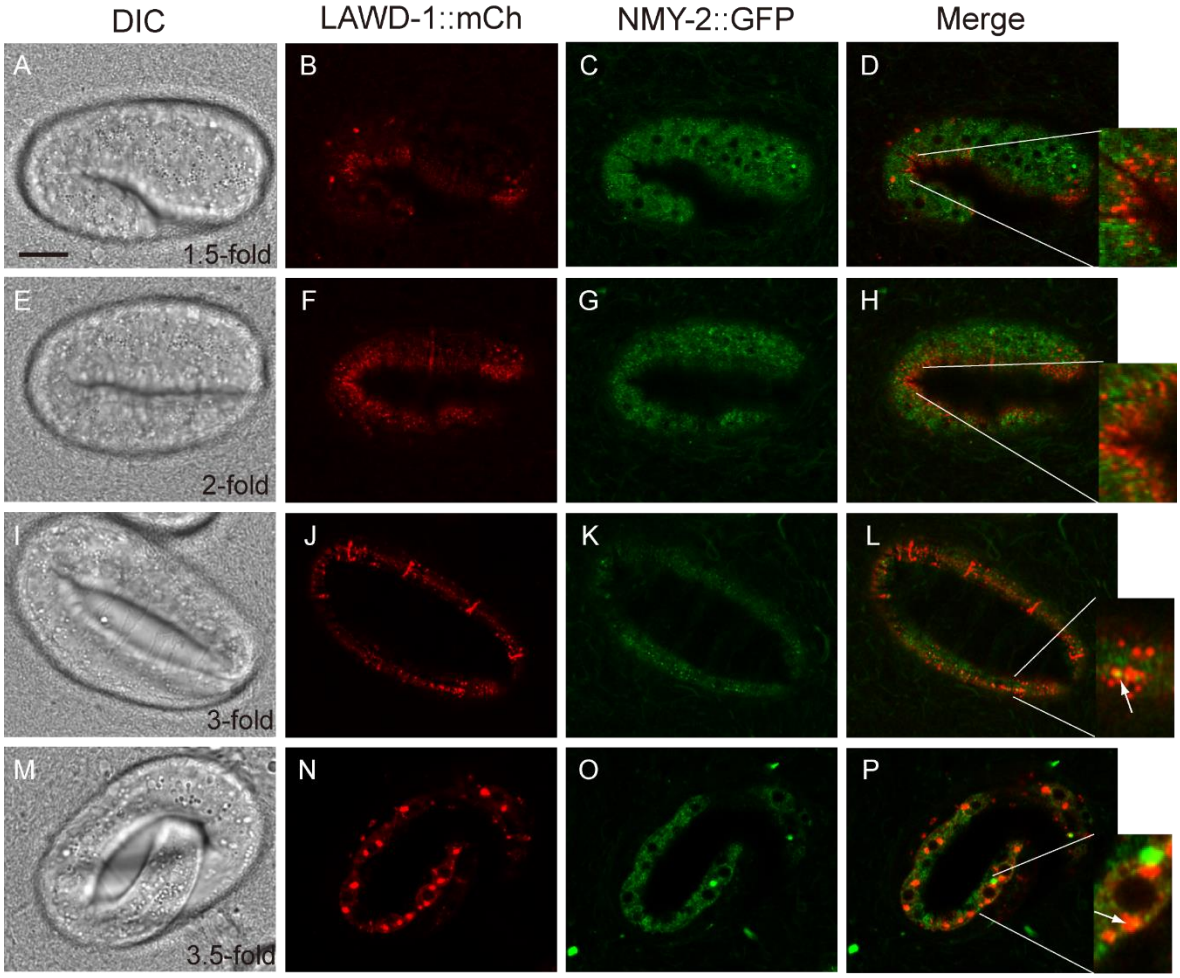

Figure 4-8 Co-expression of LAWD-1::mCh and NMY-2::GFP in seam cells during embryonic development.

A, E, I, and M. Nomarski DIC images of *C. elegans* embryos at 1.5-fold stage, 2-fold stage, 3-fold stage and 3.5-fold stage co-expressing LAWD-1::mCh and NMY-2::GFP. **B, F, J,** and **N.** LAWD-1::mCh expression in the cytosol of the developing seam cells. LAWD-1::mCh initially forms puncta in the cytosol of seam cells of the early embryo **(B),** which is then organised into filaments **(F)** followed by formation of a band-like structure **(J).** Near the end of embryo elongation, LAWD-1::mCh forms larger puncta in close proximity to the nuclei of seam cells **(N)**. **C, G, K, and O.** NMY-2::GFP expression observed in seam cells of the same embryos (left). **D, H, L, and P.** LAWD-1::mCh expression pattern is similar to that of NMY-2::GFP, but does not show co-localisation despite being in close proximity (arrows in inserts of L and P). Both reporters form band like structure at 3-fold stages and LAWD-1::mCh

appears to localise between NMY-2::GFP filaments (insert of H). Panel inserts magnify indicated regions of embryos. Scale bar = 10 µm.

4.6 LAWD-1::mCh undergoes dynamic re-organisation in seam cells during embryonic elongation.

In addition to NMY-2, F-actin is also an integral component of the actomyosin network. Since LAWD-1::mCh was detected in later stages of seam cell embryonic development, the co-expression pattern of LAWD-1::mCh and the hypodermal-specific *lin-26p::lifeact::GFP* was analysed by confocal microscopy. At the 1.5-fold stage, F-actin as detected by Lifeact::GFP formed random filaments in the cytoplasm (Figure 4-9 D). During the same stage, LAWD-1::mCh formed diffuse puncta positioned between F-actin filaments in the seam cell (Figure 4-9 D). At the 2-fold stage, both F-actin and LAWD-1::mCh were associated with a filamentous network, but displayed minimal co-localisation (Figure 4-9 H). Beyond the 2-fold stage, LAWD-1::mCh showed close proximity with F-actin in the seam cell and formed a narrow band-like structure that was also observed in the LAWD-1::mCh; NMY-2::GFP double fluorescent strain (Figure 4-9 L, P).

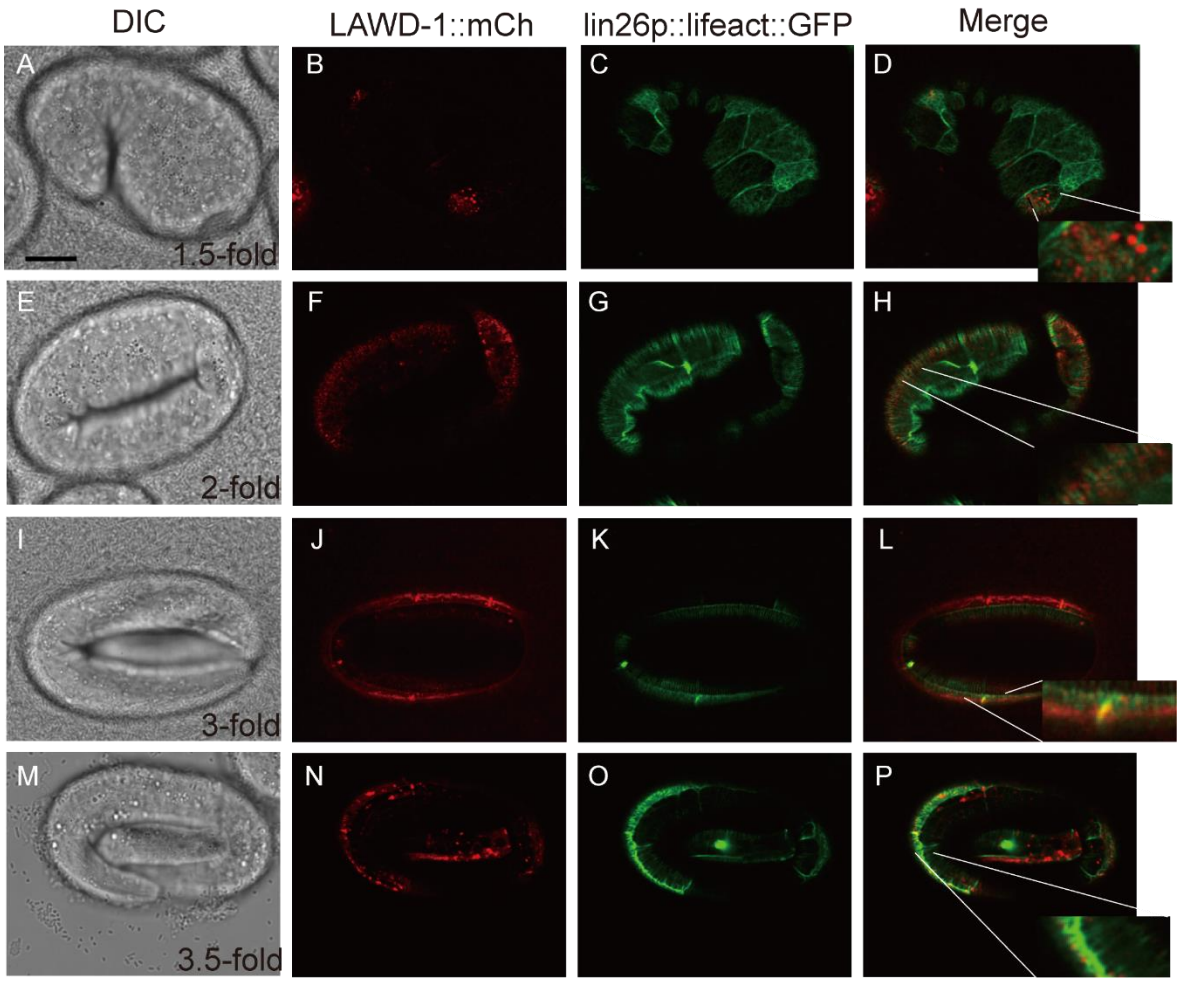

Figure 4-9 Co-expression of LAWD-1::mCh and lin-26p::lifeact::GFP in seam cells during embryonic development

A, E, I, M. Nomarksi DIC images of *C. elegans* embryos at 1.5-fold stage, 2-fold stage, 3-fold stage and 3.5-fold stage, respectively. **B, F, J, and N.** LAWD-1::mCh expression in the cytosol of developing seam cells. LAWD-1::mCh initially forms puncta in the cytosol of seam cells of the early embryo **(B)**, which is then organised into filaments **(F)** followed by formation of a band-like structure **(J)**. Near the end of embryo elongation, LAWD-1::mCh forms larger puncta in close proximity to the nuclei of seam cells **(N)**. **C, G, K, and O.** *lin-26p::lifeact::GFP* expression observed in the in the seam cells of the same animals (left). Actin organisation changes during elongation, short filaments are formed from random filaments (insert D) at earlier stages. **D, H, L, and P.** Co-expression of LAWD-1::mCh and *lin26p::lifeact::GFP* shows a lack of co-localisation at earlier stages (D and H) and partial co-localisation at the 3-fold **(L)** and 3.5-fold **(P)** stages of development. Scale bar = 10 µm.

4.7 LAWD-1::mCh co-localises with apical marker HMP-1::GFP in larval tissues

The co-expression pattern of LAWD-1::mCh and HMP-1::GFP was also examined in larval tissues, although LAWD-1 function was not explored in these tissues. As expected, HMP-1::GFP was detected in the spermatheca and vulva, and also in the anchor cell, a cell that plays a key role in signalling vulva formation (198). LAWD-1::mCh was found to co-localise with HMP-1::GFP in these tissues and along the apical surface of vulval precursor cells (Figure 4-10). These observations combined with an analysis of LAWD-1::mCh localisation in the embryo indicate that LAWD-1::mCh is apically enriched not only in the embryo epithelia but also in larval tissues as well.

4.8 LAWD-1::mCh does not co-localise with basolateral marker DLG-1::GFP in larval tissues

To verify the apical localisation of LAWD-1::mCh in post-embryonic tissues, the expression of LAWD-1::mCh was also studied in the double fluorescent strains expression DLG-1::GFP, which is also expressed in the spermatheca and vulva. Confocal image analysis was consistent with the observation in the embryo in that LAWD-1::mCh does not co-localise with DLG-1::GFP in larval tissues (Figure 4-11). Therefore LAWD-1::mCh does not appear to have a basolateral localisation in epithelial tissues.

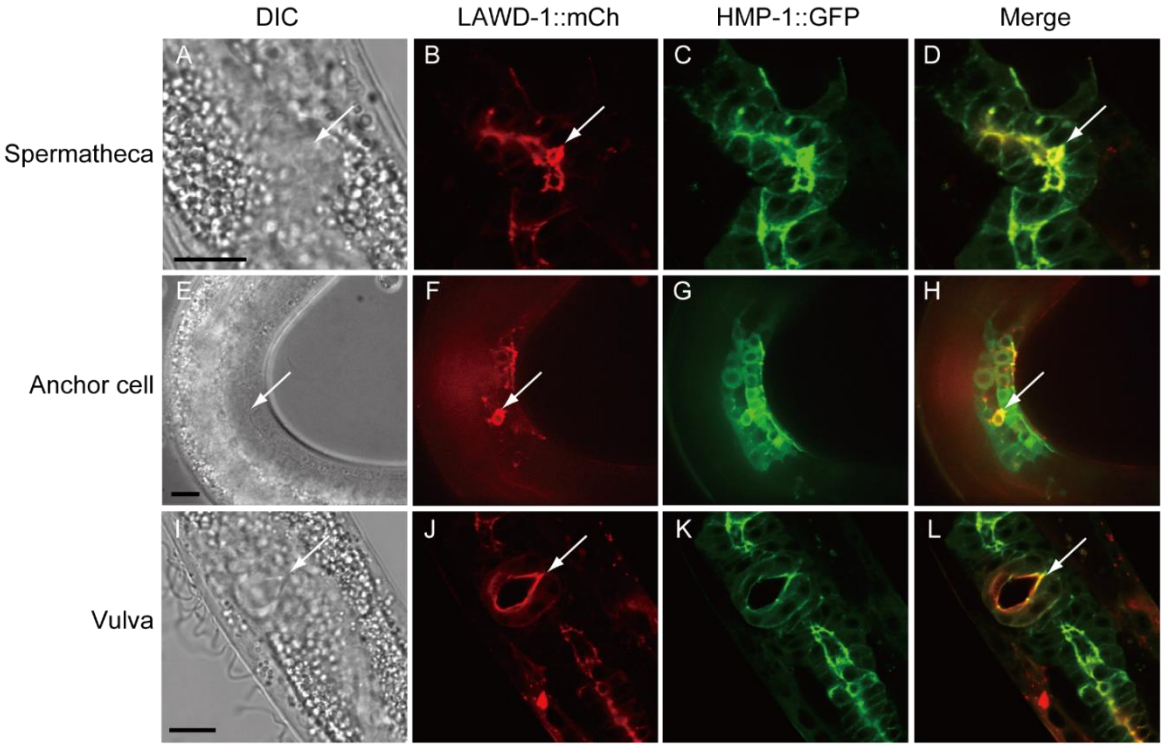

Figure 4-10 Co-expression of LAWD-1::mCh and HMP-1::GFP in larval tissues.

A. Nomarski DIC image of the spermatheca of an L4 stage animal. **B-D.** Fluorescent images showing LAWD-1::mCh, HMP-1::GFP and co-expression pattern of the two reporters in the spermatheca the animal shown in A). LAWD-1::mCh and HMP-1::GFP co-localise along the apical surface of the spermathecal lumen (arrow in D). **E.** DIC image of the developing vulva of an L3 stage animal. **F-H.** Fluorescent images showing LAWD-1::mCh, HMP-1::GFP and co-expression pattern of the two reporters in the vulva precursor cells of the animal shown in E). LAWD-1::mCh is expressed in the anchor cell and on the apical surface of vulval precursor cells; LAWD-1::mCh co-localises with HMP-1::GFP in the anchor cell (arrow in H). **I.** DIC image of the vulva of an L4 stage animal. **J-L.** Fluorescent images showing LAWD-1::mCh, HMP-1::GFP and co-expression pattern of the two reporters in the vulva of an L4 stage animal shown in I). LAWD-1::mCh partially co-localises with HMP-1::GFP along the apical surface of the vulval lumen (arrow in L). Scale bar = 10 µm.

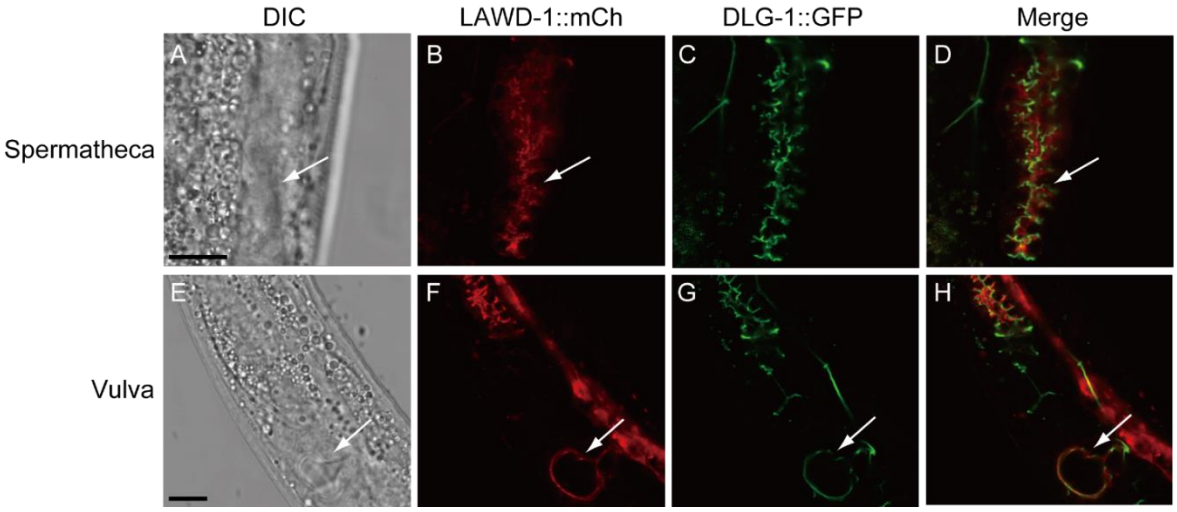

Figure 4-11 Co-expression of LAWD-1::mCh and DLG-1::GFP in larval tissues.

A. Nomarski DIC image of the spermatheca of an L4 stage animal. **B-D.** Fluorescent images showing LAWD-1::mCh, DLG-1::GFP and co-expression pattern of the two reporters in the spermatheca of the animal shown in A). LAWD-1::mCh and DLG-1::GFP do not co-localise; LAWD-1::mCh is associated with the apical surface of the spermathecal lumen whereas DLG-1::GFP is more distant (arrow in D). **E.** DIC image of the vulva of an L4 stage animal. **F-H.** Fluorescent images showing LAWD-1::mCh, DLG-1::GFP and co-expression pattern of the two reporters in the vulva of an L4 stage animal shown in E). LAWD-1::mCh does not co-localise with DLG-1::GFP in the vulva (arrow in H). Scale bar = 10 µm.

4.9 CRISPR-Cas9 knock-in LAWD-1::mCh strain confirms expression patterns obtained using an integrated transgenic reporter

Development of the CRISPR-Cas9 technology has allowed the precise engineering of sequence deletions and insertions into any region of a particular gene (9). Since the integrated strain LAWD-1::mCh used in this study was made after ^{137}Cs gamma irradiation of an extrachromosomal array, germline and early embryonic LAWD-1 expression would likely be silenced. In order to detect LAWD-1::mCh expression in the early embryo, a different reporter construct was needed. Making of the reporter was first attempted by fosmid recombineering and biolistics, but only extrachromosomal arrays were obtained. Subsequently, an attempt was made to generate a CRISPR-Cas9 (C-C) knock-in reporter, but this was unsuccessful. Instead, a LAWD-1::mCh knock-in strain was obtained commercially from SunyBiotech (China). Image analysis of this strain showed that LAWD-1::mCh(C-C) expression was fainter due to its single copy nature when compared to the integrated strain. However, the expression pattern of LAWD-1::mCh(C-C) was in agreement with the LAWD-1::mCh integrated strain. Similar to the integrated reporter, LAWD-1::mCh(C-C) was first observed in the developing intestine at bean stage (Figure 4-12 F), and formed puncta in later stages in developing intestine (Figure 4-12 G, H). Of note, LAWD-1::mCh(C-C) was not detected at earlier stages of embryogenesis.

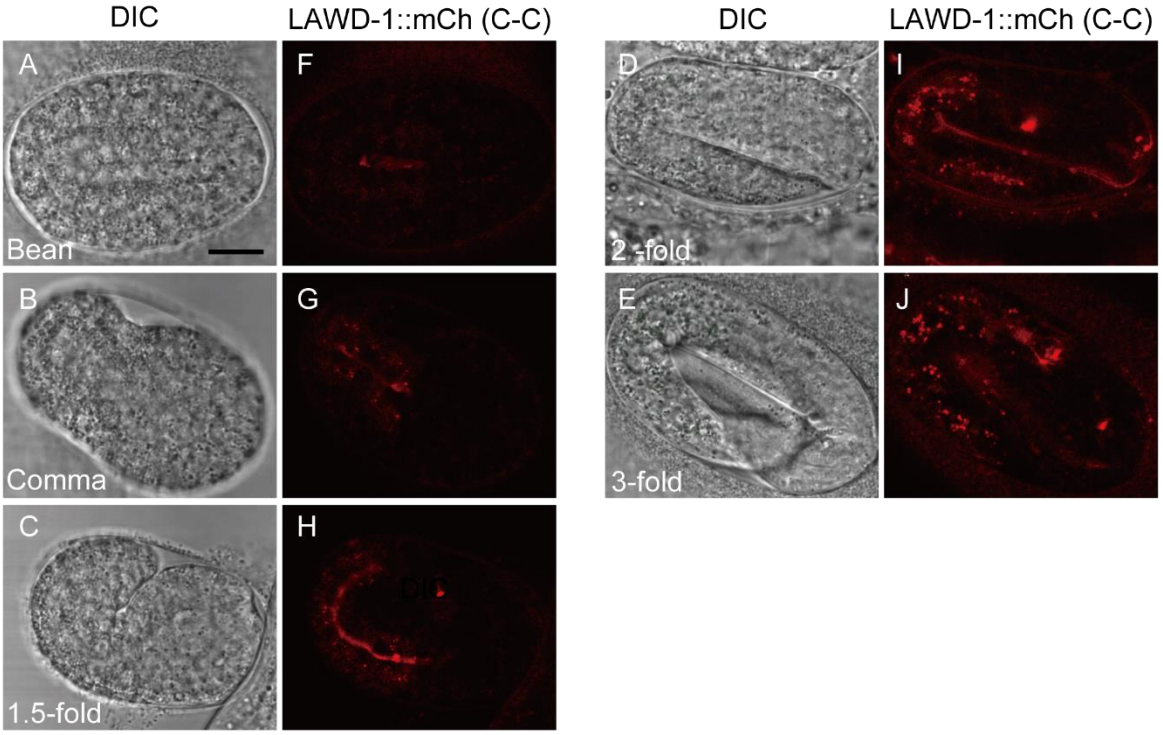

Figure 4-12 Intestinal expression of LAWD-1::mCh in a CRISPR-Cas9 engineered strain during embryonic development.

A-E. Nomarski DIC images of *C. elegans* embryos at **A.** bean stage, **B.** Comma stage, **C.** 1.5-fold stage, **D.** 2-fold stage, and **E.** 3-fold stage. **F-J.** LAWD-1::mCh (C-C) expression in embryos corresponding to A-E). The CRISPR-Cas9 engineered LAWD-1::mCh (C-C) reporter is expressed in a similar apical intestinal pattern as previously observed for the integrated fosmid transgenic reporters expressing LAWD-1::mCh (C-C) and LAWD-1::GFP used in earlier experiments. Scale bar = 10 µm.

4.10 CRISPR-Cas9 knock-in LAWD-1::mCh strain showed same expression pattern in developing seam cells as integrated reporter strain LAWD-1::mCh in embryos and in larva

The expression pattern of LAWD-1::mCh(C-C) was also examined in seam cells of the embryo and larva (Figure 4-13). However, the fluorescent signal was more difficult to detect in embryos as compared with the integrated strain LAWD-1::mCh, probably due to the single-copy nature of expression. In larval stages, a similar pattern of seam cell expression was also observed, indicating the single copy endogenous LAWD-1 is indeed expressed in the lateral epidermis of the *C. elegans*.

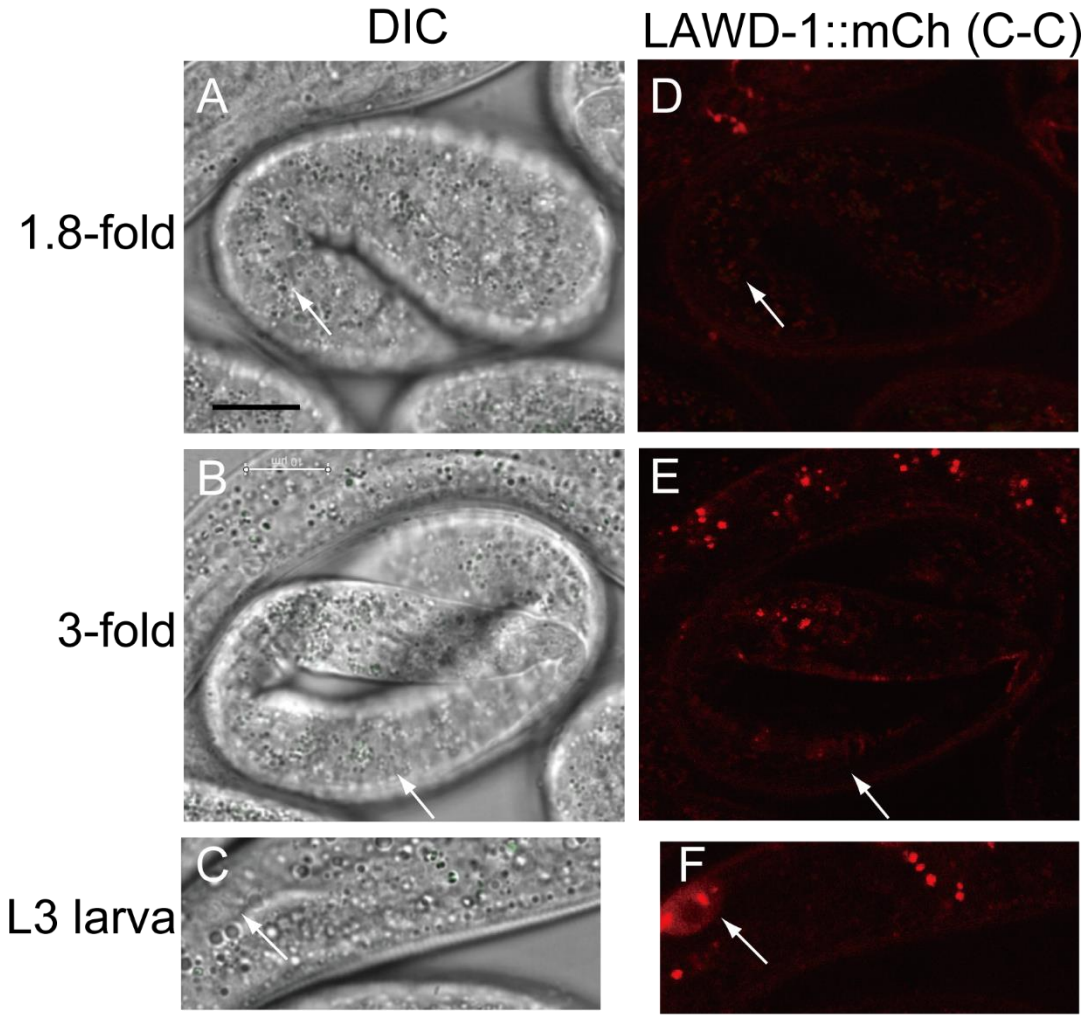

Figure 4-13 Hypodermal expression of CRISPR-Cas9 engineered LAWD-1::mRFP strain in embryos and larva.

A. Nomarski DIC image of a 1.8-fold stage *C. elegans* embryo expressing LAWD-1::mCh. **B.** DIC image of a 3.5-fold stage *C. elegans* embryo expressing LAWD-1::mCh. **C.** DIC image of section of an L3 stage *C. elegans* larva. **D.** LAWD-1::mCh is detected (arrow) in the developing seam cells of the embryo. **E.** LAWD-1::mCh forms a band-like structure (arrow) in the embryo, which although fainter is similar to that of LAWD-1::mCh expression pattern observed in previous experiments. F. LAWD-1::mCh forms puncta close to the nucleus of the seam cell (arrow). Scale bar = 10 µm.

4.11 Discussion

lawd-1 is a large gene that encodes multiple protein isoforms. There is also evidence that *lawd-1* has two promoters, P1 and P2 (Figure 3-1A) (PEK, personal communication). Although cDNA sequences are available to support the existence of multiple isoforms, it has not been possible to confirm the total number of transcripts or to determine their temporal and spatial patterns of expression. Thus, there was a risk on focusing expression studies using a single isoform, so it was decided to use a genomic reporter.

Due to the large size of the *lawd-1* gene, and the desire to retain all cis-acting regulatory information, it was not possible to express the entire gene region on a bacterial plasmid. Instead, a fosmid was identified that carried the entire *lawd-1* gene region. The availability of this fosmid also meant that it was possible to precisely insert mCherry and *GFP* tags into the 3' end of the gene using recombineering methods developed by Tursun (191). Based on the gene structure (Figure 3-1A), it was predicted that only isoform c was likely to be excluded from detection because it did not share the common C-terminus encoded by the other transcripts. An attempt was also made to generate N-terminal tagged LAWD-1 reporters. However, although mCh::LAWD-1 transgenic animals were obtained, they were non-fluorescent, although the sequence had been verified. It is speculated that the presence of N-terminal WD40 repeats might interfere with the maturation and fluorescence of GFP. Biolistic bombardment proved successful in generating extrachromosomal arrays, but not integrated constructs. This might have been caused by the large size of the fosmid, which might have been fragmented during biolistic bombardment.

Several lines carrying LAWD-1::mCh extrachromosomal arrays were also obtained and verified by PCR and partial sequencing. However, expression from these reporters was weaker than the lines obtained by ^{137}Cs gamma irradiation, so they were not used for further study (Data not shown).

The strong similarity in the spatial and temporal expression patterns of the integrated and independent LAWD-1::mCh and LAWD-1::GFP reporters combined with the ability of LAWD-1::mCh to rescue the *lawd-1* (*tm4605*) mutant phenotype, indicates that they serve as faithful reporters of endogenous gene expression. The similarity in both the spatial and temporal expression of the LAWD-1::mCh(C-C) CRISPR-Cas9 knock-in reporter and the integrated reporter further supports the validity of the observed expression patterns. Interestingly, although the LAWD-1::GFP strain had been outcrossed three times, it was relatively unhealthy, so it was not used in later co-expression analyses. Since the *gfp* tagged fosmid construct was randomly integrated into the genome, it is possible that it caused disruption of a gene during the integration process.

Before analysing the spatial and temporal pattern of LAWD-1::mCh expression in embryos and larvae virtually nothing was known about the role of this gene in development. Co-expression studies using established markers of epithelial polarity HMP-1::GFP and DLG-1::GFP served to establish that LAWD-1::mCh expression is restricted to epidermal cells and that it is specifically enriched along the apical surface. The Notched head phenotype, which is a possible manifestation of defects in the head hypodermis raises the possibility that LAWD-1 might be detected in other hypodermal cells such as the dorsal and ventral hypodermis. So far, expression of the LAWD-1::mCh reporter has not been detected in these cells,

but it is possible that the LAWD-1::mCh signal could be amplified by fixation and immunohistochemical detection.

A very interesting observation made in larval tissues is that LAWD-1::mCh was strongly expressed in the anchor cell. The anchor cell secretes the LIN-3 and LAG-2 signalling molecules to induce vulva formation (198). Invasion by the anchor cell into the vulva precursor cells is an important event during L3/L4 stage of larval development (198). Since this study mainly focused on the possible role of LAWD-1 during early development, the role of LAWD-1 in anchor cell was not further explored. Therefore, it would be interesting to see if LAWD-1 plays a role in the execution phase of vulva formation. LAWD-1::mCh expression was also observed in the larval and adult rectum, which is another tubular structure. It was further noted that *lawd-1* (*tm4605*) mutants exhibited a protruding rectum phenotype, which was categorised as a general morphogenetic defect in Table 3-1. Taken together, the role of LAWD-1 in post-embryonic morphogenesis would be a potential future direction of study.

During intestinal development and embryo elongation, co-expression of LAWD-1::mCh with the NMY-2::GFP and *lin-26p*::*lifeact::GFP* provided important insights about the potential association of LAWD-1 with the actomyosin contractility network. As discussed in Chapter 1.5.1 the actomyosin network provides the main contractile force driving elongation before the 2-fold stage. After the 2-fold stage, additional contractile mechanisms also come into play (144). Both NMY-2::GFP and the hypodermal specific *lin-26p::lifeact::GFP* actin reporter are components of the actomyosin network and display dynamic changes in organisation during embryonic development. Similarly, LAWD-1::mCh also undergoes dynamic changes

throughout elongation after 2-fold stage that match the changes in the actomyosin network, although LAWD-1::mCh shows limited co-localisation with these markers. The role of LAWD-1 function and its participation in the actomyosin network during elongation is an area for future study. Potential connections between LAWD-1 in the elongation process are discussed in Chapter 6.

LAWD-1::mCh was also observed as large puncta in intestinal cells. These structures are dynamic and their role in intestinal remains to be investigated.

Chapter 5 Identification of LAWD-1 interacting proteins based on co-immunoprecipitation and proteomics

Genetic and imaging analyses performed in this study have so far indicated that the *lawd-1* gene is required for proper development of epithelia. The lethality and morphogenetic defects arising from loss or knockdown of *lawd-1* combined with the dynamic pattern of LAWD-1::mCh expression pattern in seam cells, changing from puncta to band-like structures during embryonic elongation, have led to the hypothesis that LAWD-1 is involved in the process of embryonic elongation. Because longer isoforms of LAWD-1 that carry N-terminal WD40 domains are predicted to form propeller shaped folds capable of forming a scaffold to mediate protein-protein interactions, proteomic analysis was performed.

5.1 Anti-GFP and anti-mRFP antibodies can detect multiple protein isoforms in boiled worm samples

Before it was possible to pursue proteomic analysis of LAWD-1, it was necessary to develop methods for visualising and detecting LAWD-1 protein. An unsuccessful first attempt had been made to raise rabbit polyclonal antibodies capable of detecting C-terminal LAWD-1 isoforms (data not shown). Therefore it was decided to use the reporter strains, which both rescued the *lawd-1*(*cr7*) and *lawd-1*(*tm4605*) mutants and expressed either LAWD-1::GFP or LAWD-1::mCh and use commercially available anti-GFP and anti-mRFP antibodies to detect LAWD-1. To test whether LAWD-1 could be detected by antibodies, whole worm protein samples were analysed by SDS-PAGE for western blot analysis using anti-GFP (Covance) or anti-mRFP (MLB Japan) antibodies. As shown in Figure 5-1, multiple

LAWD-1 protein isoforms were detected in both the LAWD-1::GFP and LAWD-1::mCh samples. The anti-GFP antibody, however (Fig 5-1A), detected three non-specific bands, based on the negative control N2, which does not express GFP. Analysis of the LAWD-1::mCh proteins detected by anti-mRFP showed that the same subset of proteins was detected; however, non-specific bands were not detected. Therefore, it was decided to use LAWD-1::mCh strain for future protein studies. DLG-1::GFP and DLG-1::mRFP were used as positive controls.

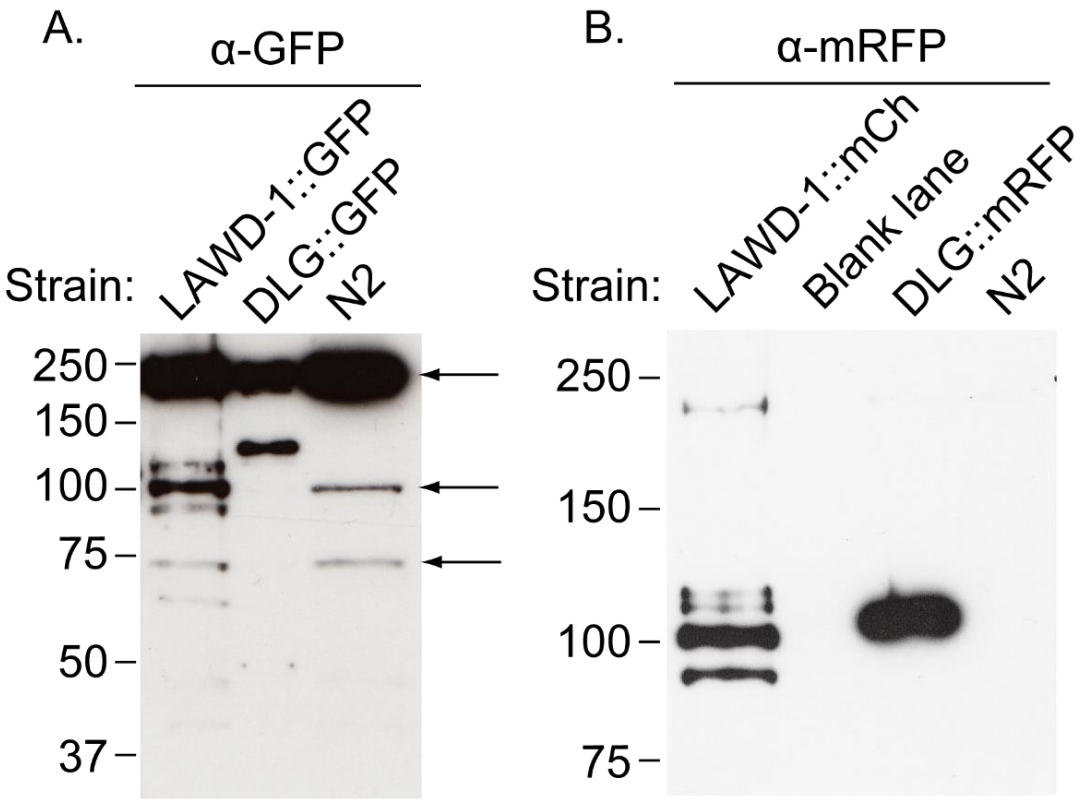

Figure 5-1 Western blot analysis of protein isoforms detected from animals expressing either LAWD-1::GFP or LAWD-1::mCh.

A. Multiple protein isoforms detected in animals expressing LAWD-1::GFP were separated on a 7% SDS-PAGE gel. N2 control detects three potentially non-specific bands; however, they are absent in the DLG::GFP positive control lane. **B.** Multiple protein isoforms were detected in animals expressing LAWD-1::mCh after separation on a 4% SDS-PAGE gel. Non-specific bands were not detected in N2 control lane. A lower percentage gel was used to resolve high molecular weight bands. Each lane contained 45 adult animals of the indicated genotype.

5.2 LAWD-1 isoforms are differentially expressed throughout development

In order to see if the pattern and expression levels of LAWD-1 proteins changed throughout development, western blot analysis was performed on animals carrying LAWD-1::mCh at the indicated stages of development (Figure 5-2). The results showed that multiple LAWD-1 isoforms were differentially expressed throughout development (Figure 5-2). Among the different isoforms, the predicted isoforms lawd-1a, b, d and e, while two new isoforms x and y were detected (Figure 3-1 and Figure 5-2). A high molecular weight band was predicted to consist of aggregates of LAWD-1 protein, because the ability to express such a large isoform was not predicted from the *lawd*-1 gene structure. These aggregates were detected at all developmental stages except in embryos (Figure 5-2A). The longest isoforms LAWD-1A and LAWD-1B, which are predicted to carry N-terminal WD40 domains, were most abundant in L1 stage samples, although it was only possible to resolve two bands of the appropriate molecular weight in adults. It was unclear whether both isoforms were present in L1 larvae, and further study will be needed to address this question. Apart from the two longest isoforms, all other predicted isoforms and those not predicted from existing cDNA data were most abundantly expressed in the L2/L3 and L4 stages (Figure 5-2C). It was also observed that some isoforms were only detected at certain stages such as the lowest molecular unknown isoform y, which was detected at L1-adult stages, although very faint in adults. Therefore, it was decided that it would be best to use mixed staged animals in the proteomic analysis in order to include all potential LAWD-1 isoforms.

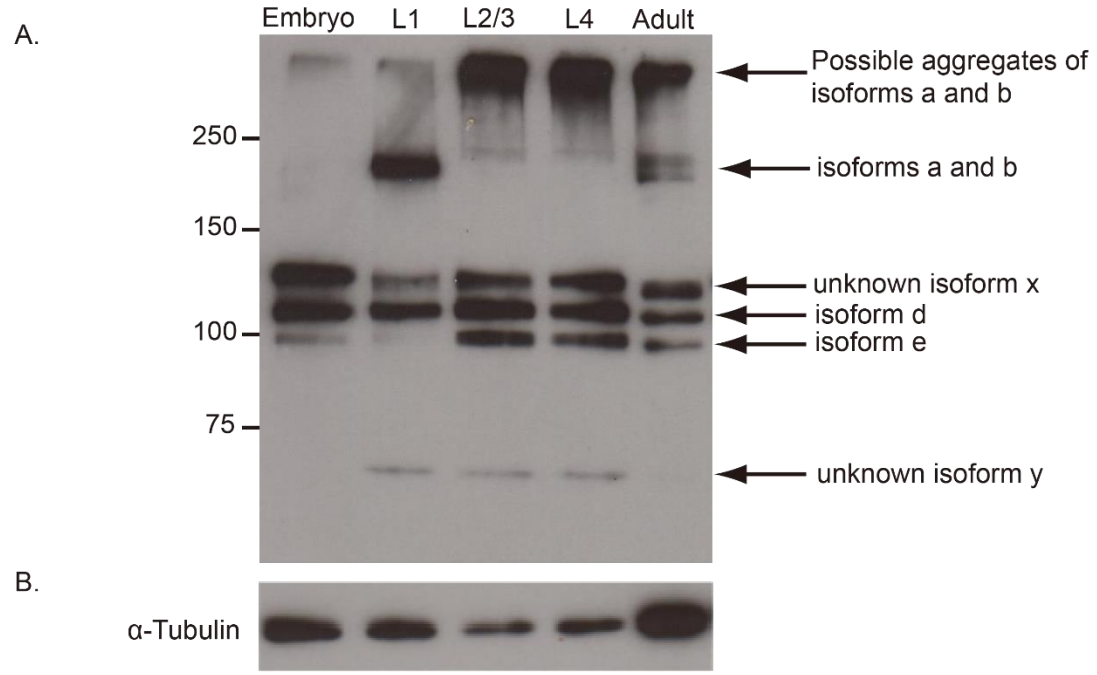
A.
Embryo
L1
L2/3
L4
Adult
250
150
100
75
Possible aggregates of isoforms a and b
isoforms a and b
unknown isoform x
isoform d
isoform e
unknown isoform y
B.
α-Tubulin

C.

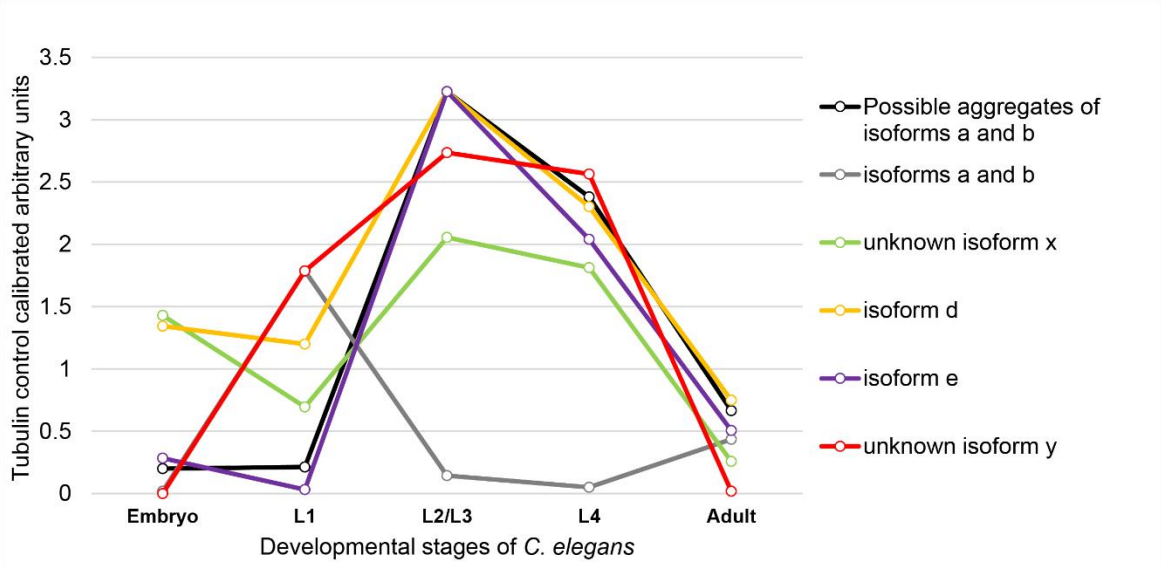
Tubulin control calibrated arbitrary units
3.5
3
2.5
2
1.5
1
0.5
0
Embryo
L1
L2/L3
L4
Adult
Developmental stages of C. elegans
Possible aggregates of isoforms a and b
isoforms a and b
unknown isoform x
isoform d
isoform e
unknown isoform y

Figure 5-2 LAWD-1::mCh isoforms are differentially expressed throughout development.

A. Western blot detection of LAWD-1::mCh protein isoforms at indicated stages of development and analysed on a 7% SDS-PAGE gel. Isoforms are marked by arrows and named based on sizes predicted from cDNA analysis (PEK unpublished data). **B.** The blot in (A) was re-probed with anti-tubulin as a loading control. **C.** The relative expression of each LAWD-1::mCh isoform was calibrated using the loading control tubulin and plotted. The expression levels of all LAWD-1 isoforms except for isoforms a and b peaked in L2/L3 stage. Isoforms a and b were most abundant during the L1 stage. Each lane was loaded with the following: 1000 embryos, 500 L1, 200 L2-L3, 100 L4 and 45 adults.

5.3 Identify optimum buffer and homogenizing conditions for co-immunoprecipitation analysis

The Chromotek mRFP nano-trap was selected to perform immunoprecipitation using LAWD-1::mCh. As a first step, conditions for obtaining worm lysates were compared. To obtain sufficient quantities of worms, they were grown and harvested from liquid culture (See section 2.2.3). The worms were then homogenised using a mini sonicator using three different buffers: Tris/NaCl, which was recommended by the manufacturer, H100 which was used in published *C. elegans* immunoprecipitation experiments (188) and RIPA buffer which contains a very strong detergent. Comparisons were performed in duplicates and the resulting lysate were analysed by SDS-PAGE. Western blot analyses indicated that only H100 buffer was successful in preserving LAWD-1 protein isoforms as only very low molecular weight bands were detected in the Tris/NaCl buffer lysates, which were likely to be due to protein degradation. The RIPA buffer lysate showed a slight improvement, but recovery of total protein was still problematic (Figure 5-3 A). After selecting the H100 lysis buffer, two methods of homogenisation were compared as the sonicator available for this study could not reach the maximum power suggested in published methods (188). The second method tested involved dounce homogenisation, which had been used successfully in other projects in the lab. Visual inspection of the blot (Figure 5-3B) indicated that dounce homogenisation was more effective in recovering LAWD-1::mCh protein isoforms.

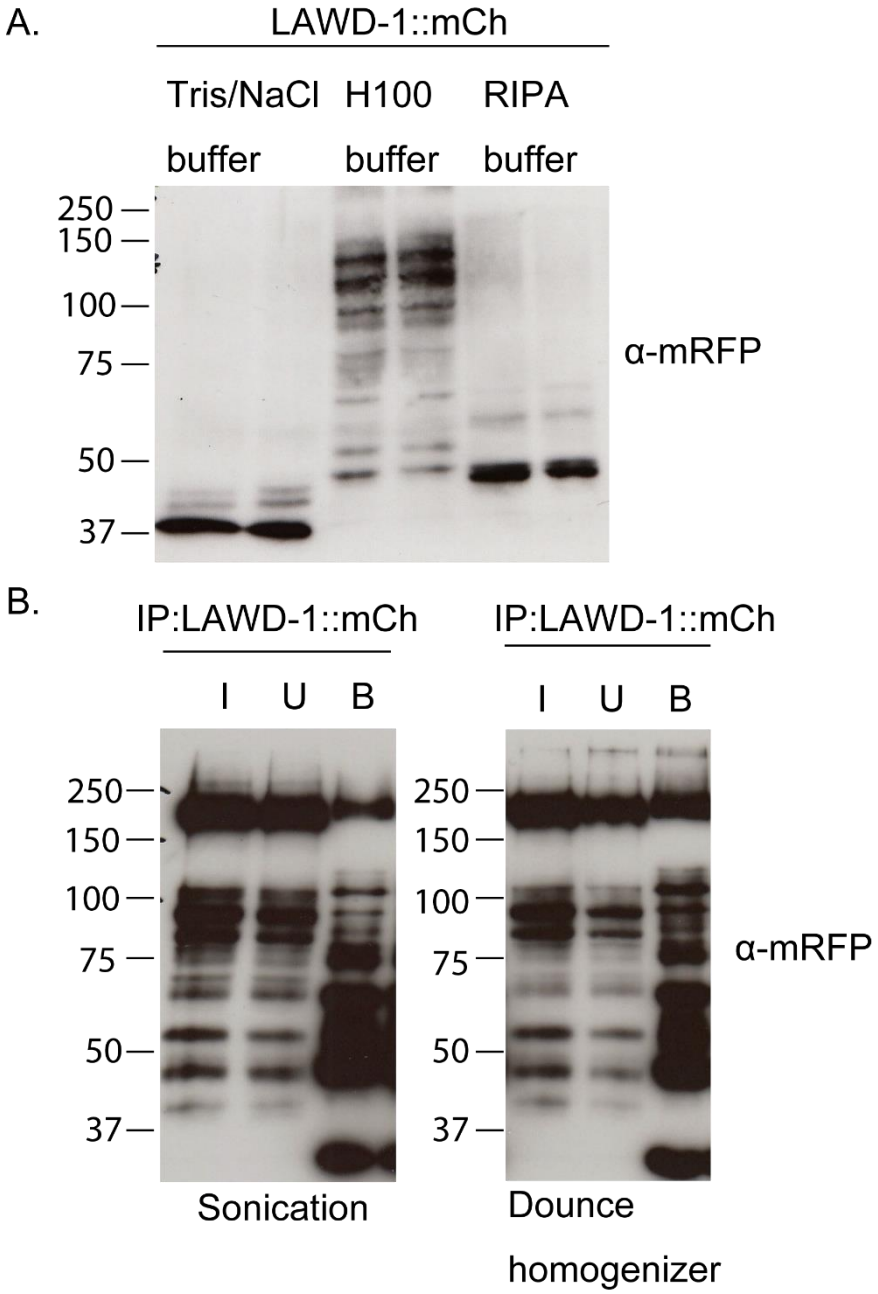

Figure 5-3 Optimising buffer and homogenization conditions for performing LAWD-1::mCh co-immunoprecipitation.

A. Western blot comparing the extraction buffers for co-immunoprecipitation: worm lysates were prepared using animals harvested after growth in liquid culture, which were homogenised using a sonication and one of three different lysis buffers. **B.** Western blot of co-immunoprecipitation methods using either mechanical extraction methods based on sonication or dounce homogenization.

5.4 Immunoprecipitation of LAWD-1::mCh and sur-5p::mCh and analysis by western blotting and silver staining.

In addition to optimising the conditions for immunoprecipitation, it was necessary to identify an appropriate negative control for the proteomic analysis. it was decided to generate a control that expressed mCh driven from the universal *sur-5* promoter (Constructs listed in Table 2-2). The construct made also contains an S-tag, which may be useful for future IP studies. The resulting strain was found to express mCherry in all *C. elegans* cells (data not shown). Having identified this control strain, proteins expressing mCh were immunoprecipitated from lysates obtained from worms expressing either LAWD-1::mCh or *sur-5p*::mCh using the mRFP nano-trap (Figure 5-4). As predicted, LAWD-1::mCh isoforms and mCherry protein alone were appropriately enriched by immunoprecipitation (Figure 5-4A). This is further verified by silver stains as unique isoforms were detected that were harvested after binding to the nano-trap, as indicated by arrowheads (Figure 5-4B).

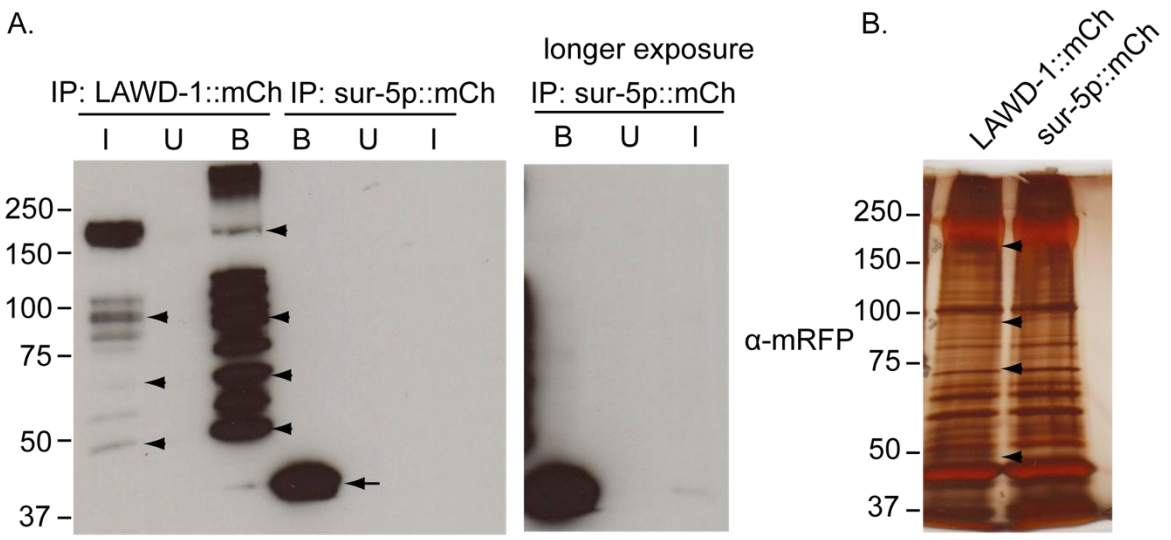

Figure 5-4 Co-immunoprecipitation of LAWD-1::mCh and sur-5p::mCh using Chromotek mRFP nanobeads followed by western blot and silver stain analyses.

A. Western blot analysis LAWD-1::mCh co-immunopreciptation process. Lysate inputs (I) were adjusted to a final concentration of 5 mg/mL. B represents 5% of total bound protein. Similar inputs were used for the control co-immunoprecipitation using *sur-5p::*mCh. **B.** Silver stain of input lysates (5% of total bound protein). Arrowheads refer to protein bands present in LAWD-1::mCh and not *sur-5::mCh*. Protein bands unique to co-IP of LAWD-1::mCh are indicated by arrowheads. I = Input, U = Unbound, B = Bound.

5.5 Proteomic identifies potential LAWD-1 interacting partners that function in epithelial development

LAWD-1::mCh and *sur-5p::mCh* worm lysate samples were immunoprecipitated using Chromotek mRFP nanotrap in the same way as described in Chapter 5.4. Samples bound to the nano-trap were sent to the University of Bristol's Proteomic Facility for mass spectroscopic analysis. After the mass spectrometry analysis was completed a list of targets were obtained where the data were analysed by Proteome Discoverer v. 2.1 software. The Mascot search engine (Matrix Science) was used to search the NCBI (nr) database. Any candidates with a Mascot score greater than the default threshold were identified as significant ($p<0.05$).

Candidates were further sorted based on the ratio of total number of unique peptides (PSM) detected in sample (E) compared with that of control (C) and then ranked based on this ratio. A cut-off value of 1.5 was used which indicated the identified peptides was 1.5 times more enriched in the sample (E) compared with control (E) (See section 2.2.3.7). The resulting list was further sorted by including only proteins where at least 30% of the protein was covered by the detected peptides and at least 10 peptides were detected. This resulted in 128 candidates, which was further filtered to 10 candidates which has functions associated with epithelial development (Table 5-1). The longest LAWD-1 isoforms LAWD-1A and LAWD-1B were also identified and ranked at the top of the list, which confirmed that LAWD-1::mCh was successfully enriched in the immunoprecipitation (Data not shown).

The list contained proteins known to be components of the actomyosin network, including NMY-1, NMY-2, MLC-4 and MLC-5. There were also proteins involved in controlling actin dynamics such as UNC-60. VAB-10B, a spectraplakin cytoskeleton involved in maintaining the structure of CeHD and possibly interacting with microtubules in epithelia has a PSM value of 43.1, which makes it the top candidate on the filtered list. 60.82% of VAB-10B protein was covered by detected unique peptides (Data not shown),

Gene Name	MW [kDa]	Description	# PSM (C)	# PSM (E)	#PSM (E)/#PSM (C)(ratio)
vab-10	561.4	Protein VAB-10, isoform	14	604	43.14286
mlc-5	16.0	Protein MLC-5	2	38	19
mlc-4	19.9	Probable myosin regulatory light chain	6	86	14.33333
nmy-2	231.1	Protein NMY-2	41	500	12.19512
nmy-1	229.2	Protein NMY-1	49	614	7.487805
mlc-7	17.29769	Protein MLC-7	12	89	7.416667
unc-60	17.0	Actin –depolymerizing factor 2	3	47	15.66667
mlc-3	17.1	Myosin essential light chain	25	147	5.88
mlc-2	17.1	Myosin regulatory light chain 2	16	327	4.605634
mlc-1	18.6	Myosin regulatory light chain 1	16	317	4.528571

Table 5-1 Top 10 LAWD-1 interacting candidates identified by mass spectroscopy involved in epithelial development.

Proteins co-immunoprecipitated with LAWD-1::mCh were detected by mass spectrometry and ranked based on three criteria: 1. at least 30% coverage of the whole protein, 2. at least 10 peptides detected, 3. PSM (number of unique peptides detected) ratio greater than 1.5. After functional assignment of all 128 candidates based on this criteria, 10 candidates were highlighted in the table, which are involved in epithelial development with VAB-10B showing significant enrichment in the LAWD-1::mCh co-immunoprecipitation sample compared with control.

5.6 VAB-10B but not VAB-10A is co-immunoprecipitated by LAWD-1::mCh

The interaction of LAWD-1::mCh and VAB-10B detected by mass spectrometry was validated by co-immunoprecipitation. A VAB-10N antibody was obtained as a kind gift from the lab of Kiyoji Nishiwaki. This antibody was first tested for its ability to detect both major VAB-10 isoforms VAB-10A and VAB-10B using whole worm samples prepared from N2. As shown in Figure 5-5, both isoforms were readily detected. Several smaller isoforms were also detected (confirmed by K. Nishiwaki); however, as their functions are not as well understood, they are not discussed further (Figure 5-5A).

After verifying the ability of the VAB-10N antibody to detect the VAB-10A and VAB-10B isoforms, three independently prepared LAWD-1::mCh lysates were bound to the Chromotek mRFP nano-trap and analysed. Western blot analyses showed that VAB-10B but not VAB-10A was co-immunoprecipitated by LAWD-1::mCh in all replicates (Figure 5-6A). The enrichment of LAWD-1::mCh isoforms in all three samples is also confirmed (Figure 5-6B). Thus, co-IP verifies that VAB-10B is associated with LAWD-1::mCh on the mRFP nano-trap beads, suggesting that VAB-10B interacts with LAWD-1::mCh.

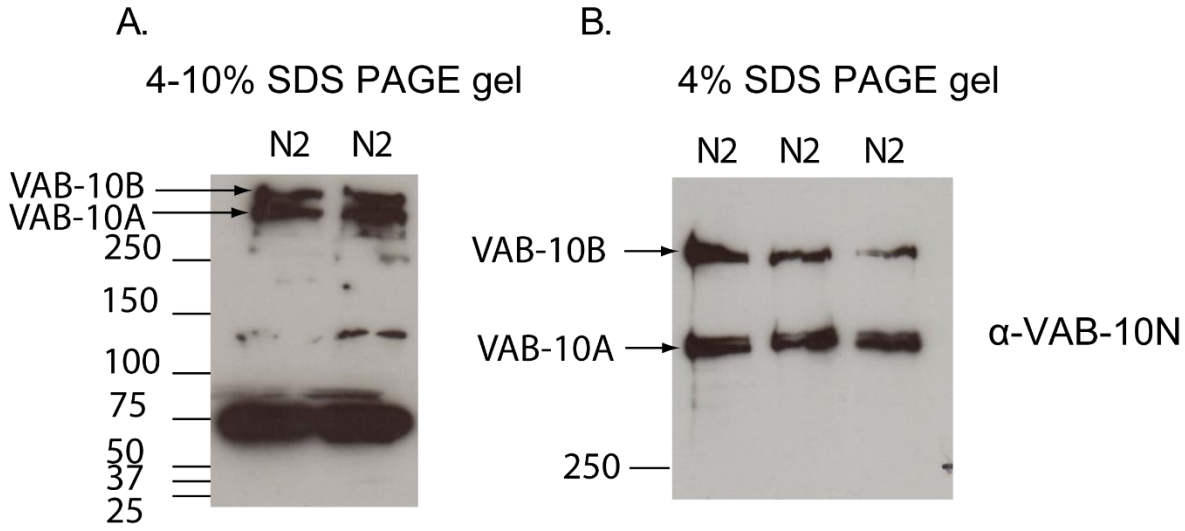

Figure 5-5 Detection of VAB-10 isoforms using the VAB-10N antibody

A. Detection of VAB-10 isoforms on 4-10% SDS-PAGE gel. **B.** Enhanced resolution of the major VAB-10A and VAB-10B isoforms on a 4% SDS-PAGE gel. The VAB-10N antibody detects a short N-terminal epitope common to both VAB-10A and VAB-10B. Each lane contains 45 adult animals.

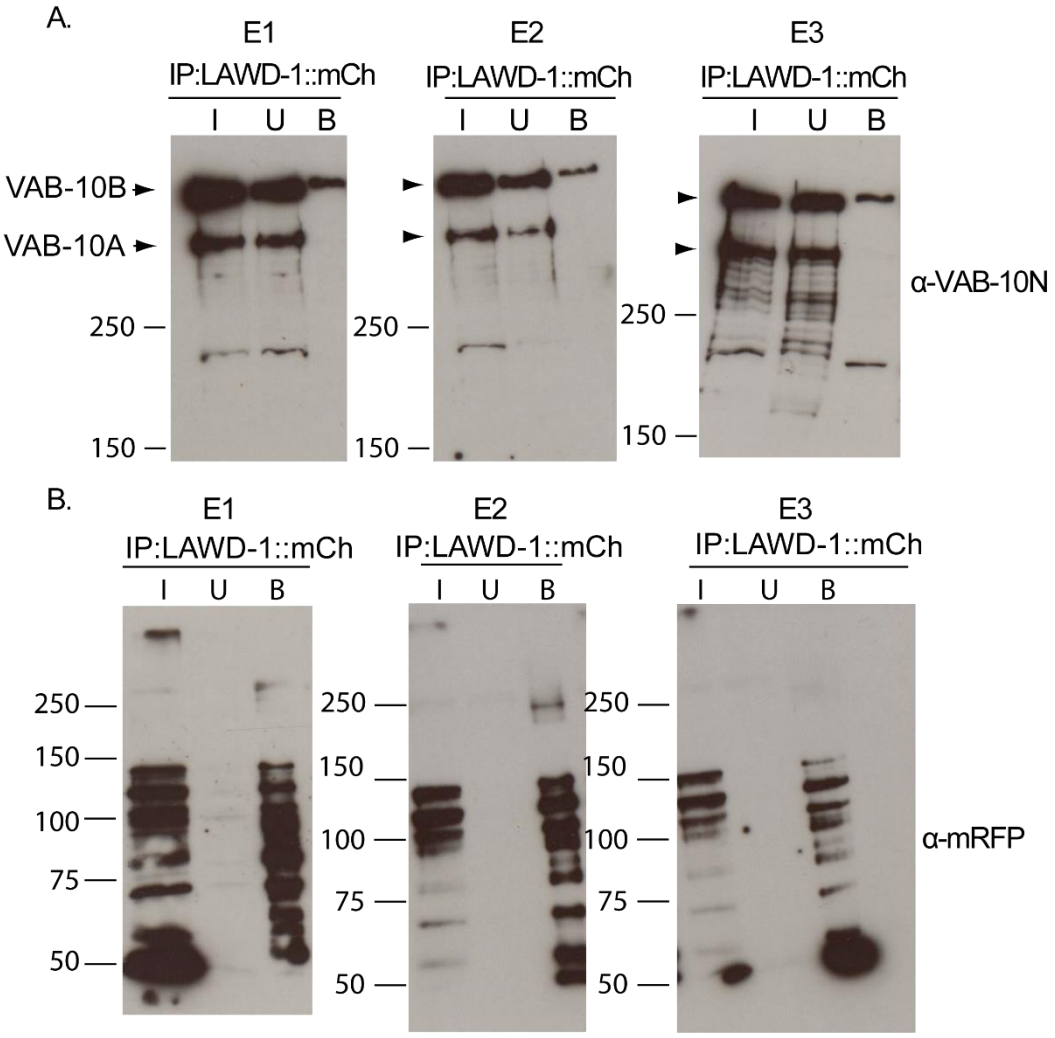

Figure 5-6 LAWD-1::mCh specifically co-immununoprecipitates VAB-10B and not VAB-10A.

A. Western blot detection of VAB-10B separated on a 4% SDS-PAGE gel after co-immunoprecipitation of LAWD-1::mCh. Three replicate experiments (E1-E3) are shown; VAB-10 was detected using the VAB-10N antibody. **B.** Confirmation that LAWD-1::mCh is present in the same samples shown in A) after co-immunoprecipitation and separation on 7% SDS-PAGE gel. LAWD-1::mCh was detected using an α-mRFP antibody. . Lysate inputs (I) were adjusted to a final concentration of 5 mg/mL; B represents 5% of total bound protein. I = Input, U = Unbound, B = Bound.

5.7 NMY-2::GFP is not co-immunoprecipitated with LAWD-1::mCh

Because a strain expressing CRISPR-Cas9 knock-in strain NMY-2::GFP was made available from the publication by Dickinson *et al*. (10), a LAWD-1::mCh and NMY-2::GFP double fluorescent strain was constructed for image analysis (Figure 4-7). This same strain was used to ask if NMY-2 was capable of being immunoprecipitated by LAWD-1::mCh.

First, an anti-GFP antibody was tested to see if it could detect NMY-2::GFP by western analysis. A doublet was detected in two independent experiments (Figure 5-7). Both bands were likely to correspond to NMY-2 protein, because the laboratory that generated the NMY-2::GFP strain confirmed that anti-NMY-2 antibody also detected two bands (Figure 5-7, Personal communication with Dr. Daniel J. Dickinson). Reciprocal immunoprecipitations were performed using samples from the same lysate. Results from the reciprocal co-IP between NMY-1::GFP and IP LAWD-1::mCh failed to identify an interaction between these proteins (Figure 5-8).

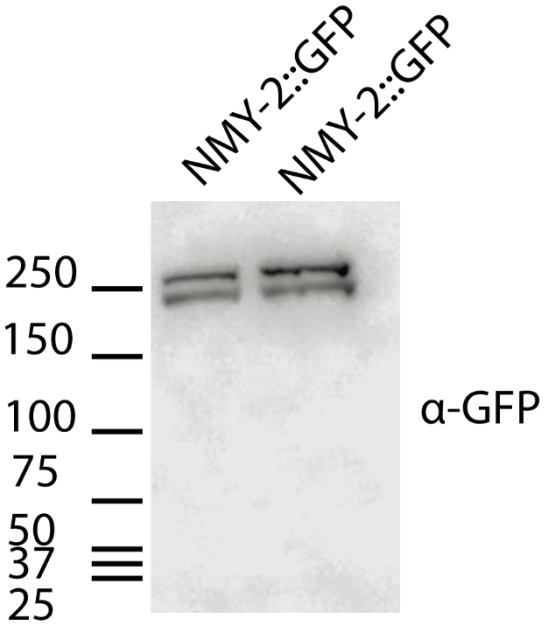

Figure 5-7 Detection of NMY-2::GFP using an α-GFP antibody

NMY-2::GFP protein was detected using an anti-GFP antibody after separation on a 10% SDS-PAGE gel. NMY-2::GFP is predicted to express only a single isoform, but an additional band is detected, the reason for which is explained in the result. Analysis was performed in duplicate using 45 adult animals in each lane.

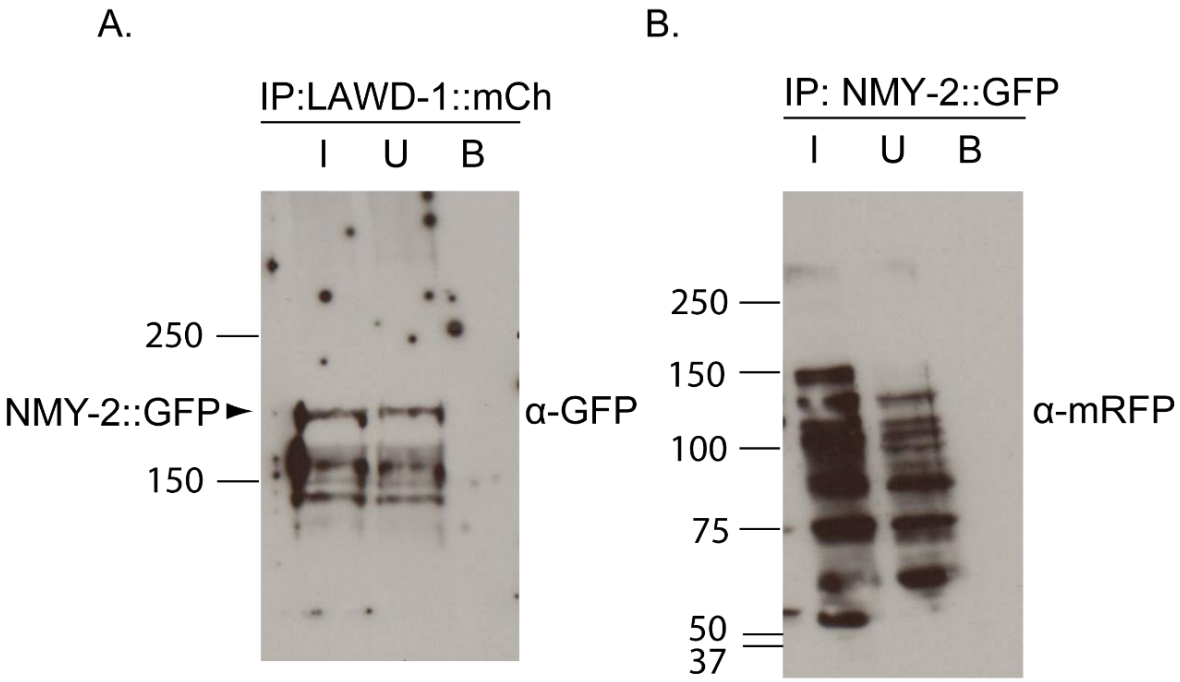

Figure 5-8 Reciprocal co-immunoprecipitation of LAWD-1::mCh and NMY-2::GFP fails to detect direct interactions.

A. Detection of NMY-2::GFP after co-immunoprecipitation by LAWD-1::mCh. **B.** Detection of LAWD-1::mCh after co-immunoprecipitation by NMY-2::GFP. A lysate from animals expressing co-expressing LAWD-1::mCh and NMY-2::GFP was prepared and the final concentration adjusted to 5 mg/mL. Aliquots of this lysates were used for immunoprecipitations performed in A) and B). NMY-2::GFP is indicated by an arrowhead. Lane B represents 5% of bound protein. I = Input, U = Unbound, B = Bound.

5.8 Discussion

The defining feature of LAWD-1 isoforms is the presence of two WD40 domains, each carrying a number of WD40 repeats. As discussed in Chapter 1.7, Certain WD40 proteins can form double propeller linked by a coiled-coiled domain and one such example is Tomosyn (174). The stable WD40 double propeller formed in N-terminus of Tomosyn acts as a negative control of the SNARE complex and inhibits vesicle fusion (174). Interestingly, *Drosophila* WD40 protein Lgl (lethal(2) giant larvae) is capable of binding to the nonmuscle myosin heavy chain (172), and since NMY-2 was also implicated in this study, it was desirable to learn if LAWD-1 WD40 domain is a functional domain and whether it is capable of interacting with other proteins, particularly those involved in epithelial development.

The longer LAWD-1A and LAWD-1B isoforms both carry WD40 domains, so it was hypothesised that these proteins could serve as scaffolds to mediate protein-protein interactions required during epithelial morphogenesis. However, it was not possible to identify other proteins with extensive similarity to LAWD-1 outside of the WD40 region that might provide clues about potential partners. Thus, it was decided to pursue an unbiased proteomic study to identify potential interacting proteins.

As a first step toward performing proteomic studies, the ability to identify LAWD-1 isoforms using LAWD-1::mCh and LAWD-1::GFP reporter strains capable of rescuing *lawd-1* mutants were explored by western blot analysis. mCherry and GFP fusions were selected because LAWD-1 fusion proteins are not only visible in live cells, but they can also be immunoprecipitated using anti-mRFP or anti-GFP nano-traps (Chromotek), which are more effective for co-IPs because of increased specificity.

Slight problems were encountered in western blots using an anti-GFP antibody. The antibody detected unspecific bands in wild type N2 whole worm samples in the absence of GFP expression. Three different anti-GFP antibodies were tested, two of them could not detect LAWD-1::GFP whereas the remaining antibody not only detected LAWD-1::GFP, but it continued to detect non-specific worm proteins. *NB*: A suitable anti-GFP antibody has since been identified. Fortunately anti-mRFP antibody detected LAWD-1::mCh specifically without detecting other bands in the absence of LAWD-1::mCh, therefore this antibody and LAWD-1::mCh was used in subsequent studies.

Developmental western blot analysis revealed the existence of multiple LAWD-1::mCh protein isoforms throughout development. The large number of transcripts predicted to be expressed from the *lawd*-1 locus poses problems when attempting to correlate proteins on a blot with specific transcripts based on size alone. At this stage, nothing is known about potential post-translational modifications that might affect the size of LAWD-1 isoforms.

The question of interest is whether certain isoforms are required during specific development stages to provide specific functions. Without pursuing further studies, which might include expressing specific cDNAs and determining whether they are capable of rescuing the *lawd-1* mutant phenotype, it is difficult to know with certainty how each isoform contributes to LAWD-1 function.

If attention is focused on the role of LAWD-1A and LAWD-1B, which are predicted to represent the longest isoforms and carry WD40 repeats, they are enriched in L1 stage larvae and in adults. The abundance of these isoforms appears to diminish between the L2 to L4 larval stages. An alternative explanation is that the

larger isoforms are trapped in a larger structure that is not adequately resolved by SDS-PAGE due to aggregation. In the simplest scenario, it is speculated that because the longest isoforms are most abundantly detected in L1 stage, they might participate in seam cell elongation. The perceived absence of the longest isoforms in the embryo and later larval stage, could mean that the lower molecular weight non-WD40 isoforms are responsible for the intestinal, vulval. Spermathecal and rectal expression of LAWD-1::mCh. Since the role of LAWD-1 in the developing intestine, spermatheca and vulva were not explored in this study, it remains to be seen if the increase in LAWD-1 expression level has significance in these developmental processes. Expression level of LAWD-1::mCh decreased in adults compared with larva, this could be an indication that there is no more dynamic change of LAWD-1 expression in adult tissues. This is consistent with the development changes of the animal as in adult germline is the most active organ but LAWD-1::mCh is not detected in germline.

Because the expression of LAWD-1::mCh isoforms is dynamic throughout development, it was decided to use mixed staged worms to produce a lysate for proteomic analysis. It was thought that this increased the probability of identifying interacting protein partners. H100 buffer turned out to be the buffer of choice as it was the only buffer capable of resolving the LAWD-1 isoforms. H100 buffer has also been used by other *C. elegans* researchers.

Proteomic analysis generated a large number of potential candidates and the candidates were further refined using criteria based on personal communication with lab colleagues (a cut-off ratio of 1.5 was used, see Chapter 5.5). The list generated a number of key regulators involved in epithelial development. The most prominent

hit was VAB-10B, a spectraplakin involved in elongation of the embryo possibly through its interaction with MT and CeHD (129).

vab-10 belongs to the spectraplakin gene family. Spectraplakins are huge cytoskeleton components which are able to cross-link the cytoskeletons and possibly their regulators. Therefore they have been called the master orchestrator of the dynamic cytoskeleton network (200). In the worm, there is a single spectraplakin gene expressing two main isoforms. VAB-10A and VAB-10B. VAB-10A is a crucial part of the CeHD structure and is also involved in cell-cell fusion through its interaction with actin (201) whereas VAB-10B is likely to interact with microtubules to stabilise the CeHD structure (129). Recent studies also showed that VAB-10B is required for Distal Tip Cell (DTC) and DTC nuclear migration (139). Therefore VAB-10B is likely to be an important cytoskeleton regulator. VAB-10 functions observed in worms so far are consistent with that in higher organisms, and the novel interaction between LAWD-1 and VAB-10B might provide further insight into the functions of spectraplakin.

VAB-10B is distinct from VAB-10A because it has a MT binding domain and multiple spectrin repeats (Figure 1-7). Although VAB-10A and VAB-10B share significant sequence similarity at their N-termini (Figure 1-7), VAB-10A was not detected in either the mass spectrometry analysis or the co-IP analysis. This is significant because it shows that the binding of LAWD-1 to VAB-10B is mediated by domains only present in VAB-10B and not VAB-10A. In the future, it would be beneficial to pinpoint the domains mediating this interaction. Both LAWD-1 and VAB-10 are large genes that are too large to express using plasmids. Such studies would need to be performed by working with smaller coding regions. It would also

be beneficial to generate a tagged version of VAB-10B suitable for proteomic analysis.

If LAWD-1 is indeed conferring its function through the WD40 domain, it is likely that LAWD-1 may somehow act as a bridge to link VAB-10B to other potential regulators. This hypothesis is also consistent with the role of VAB-10B as a protein cytoskeleton crosslinker which help recruit protein regulators to different cytoskeleton structures. The list also indicated LAWD-1 interaction with NMY-2, but this could not be verified through IP, although it is possible that the interaction is indirect. The fact that the *Drosophila* WD40 protein Lgl (lethal(2) giant larvae) can associate with nonmuscle myosin II heavy chain may be a clue that the interaction detected by the mass spectrometry may be real. Experiments from a different project in the lab focused on early embryo development and NMY-2 was also identified as a candidate but could not be verified by co-IP, therefore there is also a possibility that NMY-2 is a non-specific interacting protein.

MLC-4 is another interesting candidate as it was shown in previous studies to control the contraction of the actomyosin network through phosphorylation controlled by MEL-11 and LET-502 (153). This contraction was mainly required before the 2-fold stage of elongation, though which may not be consistent with the imaging analysis of LAWD-1 which showed that it was expressed in the lateral hypodermis in the later stages of embryogenesis. Attempts have been made to try to make a double reporter expressing LAWD-1::mCh and MLC-4::GFP, but MLC-4::GFP is expressed from an extrachromosomal array with a low transmission frequency. Hence, it was technically difficult to perform co-IP with this strain. It would be useful to make an integrated line of MLC-4::GFP to further verify this interaction.

Chapter 6 **Conclusion and future perspectives**

6.1 *lawd-1* is an essential gene that functions in epithelial morphogenesis

The present study used genetic and molecular methods to identify potential roles for the *lawd-1* gene in *C. elegans* epithelial development. During the course of this study, a number of *lawd-1* mutant alleles were obtained. All mutant alleles caused morphogenetic defects most likely associated with the process of elongation. The strongest alleles caused embryonic arrest at the 1.5-fold stage. The demonstration that a homozygous *lawd-1* null allele (*tm6954*) resulted in embryonic lethality was particularly important, because it established that *lawd-1* is indeed an essential gene. Time permitting, it would have been desirable to obtain mutant alleles that deleted the WD40 domain region in order to address questions regarding the importance of this domain in providing *lawd-1* activity. This was attempted by CRISPR-Cas9 gene editing, but the appropriate deletion was not obtained.

6.2 Identification of genes encoding proteins mediating potential interactions between LAWD-1 and the cytoskeleton

Given the synthetic lethal interaction between *lawd-1*(*cr7*) and *sma-1* (*e30*) (PEK, personal communication), it would also be fruitful to investigate the relationship between SMA-1 beta-H spectrin and LAWD-1 (160), Spectrin is another cytoskeletal protein required for morphogenesis and elongation (160). Attempts to investigate potential interactions between these proteins were hampered by the absence of reagents required for analysing SMA-1. Unfortunately, the lab that had originally identified the molecular basis of the *sma-1* mutant phenotype is no longer operational, and were unable to provide reagents. Working with another gene with

a coding region >13 kb also presented challenges. The availability of CRISPR-Cas9 gene engineering should make it possible to pursue this line of investigation.

The proteomic screen performed to identify proteins associated with LAWD-1::mCh on the basis of co-IP followed by mass spectroscopy was crucial is leading to the identification of VAB-10B as a protein capable of interacting with LAWD-1. This interaction will be discussed below. However, the screen also identified additional candidates (Table 5-1), which have not yet been analysed for their ability to interact with LAWD-1. These genes would also make good candidates for performing dual fluorescence studies. It would also be useful to see if the localisation of other known epithelial developmental regulators change in *lawd-1* mutant background.

6.3 *lawd-1* and morphogenesis of the *C. elegans* intestine

Image analyses have provided important insights into the possible function of LAWD-1. LAWD-1::mCh was expressed in many epithelial tissues, although this study focused on the developing intestine and seam cells. It was observed that LAWD-1::mCh expression in epithelial structures underwent dynamic re-arrangements in intracellular localisation during embryonic development. In the intestine, intracellular localisation of LAWD-1::mCh was confined to the apical region of the lumen.

In a recent publication investigating the molecular basis for *C. elegans* intestinal polarity, a link between *lawd-1* and the RAB-11+ recycling endosome in the intestine was found in a genome-wide RNAi screen (92). This genome-wide RNAi screen identified *lawd-1* and *vab-10* together in the 356 hits in the primary screening. Results showed that *lawd-1* RNAi can cause RAB-11 accumulation and

change of RAB-11::GFP apical morphology (92). Interestingly, RAB-11 was also identified in the mass spectrometry analysis as a possible candidate based on the three criteria described before, although it was not ranked as highly. A LAWD-1::mCh and RAB-11::GFP(intestine specific) double fluorescent strain has been built, however, co-immunoprecipitation has yet to be performed. It will be informative to see if LAWD-1::mCh is associated with RAB-11 in a co-IP experiment.

Electron microscopy will also be employed to study any potential intestine lumen defects in the *lawd-1* mutants.

6.4 *lawd-1* could act as a protein hub together with multi-cytoskeleton associated VAB-10B in the hypodermis

VAB-10B was identified as a potential interacting partner of LAWD-1::mCh. VAB-10B has been implicated to function in elongation based on its role in the CeHD (129). As discussed in Chapter 5.8, spectraplakins such as VAB-10B are capable of interacting with different cytoskeletal networks and in doing so, they contribute to dynamic changes affecting epithelial shape change in processes such as DTC migration (139). Recently published image showed that γ-tubulin reporter changed from diffused dots to organised band in the seam cells (162). This change of expression pattern is very similar to that of LAWD-1::mCh observed in the seam cell. Given that VAB-10B has a MT binding domain, this raises a question of whether LAWD-1 is involved in controlling the dynamics of MT during elongation through VAB-10B. The RAB-11+ recycling endosome has also been implicated in MT function as several MT regulatory proteins and motors were also identified in the results (92).

Mass spectrometry of proteins enriched after co-IP of mCh-tagged proteins showed a specific enrichment in LAWD-1A and LAWD-1B isoforms with WD40 domains, although most isoforms were predicted to be tagged by mCh. Although not conclusive, this provides support that these isoforms could be responsible for mediating the protein interactions being studied. The literature indicates that the primary role of the WD40 domain is to mediate protein-protein interactions (169). Studies of two *Drosophila* WD40 proteins discussed in Chapter 1 have provided clues about how a WD40 domain can interact with cytoskeleton related proteins, such as nonmuscle myosin II heavy chain (172). Apart from the actin binding domains and MT binding domains, large portion of VAB-10B is also composed of spectrin repeats (129). The role of the spectrin repeats has not yet been investigated by others. In a speculative model, it is proposed here that the interaction between LAWD-1 and VAB-10B might be mediated between the WD40 domain of LAWD-1 and the spectrin repeat region of VAB-10B (Figure 6-1). The image analysis of LAWD-1::mCh showed dynamic changes in seam cells beyond 2-fold embryonic elongation stage, and it was hypothesised that LAWD-1 might play a role in elongation at later embryonic development stages. This role could be achieved by its interaction with VAB-10B, with VAB-10B serving as the cytoskeleton cross-linker.

Taken together, these results support a model whereby LAWD-1 is involved in cytoskeleton dynamics and might specifically have a role in regulating MT dynamic changes during morphogenesis and elongation. The model presented in Figure 6-1 ties together what has been learned about LAWD-1 using approaches ranging from genetics to proteomics. There are still many questions remaining to be answered. Although the WD40 domain is proposed to mediate protein-protein interactions further analysis will need to be performed to determine whether it is this

domain, or perhaps a C-terminal LAWD-1 domain region identified by *cr7* that is responsible for the interaction with VAB-10B. This could possibly be achieved by expressing truncated versions of tagged-LAWD-1 construct based on cDNA clones and performing co-IP to identify regions responsible for interacting with VAB-10B. Reciprocal studies could also be performed by appropriately tagging VAB-10B using methods such as CRISPR-Cas9.

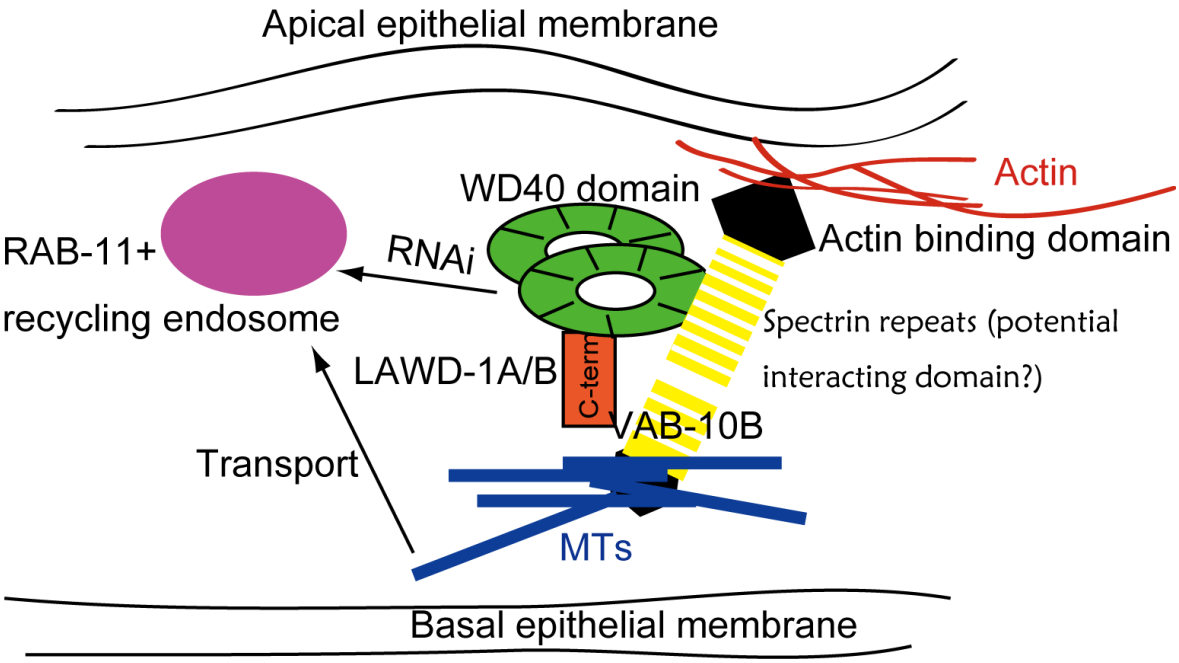

Figure 6-1 A summary of LAWD-1 localisation and interactions based on this study.

It is speculated that the WD40 domain of LAWD-1 associates with VAB-10B through its spectrin repeats. This would lead to localisation of LAWD-1 near the apical membrane of epithelia. The contribution of LAWD-1 to the dynamic changes in cytoskeleton during elongation and intestine development remains to be elucidated. It is unknown whether LAWD-1 plays a principal role as a scaffold and/or as a component of the cytoskeleton.

The detection of LAWD-1::mCh near the nuclear membrane of seam cells also raised the question as to whether LAWD-1::mCh is associated with the centrosome. As discussed in Chapter 3.3, LAWD-1 shares homology with the human WDR62, which has been implicated to play a role in MT spindle assembly (196). Although, this is a mitotic process, it is possible that LAWD-1 might be similarly associated with the epithelial MTOC. Defects in WDR62 are associated with the condition microcephaly (194), but theprecise function of WDR62 remains unknown. The studies presented here suggest that further dissection of the roles of LAWD-1A and LAWD-1B could contribute to a better understanding of the human WDR62.

Bibliography

1. Brenner S. The genetics of Caenorhabditis elegans. Genetics. 1974;77(1):71-94.
2. Sulston JE, Horvitz HR. Post-embryonic cell lineages of the nematode, Caenorhabditis elegans. Developmental biology. 1977;56(1):110-56.
3. Consortium CeS. Genome sequence of the nematode C-elegans: A platform for investigating biology. Science. 1998;282(5396):2012-8.
4. Venter JC, Adams MD, Myers EW, Li PW, Mural RJ, Sutton GG, et al. The sequence of the human genome. Science. 2001;291(5507):1304-51.
5. Lai CH, Chou CY, Ch'ang LY, Liu CS, Lin W. Identification of novel human genes evolutionarily conserved in Caenorhabditis elegans by comparative proteomics. Genome research. 2000;10(5):703-13.
6. Chalfie M, Tu Y, Euskirchen G, Ward WW, Prasher DC. Green Fluorescent Protein as a Marker for Gene-Expression. Science. 1994;263(5148):802-5.
7. Fire A, Xu S, Montgomery MK, Kostas SA, Driver SE, Mello CC. Potent and specific genetic interference by double-stranded RNA in Caenorhabditis elegans. Nature. 1998;391(6669):806-11.
8. Clark J, Ding S. Generation of RNAi libraries for high-throughput screens. Journal of biomedicine & biotechnology. 2006;2006(4):45716.
9. Chen C, Fenk LA, de Bono M. Efficient genome editing in Caenorhabditis elegans by CRISPR-targeted homologous recombination. Nucleic acids research. 2013;41(20):e193.
10. Dickinson DJ, Ward JD, Reiner DJ, Goldstein B. Engineering the Caenorhabditis elegans genome using Cas9-triggered homologous recombination. Nature methods. 2013;10(10):1028-+.
11. Arribere JA, Bell RT, Fu BX, Artiles KL, Hartman PS, Fire AZ. Efficient marker-free recovery of custom genetic modifications with CRISPR/Cas9 in Caenorhabditis elegans. Genetics. 2014;198(3):837-46.
12. Paix A, Wang YM, Smith HE, Lee CYS, Calidas D, Lu T, et al. Scalable and Versatile Genome Editing Using Linear DNAs with Microhomology to Cas9 Sites in Caenorhabditis elegans. Genetics. 2014;198(4):1347-+.
13. Farboud B, Meyer BJ. Dramatic Enhancement of Genome Editing by CRISPR/Cas9 Through Improved Guide RNA Design. Genetics. 2015;199(4):959-U106.
14. Michaux G, Legouis R, Labouesse M. Epithelial biology: lessons from Caenorhabditis elegans. Gene. 2001;277(1-2):83-100.
15. Knust E. Regulation of epithelial cell shape and polarity by cell-cell adhesion (Review). Molecular membrane biology. 2002;19(2):113-20.
16. Pasti G, Labouesse M. Epithelial junctions, cytoskeleton, and polarity. WormBook : the online review of C elegans biology. 2014:1-35.
17. Takeichi M. Dynamic contacts: rearranging adherens junctions to drive epithelial remodelling. Nature reviews Molecular cell biology. 2014;15(6):397-410.
18. Goldenring JR. Recycling endosomes. Current opinion in cell biology. 2015;35:117-22.
19. Francis GR, Waterston RH. Muscle organization in Caenorhabditis elegans: localization of proteins implicated in thin filament attachment and I-band organization. The Journal of cell biology. 1985;101(4):1532-49.

20. Francis R, Waterston RH. Muscle-Cell Attachment in Caenorhabditis-Elegans. Journal of Cell Biology. 1991;114(3):465-79.
21. Zhang H, Landmann F, Zahreddine H, Rodriguez D, Koch M, Labouesse M. A tension-induced mechanotransduction pathway promotes epithelial morphogenesis. Nature. 2011;471(7336):99-103.
22. Khan LA, Zhang H, Abraham N, Sun L, Fleming JT, Buechner M, et al. Intracellular lumen extension requires ERM-1-dependent apical membrane expansion and AQP-8-mediated flux. Nature cell biology. 2013;15(2):143-56.
23. Zhang H, Labouesse M. The making of hemidesmosome structures in vivo. Developmental dynamics : an official publication of the American Association of Anatomists. 2010;239(5):1465-76.
24. Rose L, Gonczy P. Polarity establishment, asymmetric division and segregation of fate determinants in early C. elegans embryos. WormBook : the online review of C elegans biology. 2014:1-43.
25. Assemat E, Bazellieres E, Pallesi-Pocachard E, Le Bivic A, Massey-Harroche D. Polarity complex proteins. Biochim Biophys Acta. 2008;1778(3):614-30.
26. Kemphues KJ, Priess JR, Morton DG, Cheng NS. Identification of genes required for cytoplasmic localization in early C. elegans embryos. Cell. 1988;52(3):311-20.
27. Updike D, Strome S. P granule assembly and function in Caenorhabditis elegans germ cells. J Androl. 2010;31(1):53-60.
28. Goldstein B, Macara IG. The PAR proteins: fundamental players in animal cell polarization. Developmental cell. 2007;13(5):609-22.
29. Motegi F, Sugimoto A. Sequential functioning of the ECT-2 RhoGEF, RHO-1 and CDC-42 establishes cell polarity in Caenorhabditis elegans embryos. Nature cell biology. 2006;8(9):978-85.
30. Schonegg S, Hyman AA. CDC-42 and RHO-1 coordinate acto-myosin contractility and PAR protein localization during polarity establishment in C. elegans embryos. Development. 2006;133(18):3507-16.
31. Guo S, Kemphues KJ. A non-muscle myosin required for embryonic polarity in Caenorhabditis elegans. Nature. 1996;382(6590):455-8.
32. Munro E, Nance J, Priess JR. Cortical flows powered by asymmetrical contraction transport PAR proteins to establish and maintain anterior-posterior polarity in the early C. elegans embryo. Developmental cell. 2004;7(3):413-24.
33. Munro E, Bowerman B. Cellular symmetry breaking during Caenorhabditis elegans development. Cold Spring Harbor perspectives in biology. 2009;1(4):a003400.
34. Cowan CR, Hyman AA. Centrosomes direct cell polarity independently of microtubule assembly in C. elegans embryos. Nature. 2004;431(7004):92-6.
35. Bienkowska D, Cowan CR. Centrosomes can initiate a polarity axis from any position within one-cell C. elegans embryos. Current biology : CB. 2012;22(7):583-9.
36. Jenkins N, Saam JR, Mango SE. CYK-4/GAP provides a localized cue to initiate anteroposterior polarity upon fertilization. Science. 2006;313(5791):1298-301.
37. Mayer M, Depken M, Bois JS, Julicher F, Grill SW. Anisotropies in cortical tension reveal the physical basis of polarizing cortical flows. Nature. 2010;467(7315):617-21.

38. Tabuse Y, Izumi Y, Piano F, Kemphues KJ, Miwa J, Ohno S. Atypical protein kinase C cooperates with PAR-3 to establish embryonic polarity in Caenorhabditis elegans. Development. 1998;125(18):3607-14.
39. Guo S, Kemphues KJ. par-1, a gene required for establishing polarity in C. elegans embryos, encodes a putative Ser/Thr kinase that is asymmetrically distributed. Cell. 1995;81(4):611-20.
40. Levitan DJ, Boyd L, Mello CC, Kemphues KJ, Stinchcomb DT. par-2, a gene required for blastomere asymmetry in Caenorhabditis elegans, encodes zinc-finger and ATP-binding motifs. Proceedings of the National Academy of Sciences of the United States of America. 1994;91(13):6108-12.
41. Cuenca AA, Schetter A, Aceto D, Kemphues K, Seydoux G. Polarization of the C. elegans zygote proceeds via distinct establishment and maintenance phases. Development. 2003;130(7):1255-65.
42. Watts JL, Morton DG, Bestman J, Kemphues KJ. The C. elegans par-4 gene encodes a putative serine-threonine kinase required for establishing embryonic asymmetry. Development. 2000;127(7):1467-75.
43. Morton DG, Shakes DC, Nugent S, Dichoso D, Wang W, Golden A, et al. The Caenorhabditis elegans par-5 gene encodes a 14-3-3 protein required for cellular asymmetry in the early embryo. Developmental biology. 2002;241(1):47-58.
44. Petrasek Z, Hoege C, Mashaghi A, Ohrt T, Hyman AA, Schwille P. Characterization of protein dynamics in asymmetric cell division by scanning fluorescence correlation spectroscopy. Biophysical journal. 2008;95(11):5476-86.
45. Zonies S, Motegi F, Hao Y, Seydoux G. Symmetry breaking and polarization of the C. elegans zygote by the polarity protein PAR-2. Development. 2010;137(10):1669-77.
46. Motegi F, Zonies S, Hao Y, Cuenca AA, Griffin E, Seydoux G. Microtubules induce self-organization of polarized PAR domains in Caenorhabditis elegans zygotes. Nature cell biology. 2011;13(11):1361-7.
47. Beatty A, Morton DG, Kemphues K. PAR-2, LGL-1 and the CDC-42 GAP CHIN-1 act in distinct pathways to maintain polarity in the C. elegans embryo. Development. 2013;140(9):2005-14.
48. Hao Y, Boyd L, Seydoux G. Stabilization of cell polarity by the C. elegans RING protein PAR-2. Developmental cell. 2006;10(2):199-208.
49. Hoege C, Constantinescu AT, Schwager A, Goehring NW, Kumar P, Hyman AA. LGL can partition the cortex of one-cell Caenorhabditis elegans embryos into two domains. Current biology : CB. 2010;20(14):1296-303.
50. Beers M, Kemphues K. Depletion of the co-chaperone CDC-37 reveals two modes of PAR-6 cortical association in C. elegans embryos. Development. 2006;133(19):3745-54.
51. Gotta M, Abraham MC, Ahringer J. CDC-42 controls early cell polarity and spindle orientation in C. elegans. Current biology : CB. 2001;11(7):482-8.
52. Aceto D, Beers M, Kemphues KJ. Interaction of PAR-6 with CDC-42 is required for maintenance but not establishment of PAR asymmetry in C. elegans. Developmental biology. 2006;299(2):386-97.
53. Kumfer KT, Cook SJ, Squirrell JM, Eliceiri KW, Peel N, O'Connell KF, et al. CGEF-1 and CHIN-1 regulate CDC-42 activity during asymmetric division in the Caenorhabditis elegans embryo. Molecular biology of the cell. 2010;21(2):266-77.

54. Nakayama Y, Shivas JM, Poole DS, Squirrell JM, Kulkoski JM, Schleede JB, et al. Dynamin participates in the maintenance of anterior polarity in the Caenorhabditis elegans embryo. Developmental cell. 2009;16(6):889-900.
55. Balklava Z, Pant S, Fares H, Grant BD. Genome-wide analysis identifies a general requirement for polarity proteins in endocytic traffic. Nature cell biology. 2007;9(9):1066-73.
56. Hyenne V, Tremblay-Boudreault T, Velmurugan R, Grant BD, Loerke D, Labbe JC. RAB-5 controls the cortical organization and dynamics of PAR proteins to maintain C. elegans early embryonic polarity. PloS one. 2012;7(4):e35286.
57. Chisholm AD, Hsiao TI. The Caenorhabditis elegans epidermis as a model skin. I: development, patterning, and growth. Wiley interdisciplinary reviews Developmental biology. 2012;1(6):861-78.
58. Raich WB, Agbunag C, Hardin J. Rapid epithelial-sheet sealing in the Caenorhabditis elegans embryo requires cadherin-dependent filopodial priming. Current biology : CB. 1999;9(20):1139-46.
59. Sheffield M, Loveless T, Hardin J, Pettitt J. C. elegans Enabled exhibits novel interactions with N-WASP, Abl, and cell-cell junctions. Current biology : CB. 2007;17(20):1791-6.
60. Fleming T, Chien SC, Vanderzalm PJ, Dell M, Gavin MK, Forrester WC, et al. The role of C. elegans Ena/VASP homolog UNC-34 in neuronal polarity and motility. Developmental biology. 2010;344(1):94-106.
61. Chisholm AD, Hardin J. Epidermal morphogenesis. WormBook : the online review of C elegans biology. 2005:1-22.
62. Costa M, Raich W, Agbunag C, Leung B, Hardin J, Priess JR. A putative catenin-cadherin system mediates morphogenesis of the Caenorhabditis elegans embryo. The Journal of cell biology. 1998;141(1):297-308.
63. Leung B, Hermann GJ, Priess JR. Organogenesis of the Caenorhabditis elegans intestine. Developmental biology. 1999;216(1):114-34.
64. Bossinger O, Klebes A, Segbert C, Theres C, Knust E. Zonula adherens formation in Caenorhabditis elegans requires dlg-1, the homologue of the Drosophila gene discs large. Developmental biology. 2001;230(1):29-42.
65. Koppen M, Simske JS, Sims PA, Firestein BL, Hall DH, Radice AD, et al. Cooperative regulation of AJM-1 controls junctional integrity in Caenorhabditis elegans epithelia. Nature cell biology. 2001;3(11):983-91.
66. McMahon L, Legouis R, Vonesch JL, Labouesse M. Assembly of C. elegans apical junctions involves positioning and compaction by LET-413 and protein aggregation by the MAGUK protein DLG-1. Journal of cell science. 2001;114(Pt 12):2265-77.
67. Nance J, Munro EM, Priess JR. C. elegans PAR-3 and PAR-6 are required for apicobasal asymmetries associated with cell adhesion and gastrulation. Development. 2003;130(22):5339-50.
68. Totong R, Achilleos A, Nance J. PAR-6 is required for junction formation but not apicobasal polarization in C. elegans embryonic epithelial cells. Development. 2007;134(7):1259-68.
69. Achilleos A, Wehman AM, Nance J. PAR-3 mediates the initial clustering and apical localization of junction and polarity proteins during C. elegans intestinal epithelial cell polarization. Development. 2010;137(11):1833-42.

70. Feldman JL, Priess JR. A role for the centrosome and PAR-3 in the hand-off of MTOC function during epithelial polarization. Current biology : CB. 2012;22(7):575-82.
71. Harris KP, Tepass U. Cdc42 and Par proteins stabilize dynamic adherens junctions in the Drosophila neuroectoderm through regulation of apical endocytosis. The Journal of cell biology. 2008;183(6):1129-43.
72. Shibata Y, Fujii T, Dent JA, Fujisawa H, Takagi S. EAT-20, a novel transmembrane protein with EGF motifs, is required for efficient feeding in Caenorhabditis elegans. Genetics. 2000;154(2):635-46.
73. Bossinger O, Fukushige T, Claeys M, Borgonie G, McGhee JD. The apical disposition of the Caenorhabditis elegans intestinal terminal web is maintained by LET-413. Developmental biology. 2004;268(2):448-56.
74. Segbert C, Johnson K, Theres C, van Furden D, Bossinger O. Molecular and functional analysis of apical junction formation in the gut epithelium of Caenorhabditis elegans. Developmental biology. 2004;266(1):17-26.
75. Legouis R, Jaulin-Bastard F, Schott S, Navarro C, Borg JP, Labouesse M. Basolateral targeting by leucine-rich repeat domains in epithelial cells. EMBO reports. 2003;4(11):1096-102.
76. Legouis R, Gansmuller A, Sookhareea S, Bosher JM, Baillie DL, Labouesse M. LET-413 is a basolateral protein required for the assembly of adherens junctions in Caenorhabditis elegans. Nature cell biology. 2000;2(7):415-22.
77. Pilipiuk J, Lefebvre C, Wiesenfahrt T, Legouis R, Bossinger O. Increased IP3/Ca2+ signaling compensates depletion of LET-413/DLG-1 in C. elegans epithelial junction assembly. Developmental biology. 2009;327(1):34-47.
78. Walker DS, Ly S, Lockwood KC, Baylis HA. A direct interaction between IP(3) receptors and myosin II regulates IP(3) signaling in C. elegans. Current biology : CB. 2002;12(11):951-6.
79. Thomas-Virnig CL, Sims PA, Simske JS, Hardin J. The inositol 1,4,5-trisphosphate receptor regulates epidermal cell migration in Caenorhabditis elegans. Current biology : CB. 2004;14(20):1882-7.
80. McGhee JD. The C. elegans intestine. WormBook : the online review of C elegans biology. 2007:1-36.
81. Deppe U, Schierenberg E, Cole T, Krieg C, Schmitt D, Yoder B, et al. Cell lineages of the embryo of the nematode Caenorhabditis elegans. Proceedings of the National Academy of Sciences of the United States of America. 1978;75(1):376-80.
82. Sulston JE, Schierenberg E, White JG, Thomson JN. The embryonic cell lineage of the nematode Caenorhabditis elegans. Developmental biology. 1983;100(1):64-119.
83. Aono S, Legouis R, Hoose WA, Kemphues KJ. PAR-3 is required for epithelial cell polarity in the distal spermatheca of C. elegans. Development. 2004;131(12):2865-74.
84. White EA, Glotzer M. Centralspindlin: at the heart of cytokinesis. Cytoskeleton. 2012;69(11):882-92.
85. Portereiko MF, Mango SE. Early morphogenesis of the Caenorhabditis elegans pharynx. Developmental biology. 2001;233(2):482-94.
86. Portereiko MF, Saam J, Mango SE. ZEN-4/MKLP1 is required to polarize the foregut epithelium. Current biology : CB. 2004;14(11):932-41.

87. Von Stetina SE, Mango SE. PAR-6, but not E-cadherin and beta-integrin, is necessary for epithelial polarization in C. elegans. Developmental biology. 2015;403(1):5-14.
88. Cox-Paulson EA, Walck-Shannon E, Lynch AM, Yamashiro S, Zaidel-Bar R, Eno CC, et al. Tropomodulin protects alpha-catenin-dependent junctional-actin networks under stress during epithelial morphogenesis. Current biology : CB. 2012;22(16):1500-5.
89. Zhang H, Abraham N, Khan LA, Hall DH, Fleming JT, Gobel V. Apicobasal domain identities of expanding tubular membranes depend on glycosphingolipid biosynthesis. Nature cell biology. 2011;13(10):1189-201.
90. Shafaq-Zadah M, Brocard L, Solari F, Michaux G. AP-1 is required for the maintenance of apico-basal polarity in the C. elegans intestine. Development. 2012;139(11):2061-70.
91. Zhang H, Kim A, Abraham N, Khan LA, Hall DH, Fleming JT, et al. Clathrin and AP-1 regulate apical polarity and lumen formation during C. elegans tubulogenesis. Development. 2012;139(11):2071-83.
92. Winter JF, Hopfner S, Korn K, Farnung BO, Bradshaw CR, Marsico G, et al. Caenorhabditis elegans screen reveals role of PAR-5 in RAB-11-recycling endosome positioning and apicobasal cell polarity. Nature cell biology. 2012;14(7):666-76.
93. Patel FB, Bernadskaya YY, Chen E, Jobanputra A, Pooladi Z, Freeman KL, et al. The WAVE/SCAR complex promotes polarized cell movements and actin enrichment in epithelia during C. elegans embryogenesis. Developmental biology. 2008;324(2):297-309.
94. Giuliani C, Troglio F, Bai Z, Patel FB, Zucconi A, Malabarba MG, et al. Requirements for F-BAR proteins TOCA-1 and TOCA-2 in actin dynamics and membrane trafficking during Caenorhabditis elegans oocyte growth and embryonic epidermal morphogenesis. PLoS genetics. 2009;5(10):e1000675.
95. Bernadskaya YY, Patel FB, Hsu HT, Soto MC. Arp2/3 promotes junction formation and maintenance in the Caenorhabditis elegans intestine by regulating membrane association of apical proteins. Molecular biology of the cell. 2011;22(16):2886-99.
96. Patel FB, Soto MC. WAVE/SCAR promotes endocytosis and early endosome morphology in polarized C. elegans epithelia. Developmental biology. 2013;377(2):319-32.
97. Leibfried A, Fricke R, Morgan MJ, Bogdan S, Bellaiche Y. Drosophila Cip4 and WASp define a branch of the Cdc42-Par6-aPKC pathway regulating E-cadherin endocytosis. Current biology : CB. 2008;18(21):1639-48.
98. St Johnston D, Ahringer J. Cell polarity in eggs and epithelia: parallels and diversity. Cell. 2010;141(5):757-74.
99. Baum B, Georgiou M. Dynamics of adherens junctions in epithelial establishment, maintenance, and remodeling. The Journal of cell biology. 2011;192(6):907-17.
100. Knust E, Bossinger O. Composition and formation of intercellular junctions in epithelial cells. Science. 2002;298(5600):1955-9.
101. Tsukita S, Furuse M, Itoh M. Structural and signalling molecules come together at tight junctions. Current opinion in cell biology. 1999;11(5):628-33.

102. Takai Y, Miyoshi J, Ikeda W, Ogita H. Nectins and nectin-like molecules: roles in contact inhibition of cell movement and proliferation. Nature reviews Molecular cell biology. 2008;9(8):603-15.
103. Laprise P, Tepass U. Novel insights into epithelial polarity proteins in Drosophila. Trends in cell biology. 2011;21(7):401-8.
104. Armenti ST, Nance J. Adherens junctions in C. elegans embryonic morphogenesis. Sub-cellular biochemistry. 2012;60:279-99.
105. Oda H, Uemura T, Shiomi K, Nagafuchi A, Tsukita S, Takeichi M. Identification of a Drosophila homologue of alpha-catenin and its association with the armadillo protein. The Journal of cell biology. 1993;121(5):1133-40.
106. Shapiro L, Weis WI. Structure and biochemistry of cadherins and catenins. Cold Spring Harbor perspectives in biology. 2009;1(3):a003053.
107. Pettitt J, Cox EA, Broadbent ID, Flett A, Hardin J. The Caenorhabditis elegans p120 catenin homologue, JAC-1, modulates cadherin-catenin function during epidermal morphogenesis. The Journal of cell biology. 2003;162(1):15-22.
108. Kwiatkowski AV, Maiden SL, Pokutta S, Choi HJ, Benjamin JM, Lynch AM, et al. In vitro and in vivo reconstitution of the cadherin-catenin-actin complex from Caenorhabditis elegans. Proceedings of the National Academy of Sciences of the United States of America. 2010;107(33):14591-6.
109. Bianchini JM, Kitt KN, Gloerich M, Pokutta S, Weis WI, Nelson WJ. Reevaluating alphaE-catenin monomer and homodimer functions by characterizing E-cadherin/alphaE-catenin chimeras. The Journal of cell biology. 2015;210(7):1065-74.
110. Choi HJ, Pokutta S, Cadwell GW, Bobkov AA, Bankston LA, Liddington RC, et al. alpha E-catenin is an autoinhibited molecule that coactivates vinculin. Proceedings of the National Academy of Sciences of the United States of America. 2012;109(22):8576-81.
111. Putzke AP, Rothman JH. Repression of Wnt signaling by a Fer-type nonreceptor tyrosine kinase. Proceedings of the National Academy of Sciences of the United States of America. 2010;107(37):16154-9.
112. Sumiyoshi E, Takahashi S, Obata H, Sugimoto A, Kohara Y. The beta-catenin HMP-2 functions downstream of Src in parallel with the Wnt pathway in early embryogenesis of C. elegans. Developmental biology. 2011;355(2):302-12.
113. Christophe-Hobertus C, Szpirer C, Guyon R, Christophe D. Identification of the gene encoding Brain Cell Membrane Protein 1 (BCMP1), a putative four-transmembrane protein distantly related to the Peripheral Myelin Protein 22 / Epithelial Membrane Proteins and the Claudins. BMC genomics. 2001;2:3.
114. Simske JS, Koppen M, Sims P, Hodgkin J, Yonkof A, Hardin J. The cell junction protein VAB-9 regulates adhesion and epidermal morphology in C. elegans. Nature cell biology. 2003;5(7):619-25.
115. Lockwood C, Zaidel-Bar R, Hardin J. The C. elegans zonula occludens ortholog cooperates with the cadherin complex to recruit actin during morphogenesis. Current biology : CB. 2008;18(17):1333-7.
116. Firestein BL, Rongo C. DLG-1 is a MAGUK similar to SAP97 and is required for adherens junction formation. Molecular biology of the cell. 2001;12(11):3465-75.
117. Asano A, Asano K, Sasaki H, Furuse M, Tsukita S. Claudins in Caenorhabditis elegans: their distribution and barrier function in the epithelium. Current biology : CB. 2003;13(12):1042-6.

118. Stetak A, Hajnal A. The C. elegans MAGI-1 protein is a novel component of cell junctions that is required for junctional compartmentalization. Developmental biology. 2011;350(1):24-31.
119. Lynch AM, Grana T, Cox-Paulson E, Couthier A, Cameron M, Chin-Sang I, et al. A genome-wide functional screen shows MAGI-1 is an L1CAM-dependent stabilizer of apical junctions in C. elegans. Current biology : CB. 2012;22(20):1891-9.
120. Zahreddine H, Zhang H, Diogon M, Nagamatsu Y, Labouesse M. CRT-1/calreticulin and the E3 ligase EEL-1/HUWE1 control hemidesmosome maturation in C. elegans development. Current biology : CB. 2010;20(4):322-7.
121. Walko G, Castanon MJ, Wiche G. Molecular architecture and function of the hemidesmosome. Cell and tissue research. 2015;360(3):529-44.
122. Jonkman MF. Hereditary skin diseases of hemidesmosomes. Journal of dermatological science. 1999;20(2):103-21.
123. Mercurio AM, Rabinovitz I, Shaw LM. The alpha 6 beta 4 integrin and epithelial cell migration. Current opinion in cell biology. 2001;13(5):541-5.
124. Lipscomb EA, Simpson KJ, Lyle SR, Ring JE, Dugan AS, Mercurio AM. The alpha6beta4 integrin maintains the survival of human breast carcinoma cells in vivo. Cancer research. 2005;65(23):10970-6.
125. Margadant C, Frijns E, Wilhelmsen K, Sonnenberg A. Regulation of hemidesmosome disassembly by growth factor receptors. Current opinion in cell biology. 2008;20(5):589-96.
126. de Pereda JM, Ortega E, Alonso-Garcia N, Gomez-Hernandez M, Sonnenberg A. Advances and perspectives of the architecture of hemidesmosomes Lessons from structural biology. Cell Adhes Migr. 2009;3(4):361-4.
127. Litjens SHM, de Pereda JM, Sonnenberg A. Current insights into the formation and breakdown of hemidesmosomes. Trends in cell biology. 2006;16(7):376-83.
128. Rezniczek GA, de Pereda JM, Reipert S, Wiche G. Linking integrin alpha6beta4-based cell adhesion to the intermediate filament cytoskeleton: direct interaction between the beta4 subunit and plectin at multiple molecular sites. The Journal of cell biology. 1998;141(1):209-25.
129. Bosher JM, Hahn BS, Legouis R, Sookhareea S, Weimer RM, Gansmuller A, et al. The Caenorhabditis elegans vab-10 spectraplakin isoforms protect the epidermis against internal and external forces. The Journal of cell biology. 2003;161(4):757-68.
130. Woo WM, Goncharov A, Jin YS, Chisholm AD. Intermediate filaments are required for C-elegans epidermal elongation. Developmental biology. 2004;267(1):216-29.
131. Bercher M, Wahl J, Vogel BE, Lu C, Hedgecock EM, Hall DH, et al. mua-3, a gene required for mechanical tissue integrity in Caenorhabditis elegans, encodes a novel transmembrane protein of epithelial attachment complexes. The Journal of cell biology. 2001;154(2):415-26.
132. Hong L, Elbl T, Ward J, Franzini-Armstrong C, Rybicka KK, Gatewood BK, et al. MUP-4 is a novel transmembrane protein with functions in epithelial cell adhesion in Caenorhabditis elegans. The Journal of cell biology. 2001;154(2):403-14.
133. Hresko MC, Schriefer LA, Shrimankar P, Waterston RH. Myotactin, a novel hypodermal protein involved in muscle-cell adhesion in Caenorhabditis elegans. The Journal of cell biology. 1999;146(3):659-72.

134. Rogalski TM, Mullen GP, Bush JA, Gilchrist EJ, Moerman DG. UNC-52/perlecan isoform diversity and function in Caenorhabditis elegans. Biochemical Society transactions. 2001;29(Pt 2):171-6.
135. Ding M, Goncharov A, Jin Y, Chisholm AD. C. elegans ankyrin repeat protein VAB-19 is a component of epidermal attachment structures and is essential for epidermal morphogenesis. Development. 2003;130(23):5791-801.
136. Ding M, King RS, Berry EC, Wang Y, Hardin J, Chisholm AD. The cell signaling adaptor protein EPS-8 is essential for C. elegans epidermal elongation and interacts with the ankyrin repeat protein VAB-19. PloS one. 2008;3(10):e3346.
137. Gally C, Zhang H, Labouesse M. Functional and Genetic Analysis of VAB-10 Spectraplakin in Caenorhabditis elegans. Methods in enzymology. 2016;569:407-30.
138. Hetherington S, Gally C, Fritz JA, Polanowska J, Reboul J, Schwab Y, et al. PAT-12, a potential anti-nematode target, is a new spectraplakin partner essential for Caenorhabditis elegans hemidesmosome integrity and embryonic morphogenesis. Developmental biology. 2011;350(2):267-78.
139. Kim HS, Murakami R, Quintin S, Mori M, Ohkura K, Tamai KK, et al. VAB-10 spectraplakin acts in cell and nuclear migration in Caenorhabditis elegans. Development. 2011;138(18):4013-23.
140. Woo WM, Berry EC, Hudson ML, Swale RE, Goncharov A, Chisholm AD. The C. elegans F-spondin family protein SPON-1 maintains cell adhesion in neural and non-neural tissues. Development. 2008;135(16):2747-56.
141. Gotenstein JR, Swale RE, Fukuda T, Wu Z, Giurumescu CA, Goncharov A, et al. The C. elegans peroxidasin PXN-2 is essential for embryonic morphogenesis and inhibits adult axon regeneration. Development. 2010;137(21):3603-13.
142. Huang CC, Hall DH, Hedgecock EM, Kao G, Karantza V, Vogel BE, et al. Laminin alpha subunits and their role in C. elegans development. Development. 2003;130(14):3343-58.
143. Priess JR, Hirsh DI. Caenorhabditis elegans morphogenesis: the role of the cytoskeleton in elongation of the embryo. Developmental biology. 1986;117(1):156-73.
144. Ding M, Woo WM, Chisholm AD. The cytoskeleton and epidermal morphogenesis in C. elegans. Experimental cell research. 2004;301(1):84-90.
145. Vuong-Brender TT, Ben Amar M, Pontabry J, Labouesse M. The interplay of stiffness and force anisotropies drives embryo elongation. eLife. 2017;6.
146. WilliamsMasson EM, Malik AN, Hardin J. An actin-mediated two-step mechanism is required for ventral enclosure of the C-elegans hypodermis. Development. 1997;124(15):2889-901.
147. Bernadskaya YY, Wallace A, Nguyen J, Mohler WA, Soto MC. UNC-40/DCC, SAX-3/Robo, and VAB-1/Eph polarize F-actin during embryonic morphogenesis by regulating the WAVE/SCAR actin nucleation complex. PLoS genetics. 2012;8(8):e1002863.
148. Soto MC, Qadota H, Kasuya K, Inoue M, Tsuboi D, Mello CC, et al. The GEX-2 and GEX-3 proteins are required for tissue morphogenesis and cell migrations in C. elegans. Genes & development. 2002;16(5):620-32.
149. Sawa M, Suetsugu S, Sugimoto A, Miki H, Yamamoto M, Takenawa T. Essential role of the C. elegans Arp2/3 complex in cell migration during ventral enclosure. Journal of cell science. 2003;116(Pt 8):1505-18.

150. Wernike D, Chen Y, Mastronardi K, Makil N, Piekny A. Mechanical forces drive neuroblast morphogenesis and are required for epidermal closure. Developmental biology. 2016;412(2):261-77.
151. Roy PJ, Zheng H, Warren CE, Culotti JG. mab-20 encodes Semaphorin-2a and is required to prevent ectopic cell contacts during epidermal morphogenesis in Caenorhabditis elegans. Development. 2000;127(4):755-67.
152. Costa M, Draper BW, Priess JR. The role of actin filaments in patterning the Caenorhabditis elegans cuticle. Developmental biology. 1997;184(2):373-84.
153. Gally C, Wissler F, Zahreddine H, Quintin S, Landmann F, Labouesse M. Myosin II regulation during C. elegans embryonic elongation: LET-502/ROCK, MRCK-1 and PAK-1, three kinases with different roles. Development. 2009;136(18):3109-19.
154. Chisholm AD, Hardin J. Epidermal morphogenesis. In: Community TCeR, editor. WormBook : the online review of C elegans biology: WormBook.
155. Piekny AJ, Johnson JL, Cham GD, Mains PE. The Caenorhabditis elegans nonmuscle myosin genes nmy-1 and nmy-2 function as redundant components of the let-502/Rho-binding kinase and mel-11/myosin phosphatase pathway during embryonic morphogenesis. Development. 2003;130(23):5695-704.
156. Piekny AJ, Wissmann A, Mains PE. Embryonic morphogenesis in Caenorhabditis elegans integrates the activity of LET-502 Rho-binding kinase, MEL-11 myosin phosphatase, DAF-2 insulin receptor and FEM-2 PP2c phosphatase. Genetics. 2000;156(4):1671-89.
157. Gobel V, Barrett PL, Hall DH, Fleming JT. Lumen morphogenesis in C. elegans requires the membrane-cytoskeleton linker erm-1. Developmental cell. 2004;6(6):865-73.
158. Van Furden D, Johnson K, Segbert C, Bossinger O. The C. elegans ezrin-radixin-moesin protein ERM-1 is necessary for apical junction remodelling and tubulogenesis in the intestine. Developmental biology. 2004;272(1):262-76.
159. Norman KR, Moerman DG. alpha spectrin is essential for morphogenesis and body wall muscle formation in Caenorhabditis elegans. Journal of Cell Biology. 2002;157(4):665-77.
160. McKeown C, Praitis V, Austin J. sma-1 encodes a betaH-spectrin homolog required for Caenorhabditis elegans morphogenesis. Development. 1998;125(11):2087-98.
161. Moorthy S, Chen LS, Bennett V. Caenorhabditis elegans beta-G spectrin is dispensable for establishment of epithelial polarity, but essential for muscular and neuronal function. Journal of Cell Biology. 2000;149(4):915-30.
162. Quintin S, Gally C, Labouesse M. Noncentrosomal microtubules in C. elegans epithelia. Genesis. 2016;54(4):229-42.
163. Desai A, Mitchison TJ. Microtubule polymerization dynamics. Annual review of cell and developmental biology. 1997;13:83-117.
164. Quintin S, Wang S, Pontabry J, Bender A, Robin F, Hyenne V, et al. Non-centrosomal epidermal microtubules act in parallel to LET-502/ROCK to promote C. elegans elongation. Development. 2016;143(1):160-73.
165. Wang S, Wu D, Quintin S, Green RA, Cheerambathur DK, Ochoa SD, et al. NOCA-1 functions with gamma-tubulin and in parallel to Patronin to assemble non-centrosomal microtubule arrays in C. elegans. eLife. 2015;4:e08649.
166. McGee MD, Rillo R, Anderson AS, Starr DA. UNC-83 is a KASH protein required for nuclear migration and is recruited to the outer nuclear membrane by a

physical interaction with the SUN protein UNC-84. Molecular biology of the cell. 2006;17(4):1790-801.
167. Fridolfsson HN, Starr DA. Kinesin-1 and dynein at the nuclear envelope mediate the bidirectional migrations of nuclei. Journal of Cell Biology. 2010;191(1):115-28.
168. Antoshechkin I, Han M. The C. elegans evl-20 gene is a homolog of the small GTPase ARL2 and regulates cytoskeleton dynamics during cytokinesis and morphogenesis. Developmental cell. 2002;2(5):579-91.
169. Stirnimann CU, Petsalaki E, Russell RB, Muller CW. WD40 proteins propel cellular networks. Trends in biochemical sciences. 2010;35(10):565-74.
170. Fong HK, Hurley JB, Hopkins RS, Miake-Lye R, Johnson MS, Doolittle RF, et al. Repetitive segmental structure of the transducin beta subunit: homology with the CDC4 gene and identification of related mRNAs. Proceedings of the National Academy of Sciences of the United States of America. 1986;83(7):2162-6.
171. Smith TF. Diversity of WD-repeat proteins. Sub-cellular biochemistry. 2008;48:20-30.
172. Strand D, Jakobs R, Merdes G, Neumann B, Kalmes A, Heid HW, et al. The Drosophila lethal(2)giant larvae tumor suppressor protein forms homo-oligomers and is associated with nonmuscle myosin II heavy chain. The Journal of cell biology. 1994;127(5):1361-73.
173. Collier S, Lee H, Burgess R, Adler P. The WD40 repeat protein fritz links cytoskeletal planar polarity to frizzled subcellular localization in the Drosophila epidermis. Genetics. 2005;169(4):2035-45.
174. Ashery U, Bielopolski N, Barak B, Yizhar O. Friends and foes in synaptic transmission: the role of tomosyn in vesicle priming. Trends Neurosci. 2009;32(5):275-82.
175. George SE, Simokat K, Hardin J, Chisholm AD. The VAB-1 Eph receptor tyrosine kinase functions in neural and epithelial morphogenesis in C. elegans. Cell. 1998;92(5):633-43.
176. Chin-Sang ID, George SE, Ding M, Moseley SL, Lynch AS, Chisholm AD. The ephrin VAB-2/EFN-1 functions in neuronal signaling to regulate epidermal morphogenesis in C-elegans. Cell. 1999;99(7):781-90.
177. Stiernagle T. Maintenance of C. elegans. WormBook : the online review of C elegans biology. 2006:1-11.
178. Lewis JA, Fleming JT. Basic culture methods. "Methods in Cell Biology. Caenorhabditis elegans: Modern Biological Analysis of an Organism." H.F. Epstein and D.C. Shakes (eds) ed. San Diego: Academic Press, Inc.; 1995.
179. Fay DS. Classical genetic methods. WormBook : the online review of C elegans biology. 2013:1-58.
180. Avery L. The genetics of feeding in Caenorhabditis elegans. Genetics. 1993;133(4):897-917.
181. Fay D, Bender A. Genetic mapping and manipulation: chapter 4--SNPs: introduction and two-point mapping. WormBook : the online review of C elegans biology. 2006:1-7.
182. Mello CC, Kramer JM, Stinchcomb D, Ambros V. Efficient gene transfer in C.elegans: extrachromosomal maintenance and integration of transforming sequences. The EMBO journal. 1991;10(12):3959-70.
183. Mello C, Fire A. DNA transformation. Methods in cell biology. 1995;48:451-82.

184. Evans (ed.) TC. Transformation and microinjection. In: Community TCeR, editor. WormBook : the online review of C elegans biology: WormBook.
185. Praitis V, Casey E, Collar D, Austin J. Creation of low-copy integrated transgenic lines in Caenorhabditis elegans. Genetics. 2001;157(3):1217-26.
186. Frokjaer-Jensen C, Davis MW, Ailion M, Jorgensen EM. Improved Mos1-mediated transgenesis in C. elegans. Nature methods. 2012;9(2):117-8.
187. Hyman AA. C. elegans techniques - protein biochemistry2012.
188. Zanin E, Dumont J, Gassmann R, Cheeseman I, Maddox P, Bahmanyar S, et al. Affinity Purification of Protein Complexes in C. elegans. Method Cell Biol. 2011;106:289-322.
189. Duerr JS. Immunohistochemistry. In: Community TCeR, editor. WormBook : the online review of C elegans biology: WormBook.
190. Sambrook J, Russel D. Molecular Cloning: A Laboratory Manual. 3rd ed: Cold Spring Harbor Laboratory Press; 2001.
191. Tursun B, Cochella L, Carrera I, Hobert O. A Toolkit and Robust Pipeline for the Generation of Fosmid-Based Reporter Genes in C. elegans. PloS one. 2009;4(3).
192. Gibson DG, Young L, Chuang RY, Venter JC, Hutchison CA, Smith HO. Enzymatic assembly of DNA molecules up to several hundred kilobases. Nature methods. 2009;6(5):343-U41.
193. Praitis V, Ciccone E, Austin J. SMA-1 spectrin has essential roles in epithelial cell sheet morphogenesis in C. elegans. Developmental biology. 2005;283(1):157-70.
194. Bilguvar K, Ozturk AK, Louvi A, Kwan KY, Choi M, Tatli B, et al. Whole-exome sequencing identifies recessive WDR62 mutations in severe brain malformations. Nature. 2010;467(7312):207-U93.
195. Wasserman T, Katsenelson K, Daniliuc S, Hasin T, Choder M, Aronheim A. A Novel c-Jun N-terminal Kinase (JNK)-binding Protein WDR62 Is Recruited to Stress Granules and Mediates a Nonclassical JNK Activation. Molecular biology of the cell. 2010;21(1):117-30.
196. Lim NR, Yeap YYC, Zhao TT, Yip YY, Wong SC, Xu D, et al. Opposing roles for JNK and Aurora A in regulating the association of WDR62 with spindle microtubules. Journal of cell science. 2015;128(3):527-40.
197. Riedl J, Crevenna AH, Kessenbrock K, Yu JH, Neukirchen D, Bista M, et al. Lifeact: a versatile marker to visualize F-actin. Nature methods. 2008;5(7):605-7.
198. Sherwood DR, Sternberg PW. Anchor cell invasion into the vulval epithelium in C-elegans. Developmental cell. 2003;5(1):21-31.
199. L. M. Analyzing gels and western blots with ImageJ 2010 [Available from: http://lukemiller.org/index.php/2010/11/analyzing-gels-and-western-blots-with-image-j/.
200. Suozzi KC, Wu X, Fuchs E. Spectraplakins: master orchestrators of cytoskeletal dynamics. The Journal of cell biology. 2012;197(4):465-75.
201. Yang YH, Zhang Y, Li WJ, Jiang YX, Zhu ZW, Hu HF, et al. Spectraplakin Induces Positive Feedback between Fusogens and the Actin Cytoskeleton to Promote Cell-Cell Fusion. Developmental cell. 2017;41(1):107-+.